ESPOO 2003 VTT RESEARCH NOTES 2223

Tuomo Kärnä, Kari Kolari, Peter Jochmann, Karl-Ulrich Evers, Bi Xiangjun, Mauri Määttänen & Petter Martonen

Ice action on compliant structures

Laboratory indentation tests

VTT TIEDOTTEITA – RESEARCH NOTES 2223

Ice action on compliant structures

Laboratory indentation tests

Tuomo Kärnä & Kari Kolari

VTT Building and Transport

Peter Jochmann, Karl-Ulrich Evers, Bi Xiangjun,
Mauri Määttänen & Petter Martonen

ISBN 951–38–6200–3 (soft back ed.)
ISSN 1235–0605 (soft back ed.)

ISBN 951–38–6201–1 (URL: http://www.vtt.fi/inf/pdf/)
ISSN 1455–0865 (URL: http://www.vtt.fi/inf/pdf/)

JULKAISIJA – UTGIVARE – PUBLISHER

VTT, Vuorimiehentie 5, PL 2000, 02044 VTT
puh. vaihde (09) 4561, faksi (09) 456 4374

VTT, Bergsmansvägen 5, PB 2000, 02044 VTT
tel. växel (09) 4561, fax (09) 456 4374

VTT Technical Research Centre of Finland, Vuorimiehentie 5, P.O.Box 2000, FIN–02044 VTT, Finland
phone internat. + 358 9 4561, fax + 358 9 456 4374

VTT Rakennus- ja yhdyskuntatekniikka, Puumiehenkuja 2 A, PL 1806, 02044 VTT
puh. vaihde (09) 4561, faksi (09) 456 7027

VTT Bygg och transport, Träkarlsgränden 2 A, PB 1806, 02044 VTT
tel. växel (09) 4561, fax (09) 456 7027

VTT Building and Transport, Puumiehenkuja 2 A, P.O.Box 1806, FIN–02044 VTT, Finland
phone internat. + 358 9 4561, fax + 358 9 456 7027

Technical editing Leena Ukskoski

Otamedia Oy, Espoo 2003

Kärnä, Tuomo, Kolari, Kari, Jochmann, Peter, Evers, Karl-Ulrich, Xiangjun, Bi, Määttänen, Mauri & Martonen, Petter. Ice action on compliant structures. Laboratory indentation tests. Espoo 2003. VTT Tiedotteita – Research Notes 2223. 43 p. + app. 79 p.

Keywords marine structures, offshore structures, steady-state vibrations, ice-induced vibrations, conical structures, dynamic response, measurement, testing, numerical analysis, models

Abstract

This experimental research addresses the dynamic ice-structure interaction of marine structures. The main objective was to obtain data on the phenomenon known as steady-state vibration of vertical offshore structures. Such data is needed while researchers develop numerical and simplified models of the vibration. A further objective was to find data on ice-induced vibrations of conical structures. A common belief has been that ice cannot create significant vibrations on conical offshore structures. Recent full-scale data has shown that this assumption is not correct. Hence, the present project aimed at obtaining laboratory data on this kind of vibrations. The third aim of the project was to demonstrate that additional structural damping can be used to mitigate the dynamic response caused by ice actions.

Tests were done at the ice basin of the ARCTECLAB using the carriage of the ice basin. An experimental structure was installed on the carriage and penetration tests were done on three sheets of columnar-grained ice. The dynamic properties of the structure were modified during the test series. Two different indentors were used, a vertical cylinder and a cone. This test report provides detailed descriptions of the test set up and the test programme. The main results are also shown in terms of the measured time signals. The report serves as a background document for more detailed analysis and subsequent exploration of the data.

Preface

This experimental research was conducted jointly by the VTT Technical Research Centre of Finland, Hamburgische Shiffbauversuchsanstalt, Dalian University of Technology and Helsinki University of Technology. The need for new tests was identified while these institutes were working together in the EU funded research project "NEST – Networking Studies on Ice and Compliant Structures" (Contract No ICA5-CT-2001-50002). The tests serve also the needs for new laboratory data as identified in the research project "ARKI – Arktiset Merirakenteet (Arctic Offshore Structures)" sponsored by the Finnish Technology Agency (Dno 40857/99).

The research team would like to thank the Hamburg Ship Model Basin (HSVA), especially the ice thank crew, for the hospitality, technical support and professional execution of the test programme in the ARCTECLAB. The research activities carried out at the Major Research Infrastructure ARCTECLAB were financially supported by the Human Potential and Mobility Programme from the European Union through contract HPRI-CT-1999-00035.

Contents

1. Introduction

Ice-induced vibrations of compliant marine structures have been studied on several occasions since Peyton (1966) published his experimental results. Phenomenological and numerical models are available to analyze this phenomenon. However, details of the ice-structure interaction process that lead to this phenomenon are not properly understood. Ice-induced vibrations may occur on several kinds of structures. These include offshore structures for hydrocarbon production and aids of navigation. Designers will face the same problem in future while constructing offshore wind power generators for the ice-covered areas of the Baltic Sea. Therefore, there is now an urgent need to understand the physical phenomena involved in ice-induced vibrations.

1.1 Physical problems involved

Ice-induced vibrations that occur on vertical structures have been characterized in the past using either the concepts of resonant vibration or self-induced vibration. The latter is known also as a lock-in phenomenon. Installing a cone at the ice level is one of the methods to reduce the quasi-static global ice force and the ice induced vibrations. However, recent full-scale data from the Bohai Bay (Yue and Bi, 2000) shows that vibrations on conical structures can be excessive. It is anticipated that a similar situation may arise on offshore wind power generators.

The ice-induced vibrations have traditionally been described using macroscale or phenomenological theories. More recently, researchers are trying to understand the basic reasons for these vibrations. Hence microscale aspects of the ice-structure interaction are considered. Several concepts have been tried or proposed in attempts to understand the self-induced vibrations. These include the macroscale phenomena

- the strain rate dependence of the uniaxial compressive strength (drop at the ice strength at a critical strain rate)
- transition from nonsimultaneous failure to simultaneous failure
- two variants of the concept known as the ice failure depth

and also microscale phenomena such as

- horizontal splits as a mechanism that creates the change from nonsimultaneous to simultaneous failure
- wing-crack mechanism in ice crushing
- pressure melting under a high pressure
- velocity dependence of the kinetic friction.

Full scale observations indicate that transition from nonsimultaneous to simultaneous failure is a prerequisite for self-induced vibration. However, the basic reason for such a transition is not properly understood. It should also be noticed that the famous event on the Moliqpak structure in 1986 exhibited simultaneous ice failure with large global loads and dynamic response. However, the response was not self-induced vibration.

Previous work suggest that the following macroscale parameters influence the arise of self-induced vibration:

- ice velocity
- peak force
- structural damping
- modal amplitude at the ice level
- aspect ratio and the ice thickness.

In addition, several microscale features related to ice behaviour influence the interaction process. In the test condition we can influence:

- ice temperature
- ice quality.

1.2 Objectives

The aim of this work is to improve the understanding of the physical phenomena involved in ice induced vibrations. Therefore, tests were carried out as physical tests that support the development of theoretical modelling. While planning these tests, the following desirable features of the test set-up were identified:

- Freshwater ice or other kind of natural ice should be used to provide natural brittleness.
- Simple indentors should be used.
- Attempts should be made to measure or observe relevant physical phenomena.

2. Experimental setup

2.1 Model basin

The testes were made at a Large Scale Facility of EU, known as ARCTECLAB, which is operated by the Hamburg Ship Model Basin (Hamburgische Schiffbauversuchs-anstalt, HSVA). This institute has been operating ice research facilities for more than 25 years. The main facility is the 78 m long, 10 m wide and 2.5 m deep ice model tank (see Figure 1). An air forced cooling system generates air temperatures as low as –20 °C. A motor-driven carriage runs at velocity that can be varied between 3 mm/s and 3 m/s, and provides a towing force up 50 kN. Service carriages above water as well as underwater are available to carry experimental equipment, measuring devices e.g. a variety of load cells, dynamometers, accelerometers, and video cameras.

Figure 1. HSVA's 78 m long, 10 m wide and 2.5 m deep ice basin.

2.2 Test structure

A simple structure was built for ice-structure interaction tests. The objectives in the test structure design were the following:

- The tests structure should incorporate two eigenmodes. The first eigenfrequency f_1 should be in the range from 2 Hz to 6 Hz and the second frequency f_2 from 10 Hz to 15 Hz.
- The stiffness of the structure, at the ice-level stiffness should be adjustable, the initial target value is $k \approx 1.0$ kN/mm
- Load bearing capacity of the structure must be at least 60 kN (static force on ice-level)
- Ice-level indentors must be easily interchangeable.

The sketch of the structure, which meets the requirements presented above, is shown in Figures 2 and 3. The structure was cross-type, welded steel structure. Columns and torsion beam were fabricated from rectangular hollow sections. The vertical column was connected to the horizontal torsion beam. The torsion beam-ends were connected to the HSVA's carriage columns. The stiffness of the torsion beam connection was adjustable.

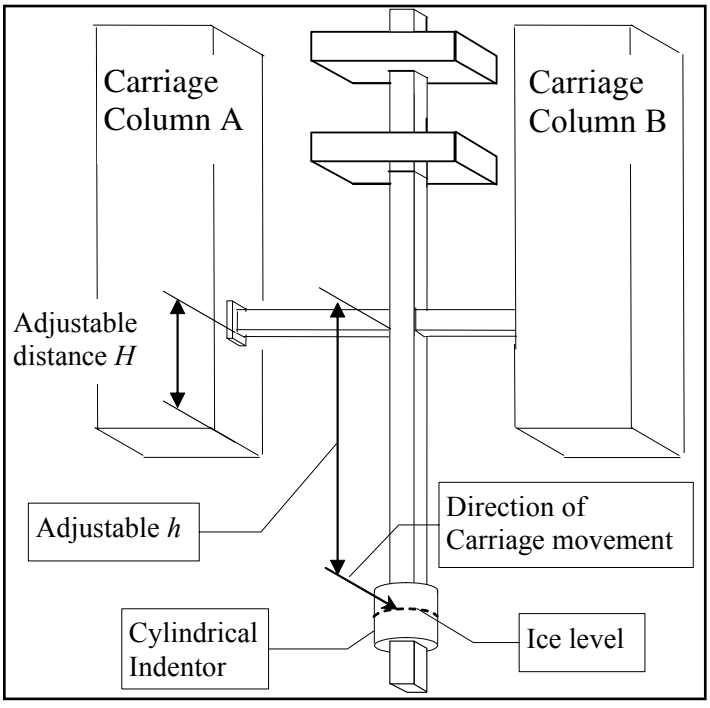

Figure 2. Sketch of the test structure and it's connection to the HSVA's Carriage.

The carriage moved along the rails located on the ice basin sides with a pre-defined velocity (Figure 3).

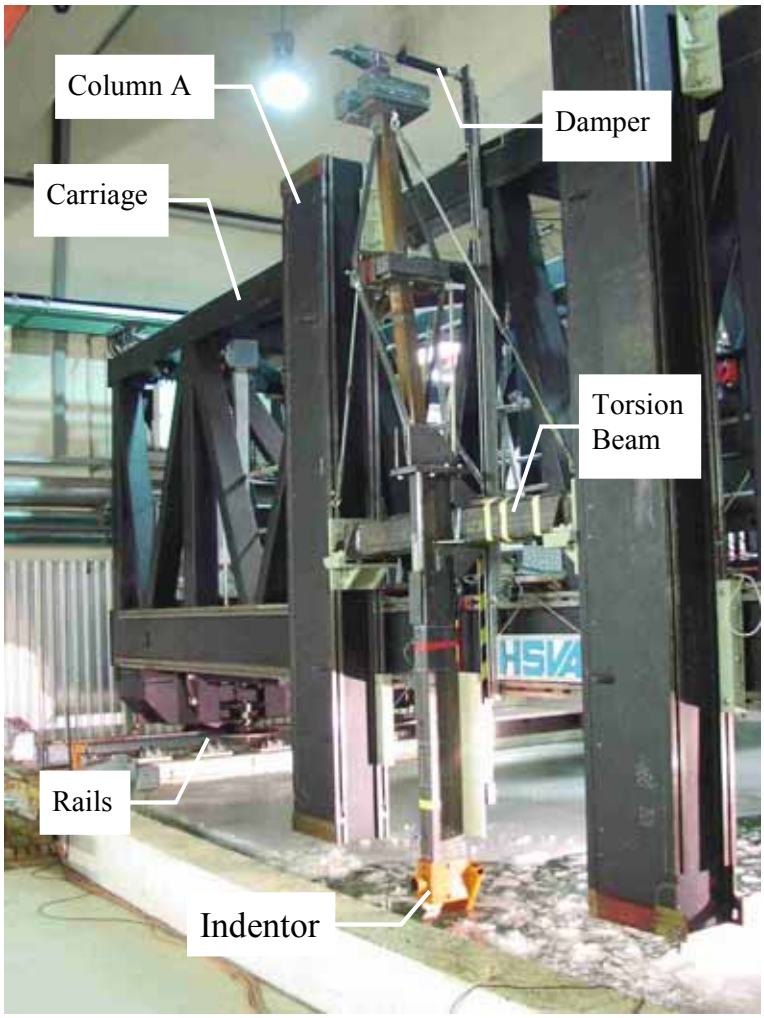

Figure 3. Test structure and the carriage.

2.2.1 Basic properties of the structure

The detailed drawings of the test structure are shown in Figures 4 and 5. It was possible to vary the two weights of the upper column (74 kg and 105 kg in Figure 4) to adjust the first two eigenfrequences. The lowermost weight of 90 kg was constant and it was located inside the lower column (RHS 200x100x8).

The rotational stiffness of the torsion-beam connection was varied by using different types of rubber springs between the structure and the carriage (Figs 6 and 7). Rubber and steel pads were used in the tests.

Ice-level stiffness was adjustable by changing the distance of structure (*H)* and the position of the indentor (*h*) as shown in Figure 2. The stiffness was experimentally verified before each test.

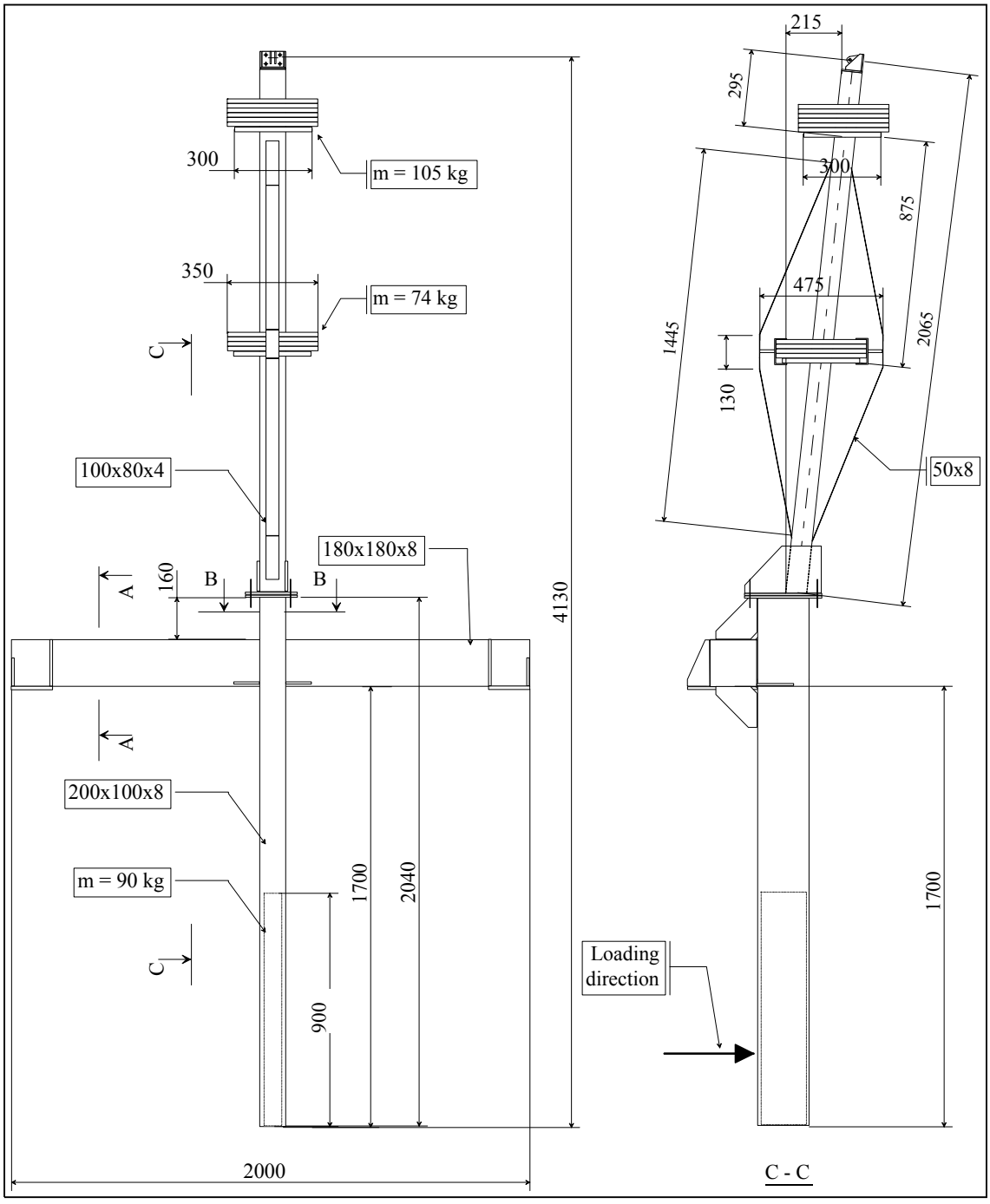

Figure 4. Front and side view of the structure.

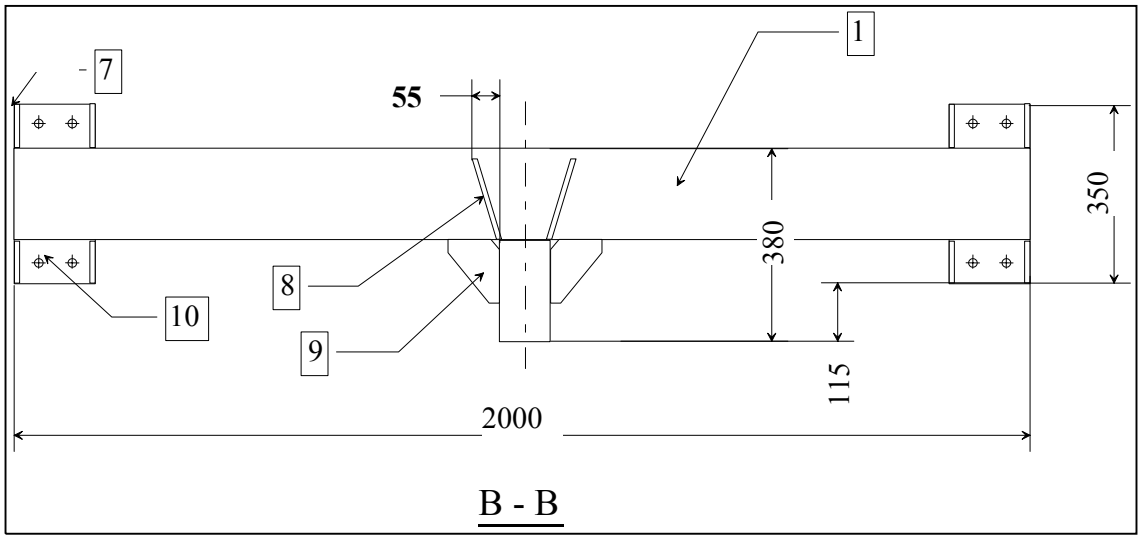

Figure 5. Top view of the structure.

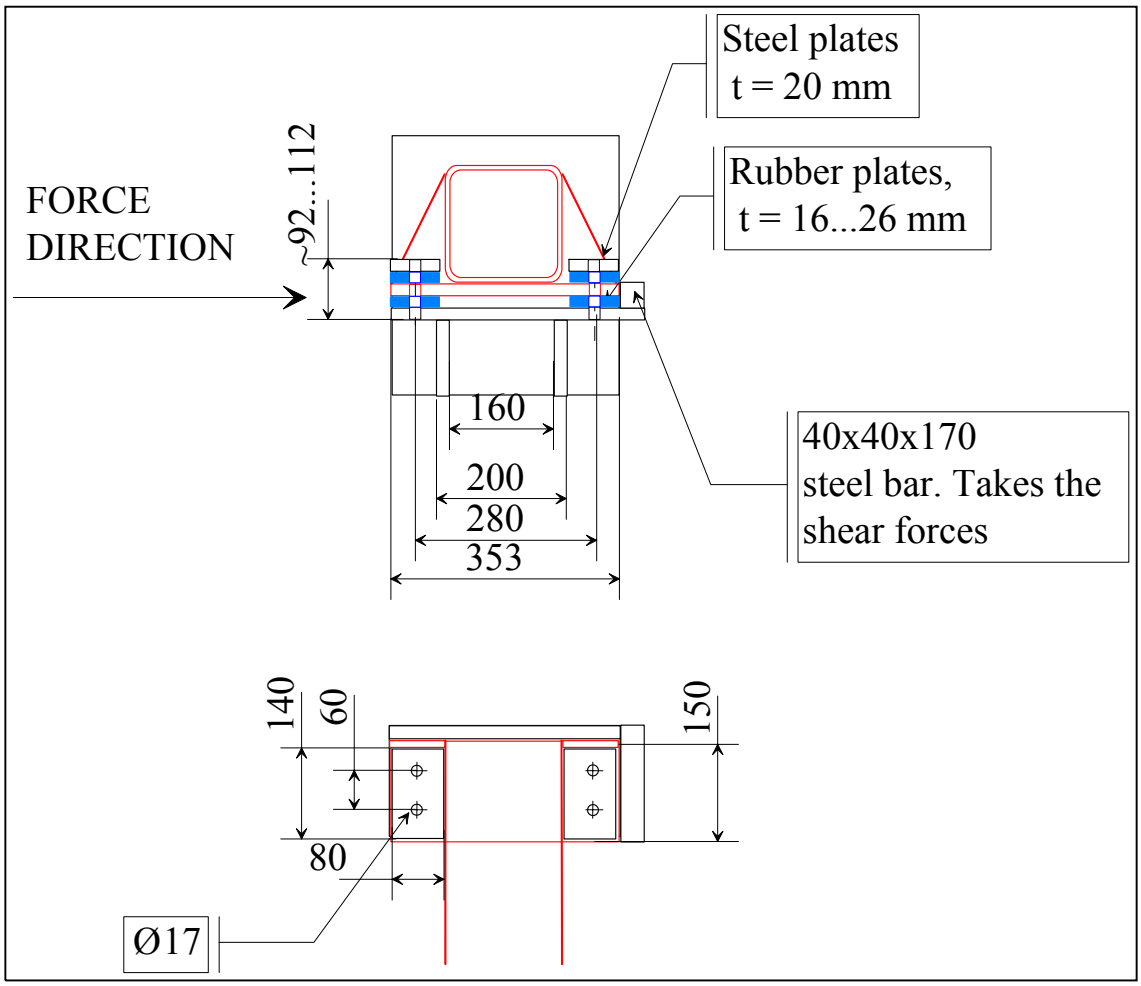

Figure 6. Torsion beam end details.

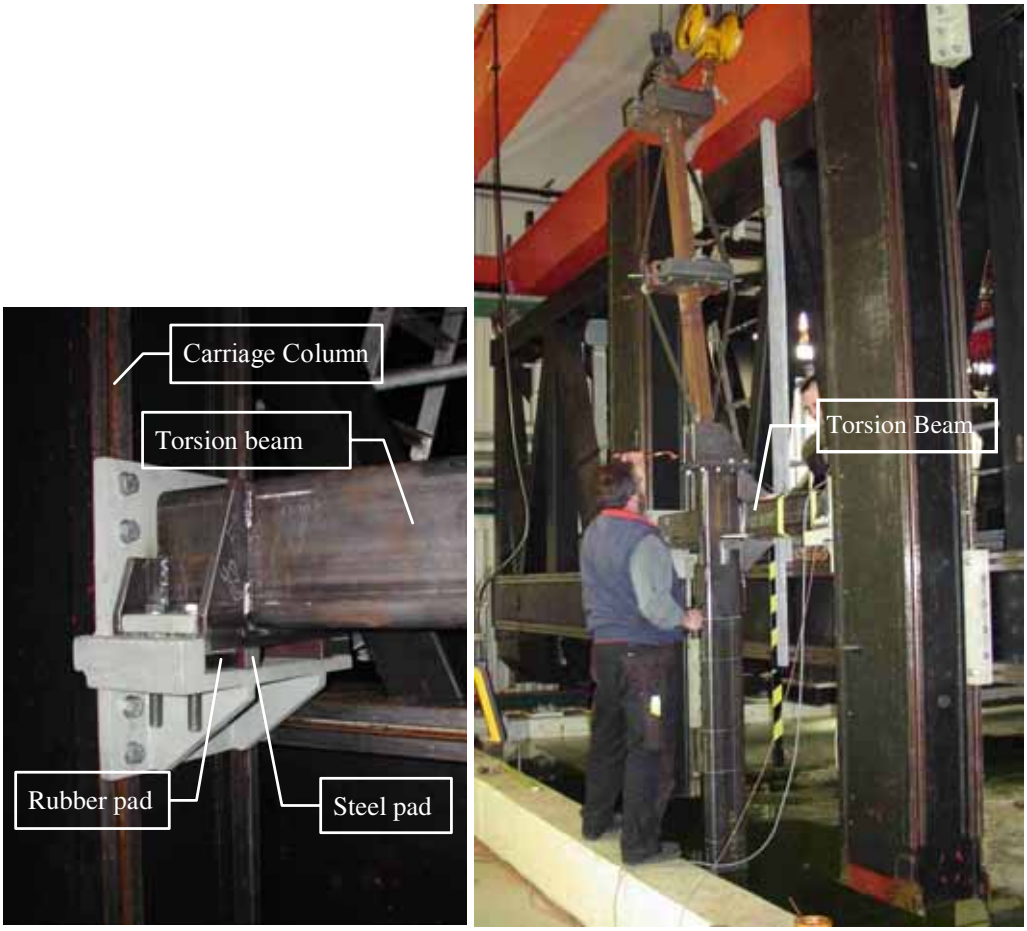

Figure 7. Structure connection to the HSVA's carriage. Klaus Niederhausen (right) tightening connection bolts between upper and lower columns.

2.2.2 Structural variants

The structure was modified before each test to achieve desired stiffness and dynamical properties. Before actual tests, stiffness and eigenfrequences were experimentally determined by calibration tests.

Ice-level stiffness modification was based on the rotational stiffness of the torsion beam and vertical location of the structure (distance *H* and *h* in Figure 2). Rotational stiffness of the torsional beam was modified by using rubber springs between the beam end and the carriage as show in Figures 6 and 7. The rubber material was a mixture of natural rubber (NR) and Styrene-Butadiene (SBR). The indentation hardness of the rubber was 60. Steel plates of 3 mm thickness were glued on the top and the bottom sides of the rubber plate to ensure designed behaviour of the rubber springs. The dimensions of the spring are shown in Figure 8. The stiffness and damping properties of the spring were measured (see Sect. 2.5). Steel pads were used instead of rubber springs when structure stiffness was set to maximum.

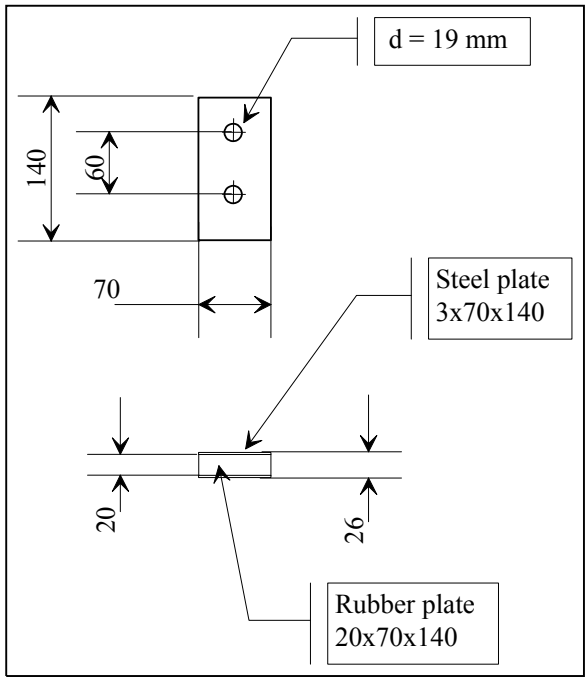

Figure 8. Rubber spring dimensions.

Table 1. Description of the structural variants. Parameter h shown in Figure 2.

Variant	*h* (m)	Description
SV1	1.60	The basic structure (Figs 4–9). Rubber springs active, No tension bars.
SV2	1.60	The same as SV1 but tension bars active in the loading direction.
SV3	1.60	Rubber springs were made inactive using steel pads as shown in Figure 7. No tension bars.
SV5	1.60	Rubber springs not active. All tension bars active. The upper part of the structure had an additional tie to increase the structural stiffness in the loading direction. The tie is shown in Figure 10.
SV6	1.60	The same as SV5 but the vertical tie is removed. (NOTE: A weld in the end of the torsional beam was damaged during a test).
SV6B	1.60	The same as SV6 after re-welding the damaged connection.
SV7	1.05	The variant SV6B was changed by installing three additional weights á 15 kg on top of the structure. The rubber springs were activated.
SV8	1.05	The same as SV7, but the torsion beam was welded directly to the consoles of the carriage columns (no rubber springs).

Two kinds of tension bars were used in the tests. The bars shown in Figure 10 (right) were used to stiffen up the upper column in the loading direction and to rise the value of second eigenmode. The tension bars shown in Figure 10 (left) were used to prevent sideward vibration of the upper column. An additional vertical tie (Figure 10 (left)) was used in some tests (SV5) to increase the structure's stiffness in the loading direction. Table 1 shows the notations and descriptions for different structural variants that were used.

A friction damper was used in some of the tests. The damper was located on the top of the structure as shown in Figure 9. Damping forces were experimentally measured by HBM U9B load cell. Two spring loaded screws were used to adjust the damping force.

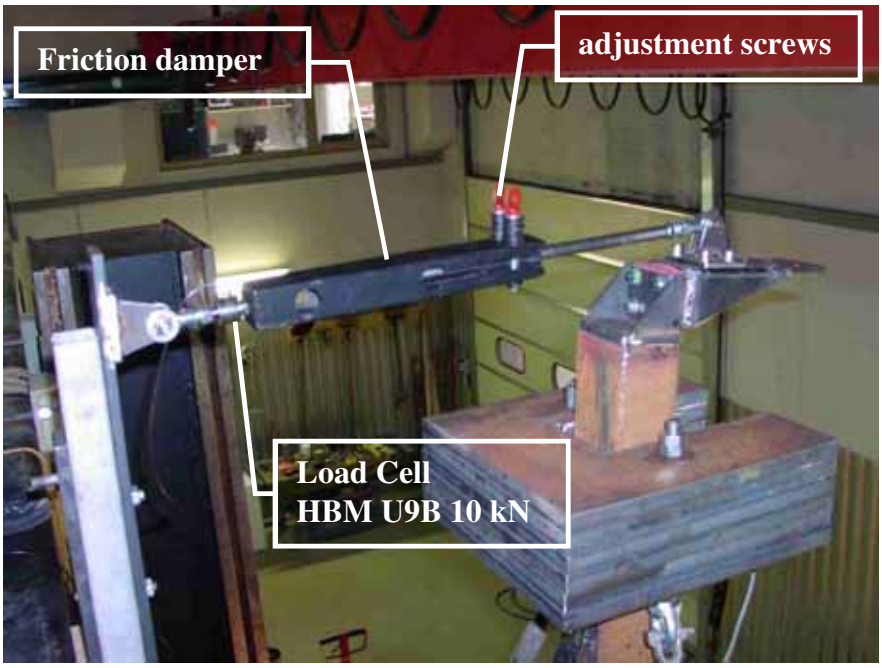

Figure 9. Friction damper on the top of the structure.

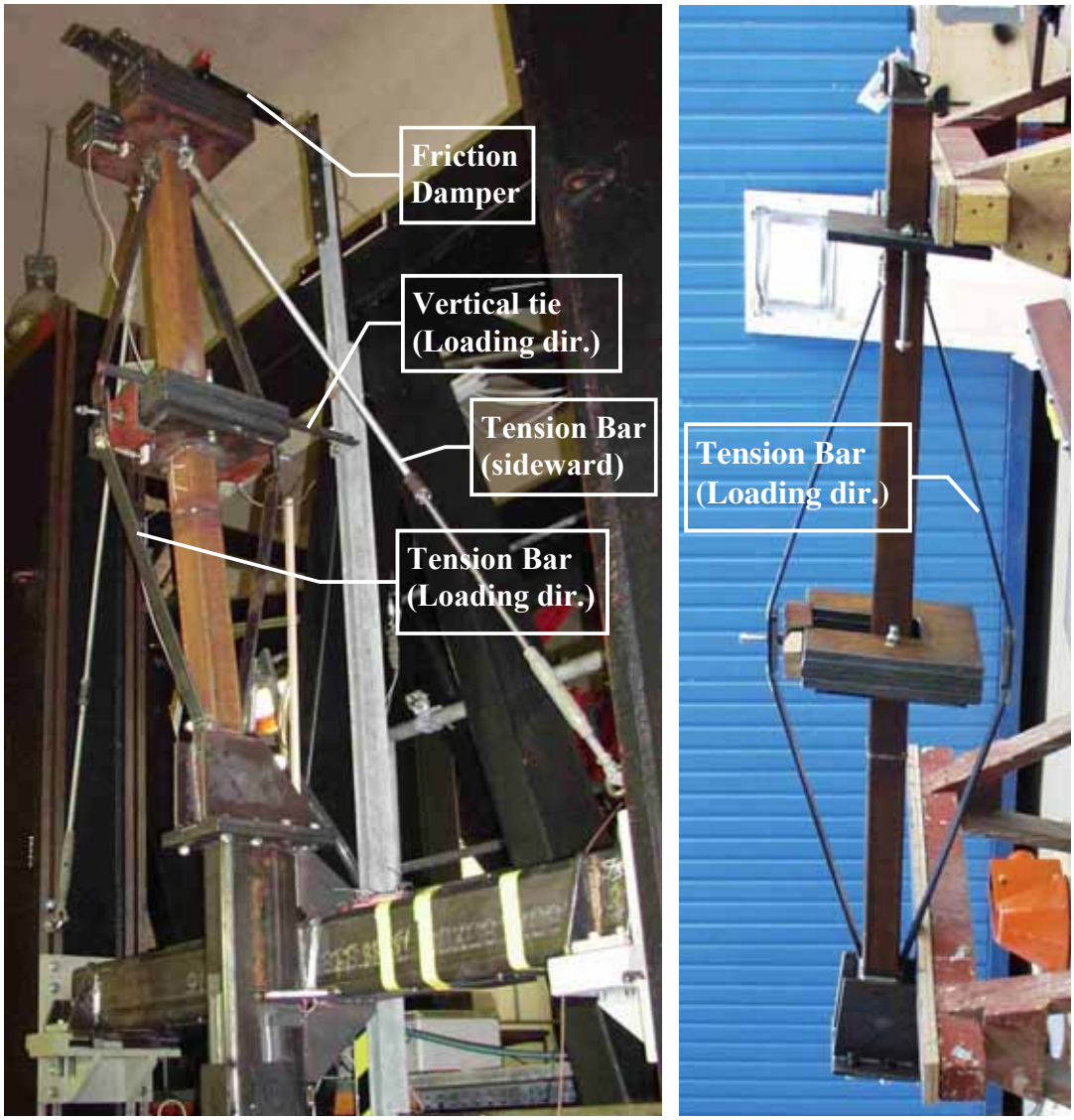

Figure 10. Upper column of the structure with all the tension bars and the vertical tie (left). Upper column tension bars under construction (right).

2.2.3 Numerical modal analysis

The structural stiffness, eigenfrequences and eigenmodes were numerically determined before manufacturing the structure. ABAQUS 6.2-1 and EMRC NISA II Finite element programs were used in the analysis. The structure was modelled using both shell and beam elements. According to the numerical analyses the beam model results were as reliable as the results given by the shell model. Figure 11 shows the 2nd eigenmode of a structural alternative when shell elements were used in the modelling.

The first 4 eigenmodes are shown in Figure 12 and the eigenfrequences in Table 2. Deflections in modes 1 and 3 were in sideward direction while modes 2 and 4 were

vibrating in loading direction. The rubber spring stiffness was assumed to be 10^{12} N/m, elastic modulus for the steel structure was set to 210 GPa and Poisson's ratio was 0,3. Static stiffness was found to be 1.05 kN/mm, when a concentrated force was acting on the lower end of the column (Fig. 13).

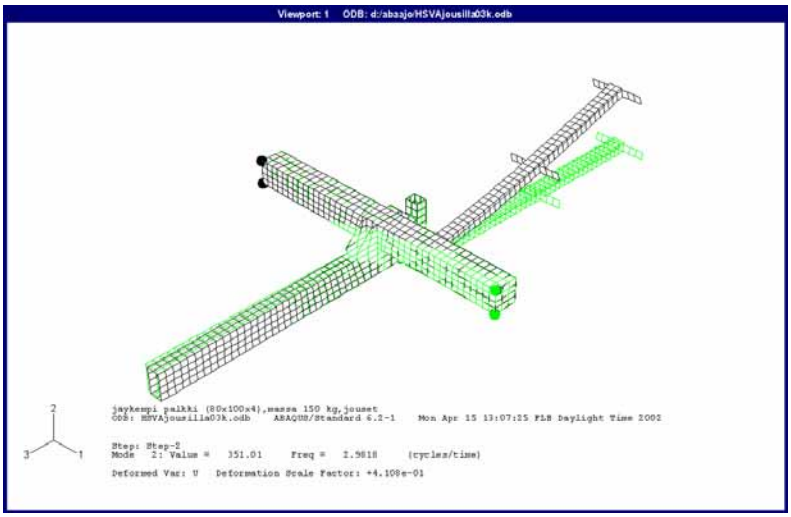

Figure 11. Second eigenmode for one of the structure alternative.

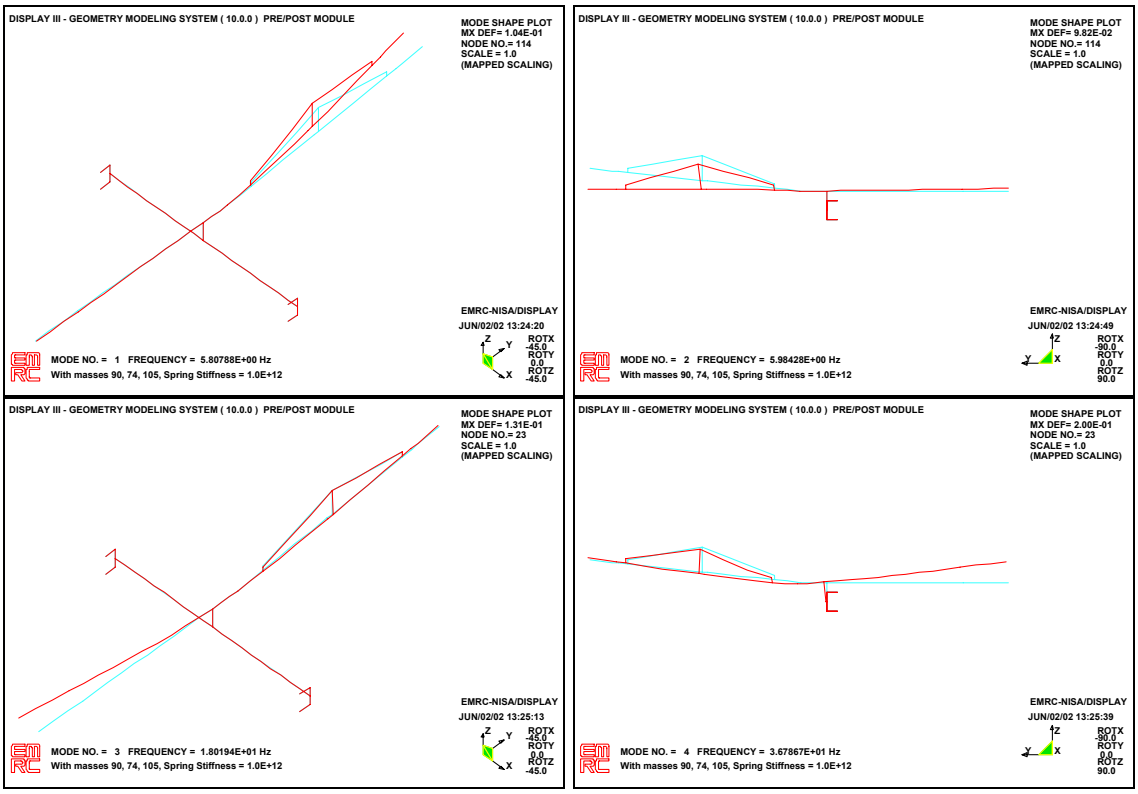

Figure 12. The first 4 Eigenmodes for the test structure.

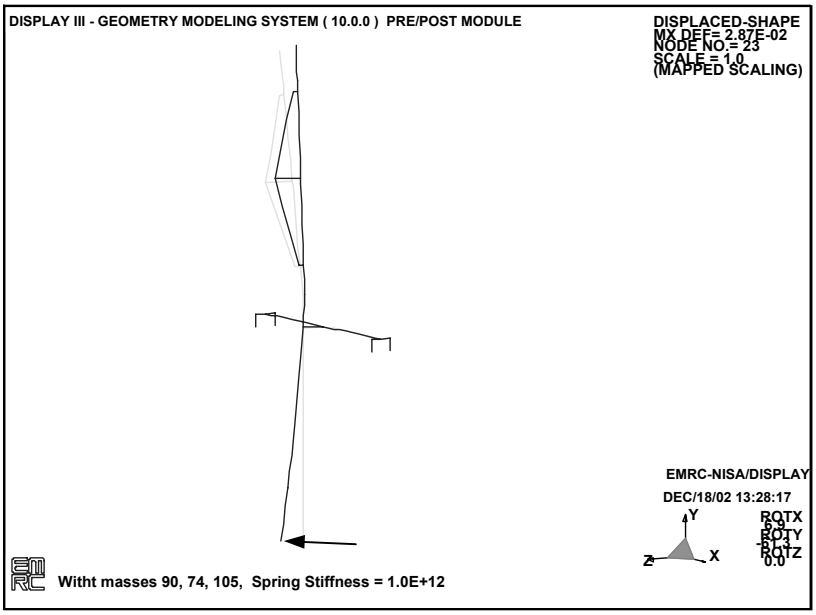

Figure 13. Column deflection in static loadig.

Table 2. Eigenfrequences (FEM).

Mode	Frequency, Hz	Remark
1	5,81	Sideward direction, tension bar inactive
2	5,98	Loading direction, tension bar active
3	18,0	Sideward direction, tension bar inactive
4	36,8	Loading direction, tension bar active

2.2.4 Indentors

Three different types of indentors were prepared for the tests; cylindrical, conical and inclined cylindrical (Figs 14 and 15). All indentors were made of steel. Indentors were fixed to the column by M10 bolts so that the position of an indentor was adjustable (*h* in Figure 2). Detailed indentor drawings are shown in Figures 16–18. The diameter of cylindrical indentor was 114 m. The angle of inclination was 30 degrees for the conical indentor.

Figure 14. Cylindrical and conical indentors.

Figure 15. Inclined cylindrical indentor.

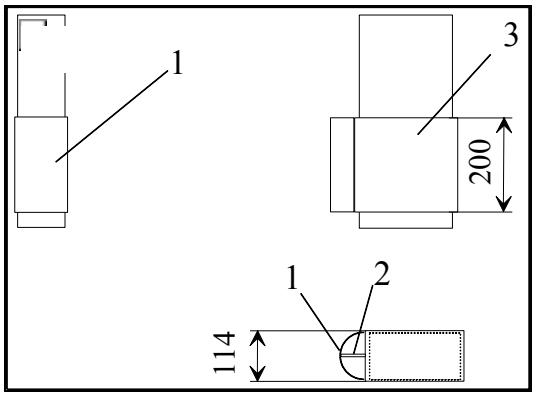

Figure 16. Cylindrical indentor drawing.

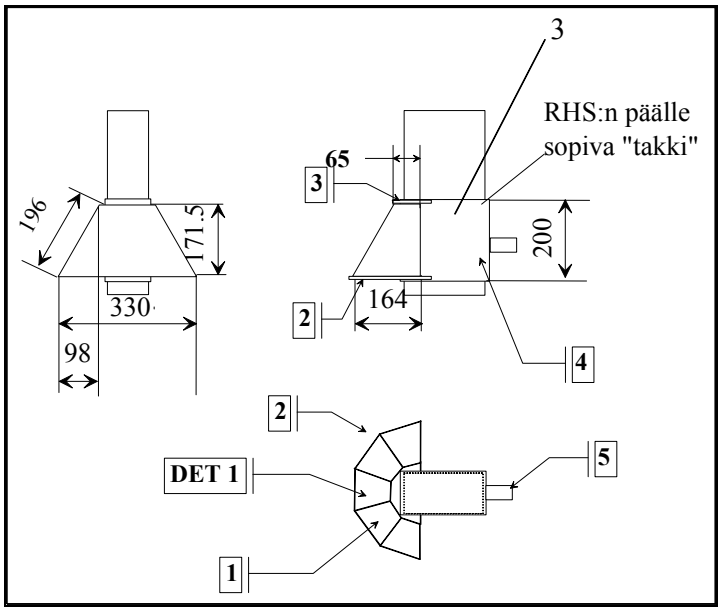

Figure 17. Conical indentor drawing.

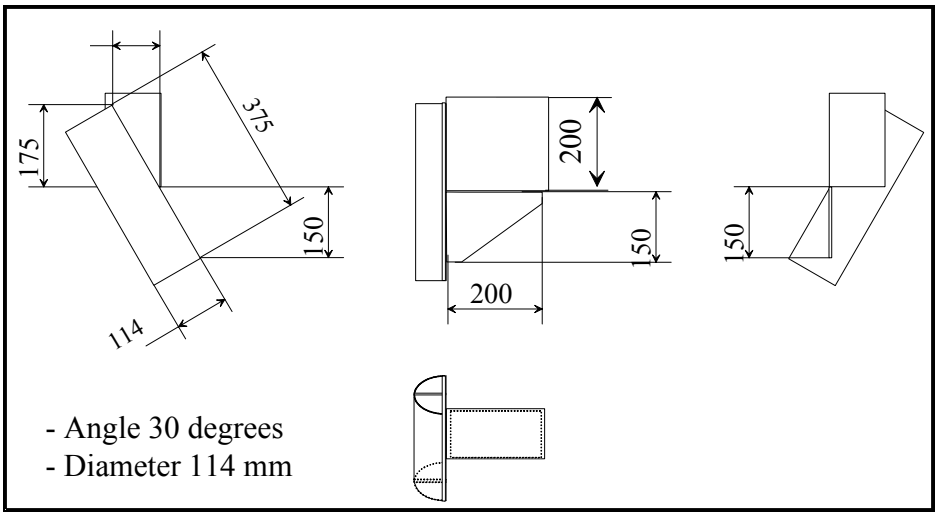

Figure 18. Inclined cylindrical indentor drawing.

2.3 Measuring equipment

Direct measurement of the ice force not feasible because the indentor had to be moved while changing the length parameter *h*. Therefore, ice force measurements were done indirectly. Bending, torsion and shear strains were measured for stress calculation. Accelerations and displacements were measured for displacement and dynamical state calculations. Damping forces were measured, when the friction damper was active. The measurement set-up is shown in Figures 19 and 20.

2.3.1 Force measurements

The damping force was measured using a "HBM U9B" load cell when the damper was active. Ice forces were measured indirectly by strain gauges (Fig. 18). Load measurement included the use of up to four electrical resistance strain gauge full bridges. These were arranged to measure the applied load through beam bending, shear and torsion. Each of the strain gauge measuring channels contained a full Wheatstone bridge with all the four bridge element being formed by active strain gauges attached on the specimen.

Strain gauges were Kyowan type. The bending gauges were composed of 4 single uniaxial gauges while torsion and shear gauge groups composed of two element rectangular rosette gauges. The k-values were 2,1 for single gauges and 2,14 for two element rectangular rosette gauges.

Calibration tests were done before each test series.

2.3.2 Displacement measurements

Displacements were measured using two Laser Distance Sensors (Micro Epsilon Type LD 1605-100). The sensors were installed to measure deflection of the lower column. The actual distance between the sensors was 500 mm. The set-up is shown in Figures 19 and 22. The distance D in Figure 20 was proportional to the vertical position of the test structure. The height positions z_{D1} and z_{D2} of the displacement sensors are shown subsequently in Table 5.

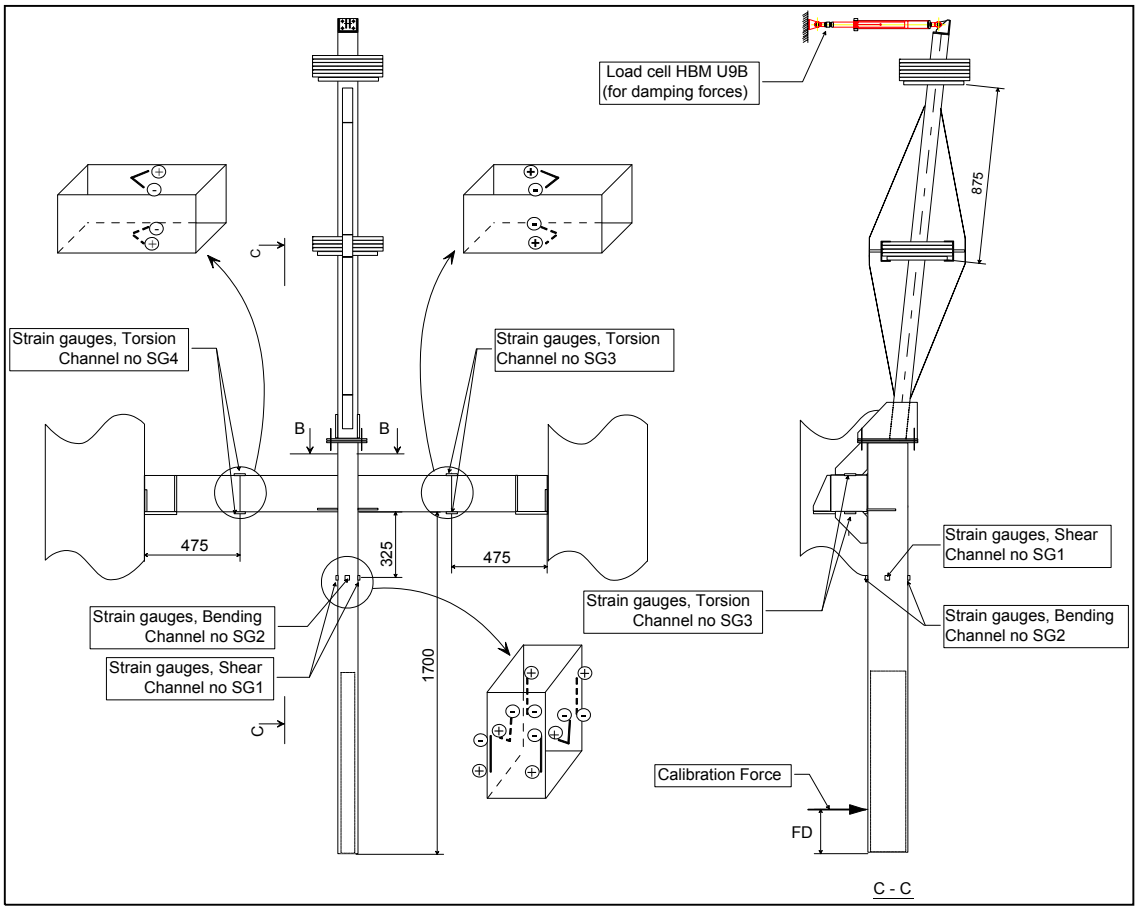

Figure 19. Force and strain measurement set-up.

2.3.3 Accelerations

Accelerations were measured using 4 HBM B12/500 sensors. The locations of the accelerometers are indicated in Figures 20, 21 and 22. Accelerometers 1 and 2 were installed into the lower column (Fig. 22). The exact height positions z_{a1} and z_{a2} of these two sensors are shown subsequently in Table 5.

Accelerometers 3 and 4 were installed below the two masses of the upper column. The accelerometer 1 was on the opposite side of the lower column during modal tests. In some of the tests also carriage accelerations were measured using sensors nearby torsion beam ends as shown in Figure 23. Accelerations were measured only into the direction parallel with loading direction, except in calibration tests where accelerometer 1 was rotated 90 degrees to measure sideway vibration also.

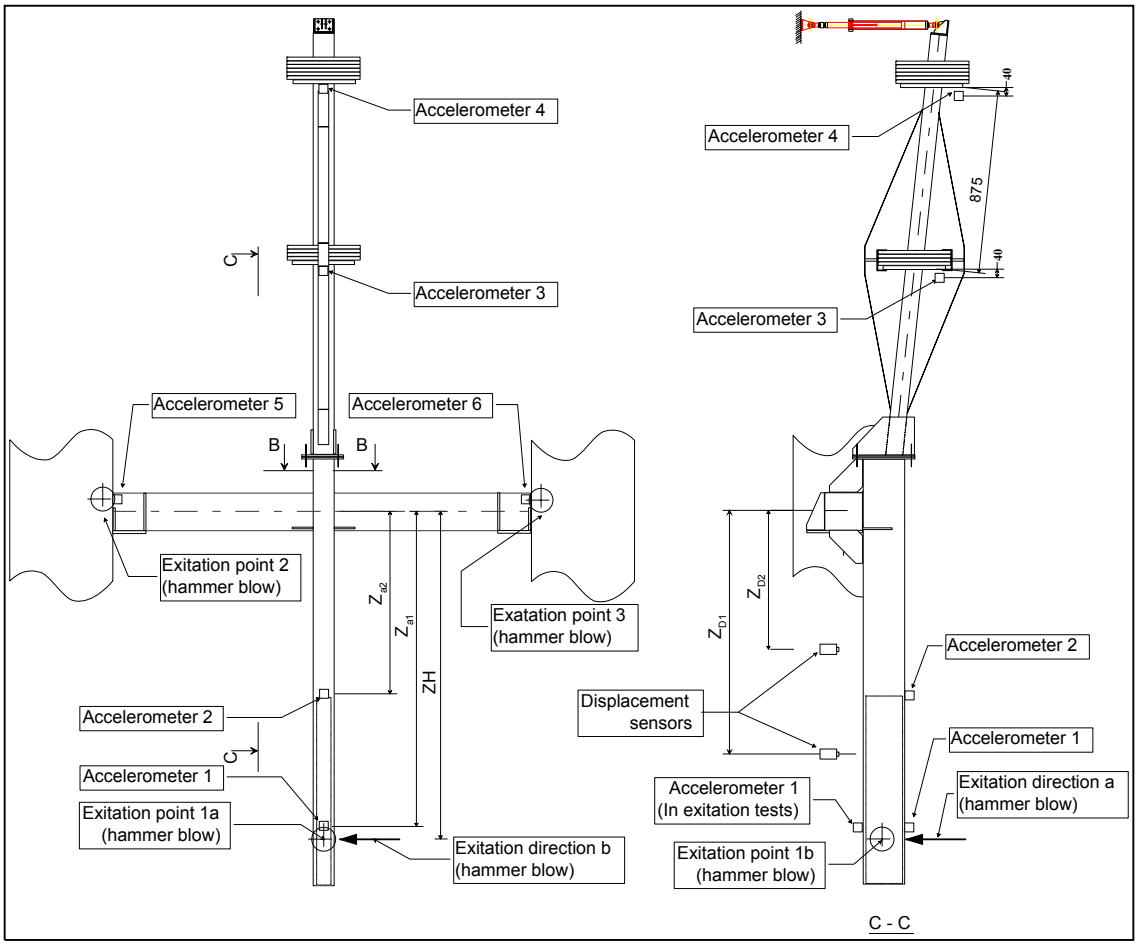

Figure 20. Displacement and acceleration measurement set-up.

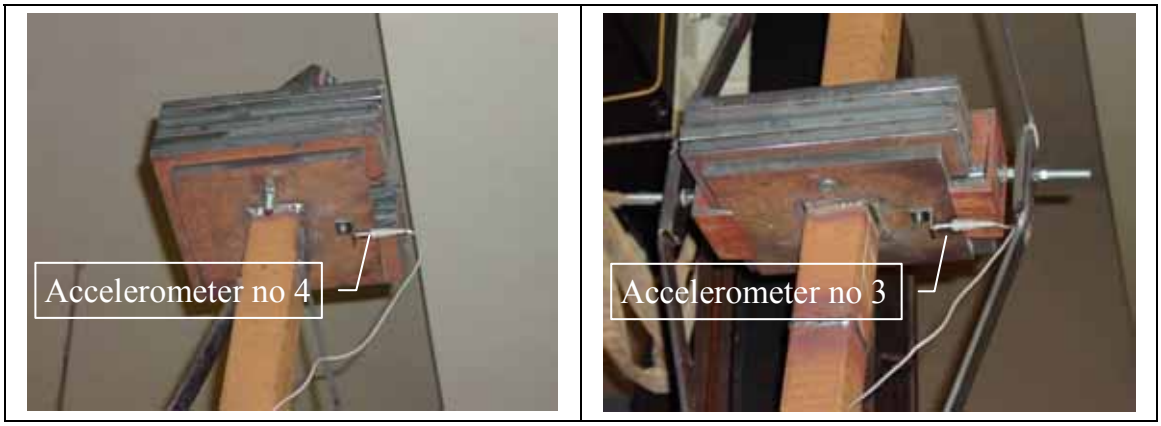

Figure 21. The 3rd and 4th accelerometers.

Figure 22. The 1st and 2nd accelerometers, displacement sensors and video camera.

2.3.4 Carriage measurements

Test carriage position and speed were measured during each test using the permanent facilities of the carriage.

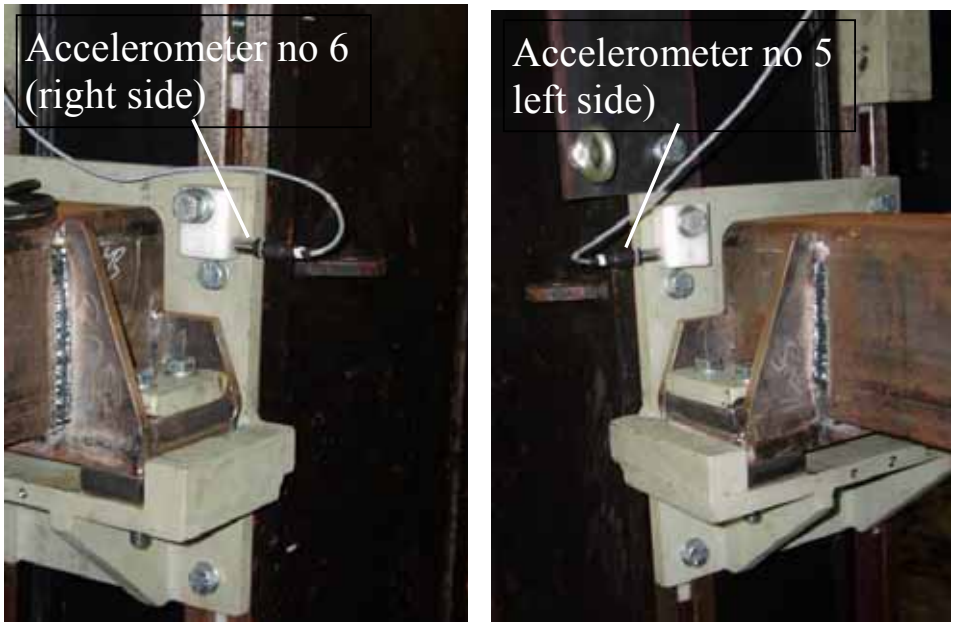

Figure 23. Carriage column acceleration measurement sensor, located at the torsion beam ends.

2.3.5 Data acquisition

The data was collected using a Spider 8 PC measurement system. Each unit of this system consists of eight carrier amplifiers. In maximum, eight units can be cascaded to a maximum of 64 channels. The carrier frequency is 4.8 kHz. The sampling frequency range is from 1 Hz to 9600 Hz. Digital filters are build in. Data was transferred via a parallel interface to the connected PC.

In the tests at moderate or high carriage velocities (v>0.08 m/s), the sampling frequency was set to 1200 Hz and the low-pass filter at 150 Hz. When the carriage velocity was lower the sampling frequency was either 600 Hz or 300 Hz while the low-pass filter was set correspondingly at 75 Hz or 40 Hz.

2.4 Visual observations

All the test runs were recorded using video cameras and digital cameras. One conventional VHS camera was attached to the carriage beam above the indentor so that the indentor behaviour and ice failure could be recorded (see Fig. 22). Freehand digital video and still cameras were used also.

Compressed air was used to blow crushed ice away in front of the indentor as shown in Figure 24.

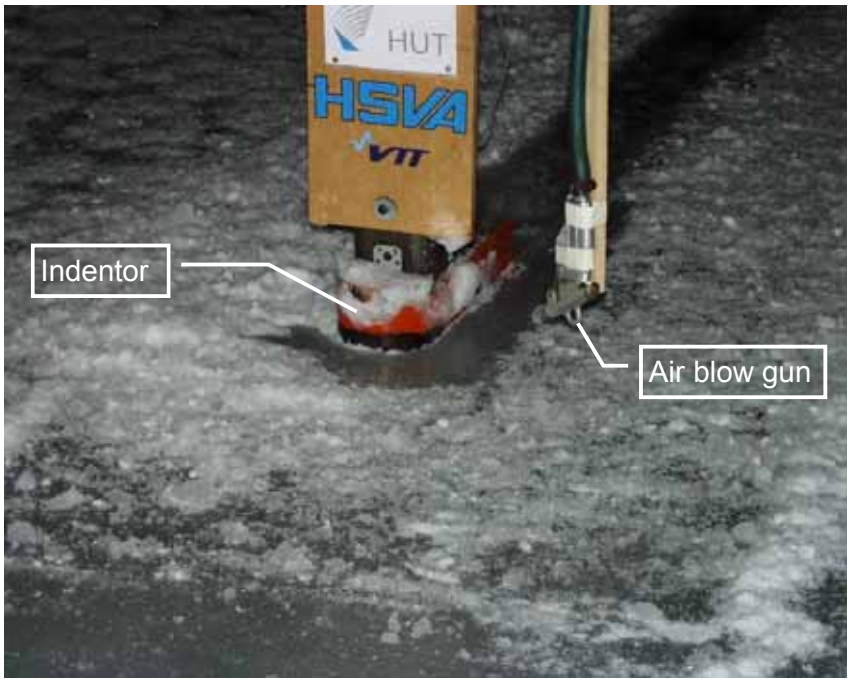

Figure 24. Test set-up for blowing cruched ice away.

2.5 Calibration methods

Calibration tests were done before each test series. The main aim of the force calibration tests was to find calibration factors for bending, shear and torsion force measurement channels. Also, dynamic calibration tests were performed before each test series using hammer blow excitation. These tests were done to measure the eigenfrequences and the structural damping of the tests structure.

Force calibration tests were performed using hydraulic jack for pulling the lower column end. The test set-up is shown in Figure 25. The calibration force was measured using a load cell between the steel frame and a rope as shown in Figure 25. Loads up to 30 kN were applied in this kind of calibration.

In dynamic calibration tests the structure was exited by a hammer blow. The excitation points are shown in Figure 20. All structural variants were exited by hammer blow into the lower column end (point 1). Some of the structural variants were also exited via points 2 and 3 where the test structure was fixed to the carriage. At the point 1, the structure was exited both in the main direction of ice loading and in the transverse direction. These directions are indicated in Figure 20 as *a* and *b* respectively. When the excitation was done in the transverse direction b, the accelerometer No 1 was rotated 90 degrees to measure accelerations in the transverse direction.

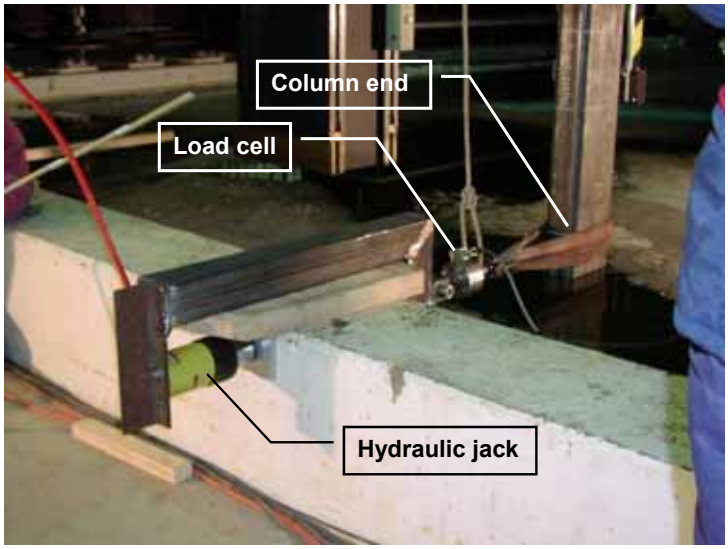

Figure 25. Force calibration test set-up.

Figure 26. Hammer blow excitation in direction "a" by Bi Xiangjun.

2.5.1 Force calibration before installation

The first calibration tests were done by VTT in Finland before the test structure was shipped to HSVA. The test set-up is shown in Figure 27. The end displacements and rotations of the torsion beam were restrained. The lower column was loaded with a point load using a variable bending arm. The objective of these calibration tests was to find calibration factors for the channels measuring bending-, shear- and torsion forces.

The shear force-measuring group was shown to be dependent on bending arm length. This was an unexpected results. Calibration factors are shown in Table 3.

Table 3. Calibration factors for VTT calibration tests.

Channel	mV/V	Factor
Shear SG1, position 1	1	-454,55 kN
Shear SG1, position 2	1	-285,71 kN
Shear SG1, position 3	1	-188,68 kN
Bending SG2, all positions	1	-22,94 kNm
Torsion SG3, all positions	1	-123,46 kNm
Torsion SG4, all positions	1	-114,94 kNm

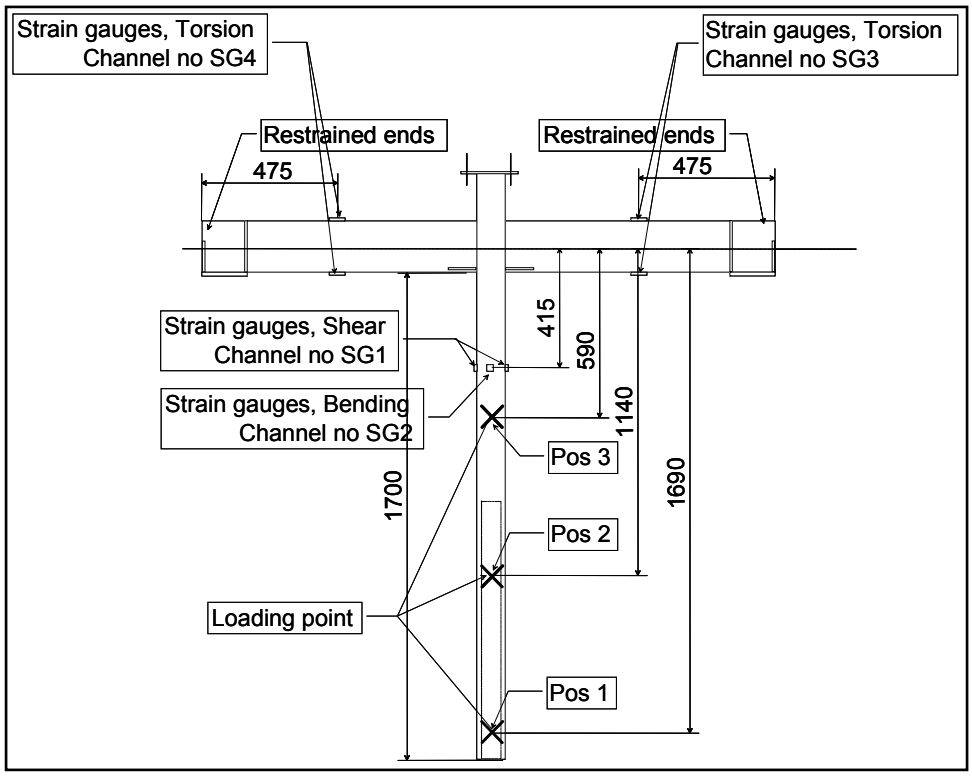

Figure 27. Test set-up for VTT calibration. Positions of strain gauges and loads.

2.5.2 Calibration tests on structural variants

The structure was varied between each test series. The variables were the following:

- Ice level distance from torsion beam (variable *h* in Figure 2)
- Tension bars and the lateral tie (active or inactive, see Figure 10)
- Stiffness of the springs at the ands of the torsion beam (Figs 6 and 7).

Force and dynamic calibration test were done before each test series or immediately afterwards. The results of mechanical calibration tests are shown in Table 4.

Table 4 shoes the positions of the accelerometers and displacement transducers for each structural variant. Selected results of the impact tests are shown in Table 6, as analysed during the test campaign. Further results can be obtained by a further analysis of the original data files.

Table 4. Calibration factors for each mechanical calibration tests.

Calibration file	SG1, kN	SG2, kN	SG3, kNm	SG4, kNm	FL[1)], mm
SG_02_05_17_15_27_mech	-444.196	-19.978	-41.324	-39.648	1620
SG_02_05_17_15_56_mech	-453.480	-19.581	-40.640	-39.597	1620
SG_02_05_17_20_30_mech_SV3	-444.603	-19.716	-38.177	-41.584	1620
SG_02_05_22_18_04_mech_SV5	-506.316	-17.778	-46.847	-51.055	1740
SG_02_05_27_14_33_mech_SV6	-402.017	-20.359	-47.330	-37.045	1570
SG_02_05_28_19_45_mech_SV6b	-415.944	-20.310	-40.465	-42.350	1570
SG_02_05_30_15_25_mech_SV7	-268.947	-40.899	-62.384	-72.282	890
SG_02_06_04_14_58_mech_SV8	-266.840	-41.269	-65.065	-69.706	990

[1)] FL is the distance of the loading point from neutral axis of the torsion beam

Table 5. Positions of the sensors (see Fig. 20).

Structure	z_H mm	z_{a1} mm	z_{a2} mm	z_{D1} mm	z_{D2} mm
SV3	1490	1475	935	752	1255
SV5	1490	1475	345	1255	752
SV6	1490	1505	995	1255	752
SV6B	1490	1505	995	1255	752
SV7	950	950	365	-	645
SV8	950	950	365	-	645

Table 6. Results of the impact tests.

Structure	f_1, *Hz*	ξ_1	f_2, *Hz*	ξ_2
SV3	6.6	0.05	18.4	0.04
SV6	6		18	
SV7	5.3	0.12	15.1	0.08
SV8	6.7	0.007	17.2	0.02

3. Ice

Sheets of columnar grained ice were grown in the ice basin from a water that had a salinity of 9.1 ppt. The whole water solution was first cooled to about -0.2 ^{o}C. When the water surface froze the ice was skimmed twice and the water was then seeded by spraying. After this, the growth of a columnar grained ice started at a rate of 18 mm/h to 20 mm/h at a room temperature of -20 ^{o}C. The salinity of the newly formed ice was about 4 ppt.

First tentative tests were done on 22.05.2002 when the first ice sheet had reached a target thickness of 40 mm. It was found that the ice was too weak. The reason for this problem was studied. It was found that a saline ice contains immediately after the freezing process about 30 % water that weakens the ice. The ice will achieve a state of equilibrium later on when this additional water is fully frozen. Therefore, the target thickness for the ice sheets was raised to 80 mm. The subsequent experience showed that ice sheets that had a thickness of 80 mm to 90 mm were strong enough for the tests.

Three ice sheets were used in the tests. The strength of the ice sheet was studied by making uniaxial compressive tests and bending tests (Fig. 28).

Figure 28. Uniaxial compressive test.

Appendix A shows the results of the compressive tests. Bending tests were also made to further characterize the ice. Appendix B shows the results of the bending tests.

4. Test programme

Several parameters were varied in the test. Most of the tests were done using the cylindrical indentor (Figs 14 and 16). The faceted cone depicted in Figures 14 and 17 was also used in one series of tests. The inclined cylindrical indetor (Fig. 15) was used only in preliminary tests. The main variables in these tests were the mean velocity of ice penetration and the structural variant. Table 1 provides a description of the structural variants. The height position (parameter *h*, Fig. 1) was also varied.

Three ice sheets were used in the actual tests that were conducted between 24.05.2002 and 06.06.2003. Tables 7 to 12 show details of the parametric variations in different tests. In these tables, h_{ice} is the ice thickness and *v* is the nominal velocity.

Table 7. Tests with the structural variant SV5 and the vertical cylindrical indentor (V). The damper was in use.

Test	Date	Sheet No	h_{ice} (mm)	*h* (m)	*v* (mm/s)
SV5V02	24.05.2002	1	92...93	1.60	3
SV5V05(2)	24.05.2002	1	92...93	1.60	5
SV5V10	24.05.2002	1	92...93	1.60	10
SV5V20	24.05.2002	1	92...93	1.60	20
SV5V40	24.05.2002	1	92...93	1.60	40
SV5V50PR(1)	24.05.2002	1	92...93	1.60	50
SV5V60	24.05.2002	1	92...93	1.60	60
SV5V80	24.05.2002	1	92...93	1.60	80
SV5V100PR	24.05.2002	1	92...93	1.60	100
SV5V150	24.05.2002	1	92...93	1.60	150
SV5V200PR	24.05.2002	1	92...93	1.60	200
SV5V500	24.05.2002	1	92...93	1.60	500

(1) PR = Preliminary tests ; (2) The damper became ineffecive during this test

Table 8. Tests with the structural variant SV6 and the vertical cylindrical indentor (V).

Test	Date	Sheet No	h_{ice} (mm)	*h* (m)	*v* (mm/s)
SV6V05	24.05.2002	1	94...97	1.60	5
SV6V10	24.05.2002	1	94...97	1.60	10
SV6V20	24.05.2002	1	94...97	1.60	20
SV6V40	24.05.2002	1	97	1.60	40
SV6V60	24.05.2002	1	94...97	1.60	60
SV6V80	24.05.2002	1	94...97	1.60	80
SV6V100	24.05.2002	1	94...97	1.60	150
SV6V150	24.05.2002	1	94...97	1.60	150
SV6V200	24.05.2002	1	94...97	1.60	200
SV6V500	24.05.2002	1	94...97	1.60	500

Table 9. Tests with the structural variant SV6B and the vertical cylindrical indentor (V).

Test	Date	Sheet No	h_{ice} (mm)	h (m)	v (mm/s)
SV6BV100	29.05.2002	2	77	1.60	100
SV6BV150	29.05.2002	2		1.60	150
SV6BV200	29.05.2002	2	80	1.60	200
SV6BV250	29.05.2002	2	76	1.60	250
SV6BV300	29.05.2002	2		1.60	300
SV6BV350	29.05.2002	2	77	1.60	350
SV6BV400	29.05.2002	2	77	1.60	400
SV6BV450	29.05.2002	2		1.60	450
SV6BV500	29.05.2002	2		1.60	500
SV6BV600	29.05.2002	2	79	1.60	600
SV6BV_SW1	29.05.2002	2		1.60	50...100 (2)
SV6BV_SW2(1)	29.05.2002	2	80	1.60	95
SV6BV_SW2	29.05.2002	2	82	1.60	80...180(3)

(1) The damper was used by increasing the damping force from zero to a maximum
(2) The velocity was varied in steps from 50 mm/s to 100 mm/s
(3) The velocity was varied in steps from 80 mm/s to 180 mm/s

Table 10. Tests with the structural variant SV7 and the vertical cylindrical indentor (V).

Test	Date	Sheet No	h_{ice} (mm)	h (m)	v (mm/s)
SV7V_AP1(1)	30.05.2002	2		1.05	50...250
SV7V_AP2(1)	30.05.2002	2		1.05	200...700
SV7V_SW1	30.05.2002	2	98	1.05	50...150
SV7V_SW2	30.05.2002	2	95...98	1.05	170...250
SV7V_SW3	30.05.2002	2		1.05	275, 300
SV7V_SW4	30.05.2002	2	95	1.05	400, 500
SV7V_SW5	30.05.2002	2	98	1.05	200, 220, 240
SV7V_SW6	30.05.2002	2		1.05	10...50

(1) Two "Approach" tests were done by driving the structure in the partially refrozen channel produced in the previous tests, one day before

Table 11. Tests with the structural variant SV8 and the vertical cylindrical indentor (V).

Test	Date	Sheet No	h_{ice} (mm)	h (m)	v (mm/s)
SV8V_SW1	05.06.2002	3	73	1.05	3, 8, 13, 17
SV8V_SW2	05.06.2002	3	79	1.05	18, 28, 38, 48, 58
SV8V_SW3	05.06.2002	3	81	1.05	58, 78, 98, 118, 138
SV8V_SW4	05.06.2002	3	81	1.05	138, 168, 198, 228, 257
SV8V_SW5	05.06.2002	3	80	1.05	258, 308, 358, 407, 457
SV8V_SW6	05.06.2002	3	81	1.05	456, 517, 637, 697
SV8V_SV6	05.06.2002	3	81	1.05	
SV8V_F1(2)	05.06.2002	3		1.05	
SV8V_F2(2)	05.06.2002	3		1.05	
SV8V_60(1)	05.06.2002	3		1.05	60
SV8V_F3(2)	05.06.2002	3		1.05	

(1) The damper was in use
(2) The ice fracture process was strudied at a very low indentation velocity

Table 12. Tests with the structural variant SV8 and the faceted cone (C).

Test	Date	Sheet No	h_{ice} (mm)	h (m)	v (mm/s)
SV8C_used_SW1(1)	06.06.2002	3	90...100	1.05	
Sv8C_20	06.06.2002	3	94...100	1.05	20
Sv8C_50	06.06.2002	3	85...90	1.05	50
Sv8C_100	06.06.2002	3	95...100	1.05	100
Sv8C_150	06.06.2002	3	86...90	1.05	150
Sv8C_200	06.06.2002	3	94...95	1.05	200
Sv8C_400	06.06.2002	3	90	1.05	400

(1) An "Approach" tests were done by driving the structure at an increasing velocity in the partially refrozen channel produced in the previous tests, one day before

5. Test results

Appendix C provides representative ice signals from the tests. Besides the directly measured signals, the Appendix C shows also estimated of the ice force signal. This signal was obtained indirectly from a two-degree-of-freedom model for the structure. The model was derived by applying a regression analysis on the static and calibration tests. A separate report on this method is stored with the data files.

Figures 29 to 32 show results obtained with the test structure SV6 having the two lowest natural frequencies at 7 Hz and 17 Hz. Figure 29 shows results in conditions where a cylindrical indentor was moving at a low velocity against the ice sheet. The force signal has a saw-tooth pattern, which is typical for this kind of condition. The waterline stiffness of the structure appears to be the main controlling parameter of the interaction. As the ice velocity is low, the structure follows more or less passively the displacement of the ice edge during a loading phase. A phase of transient vibrations is triggered when the ice fails. These transients influence the ice force during each loading phase.

The inertia forces of the structure start to control the interaction as the indentation velocity increases. Steady state vibrations may occur, in particular if the structural damping is low. In this test structure, the first eigenmode dominated the dynamic response in tests with medium indentation velocities (Figs 30 and 31). At high indentation velocities the second mode dominated as seen in Figure 32.

Figure 33 shows the response of the test structure SV8 in conditions where the faceted cone was used as the indentor. Comparisons with conditions where the same structure had a vertical indentor show that the cone reduced the response when the indentation velocity was smaller than about 180 mm/s. A resonant condition was found at the indentation velocity of 200 mm/s. This was caused by the particular ice failure mode that prevailed at all ice velocities while the cone was used. The grain boundaries of the columnar grained ice were weak. Therefore, the ice did not fail by a bending failure mode that is common for conical structures. Instead, sequential shear failures occurred along the grain boundaries due to the vertical load component created by the cone. The ice failure length varied between 30 mm and 40 mm for the 90 mm thick ice sheet. Figure 34 shows how a fractured piece of ice of this length extrudes upward between the indentor and the intact ice sheet. Due to this failure process, the ice force fluctuations can be characterised as a narrow band periodical force.

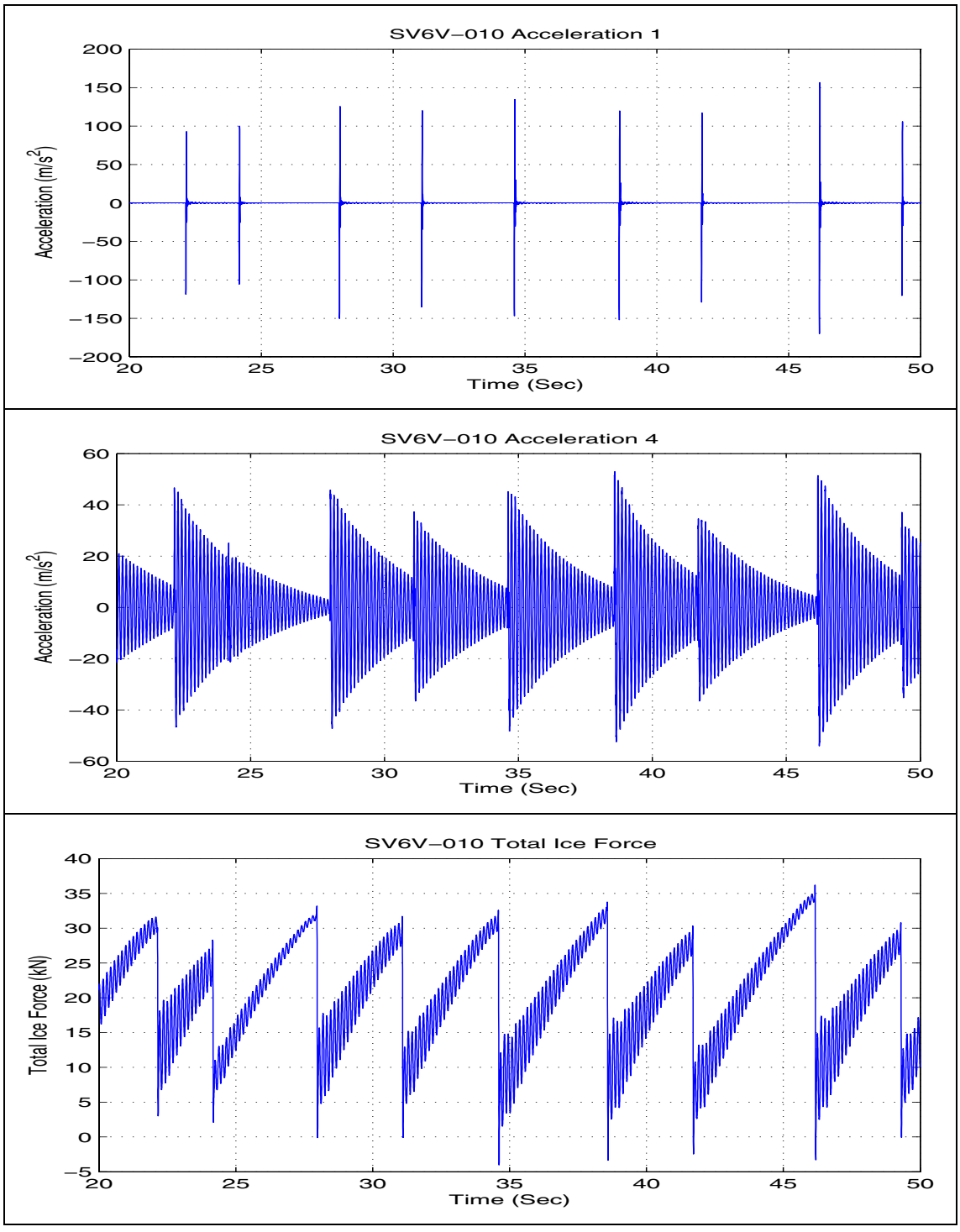

Figure 29. Measured accelerations close to the water level (Acceleration 1) and at the top of the structure (Acceleration 4) at a low indentation velocity of 10 mm/s.

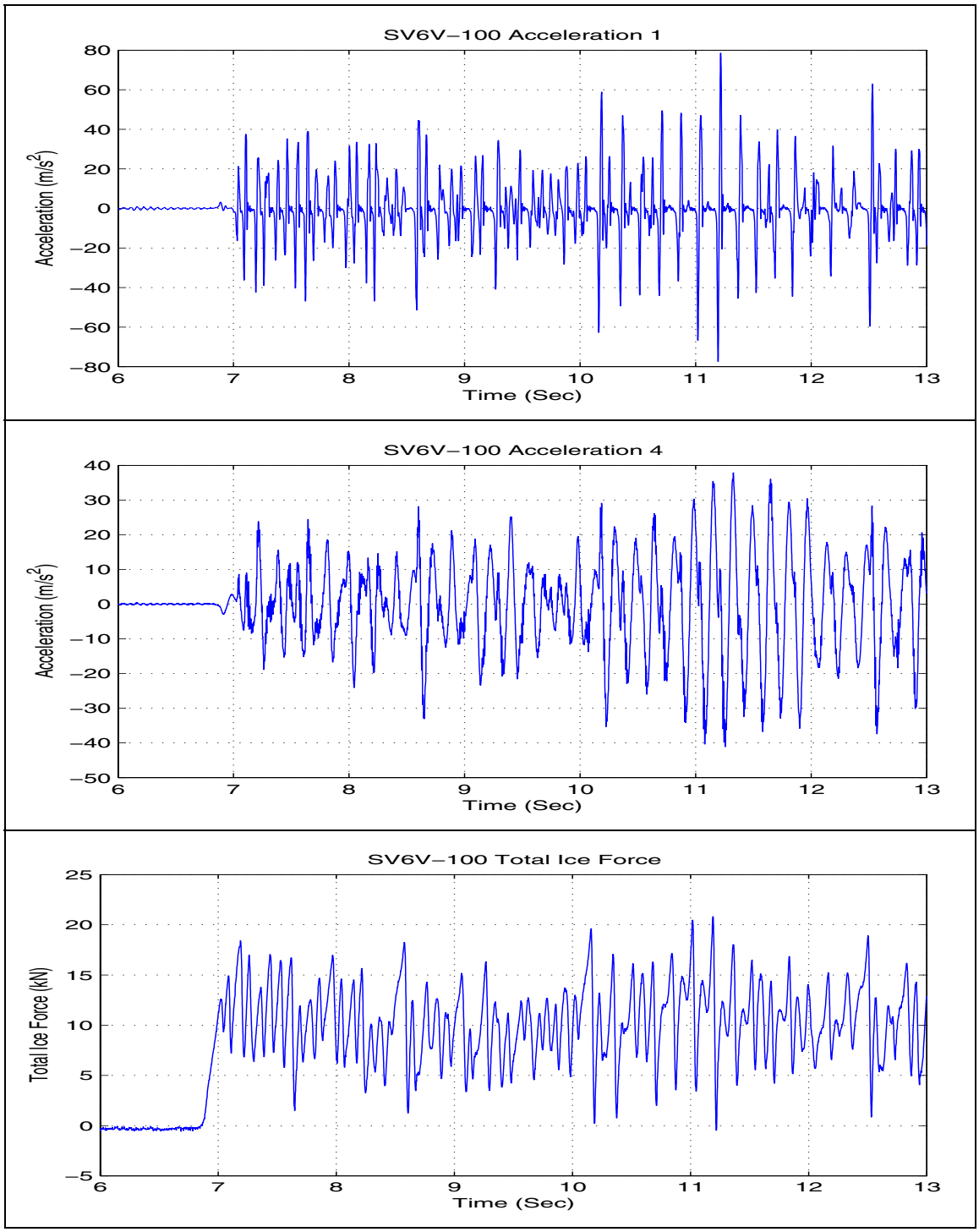

Figure 30. Measured accelerations close to the water level (Acceleration 1) and at the top of the structure (Acceleration 4) at a medium indentation velocity of 100 mm/s.

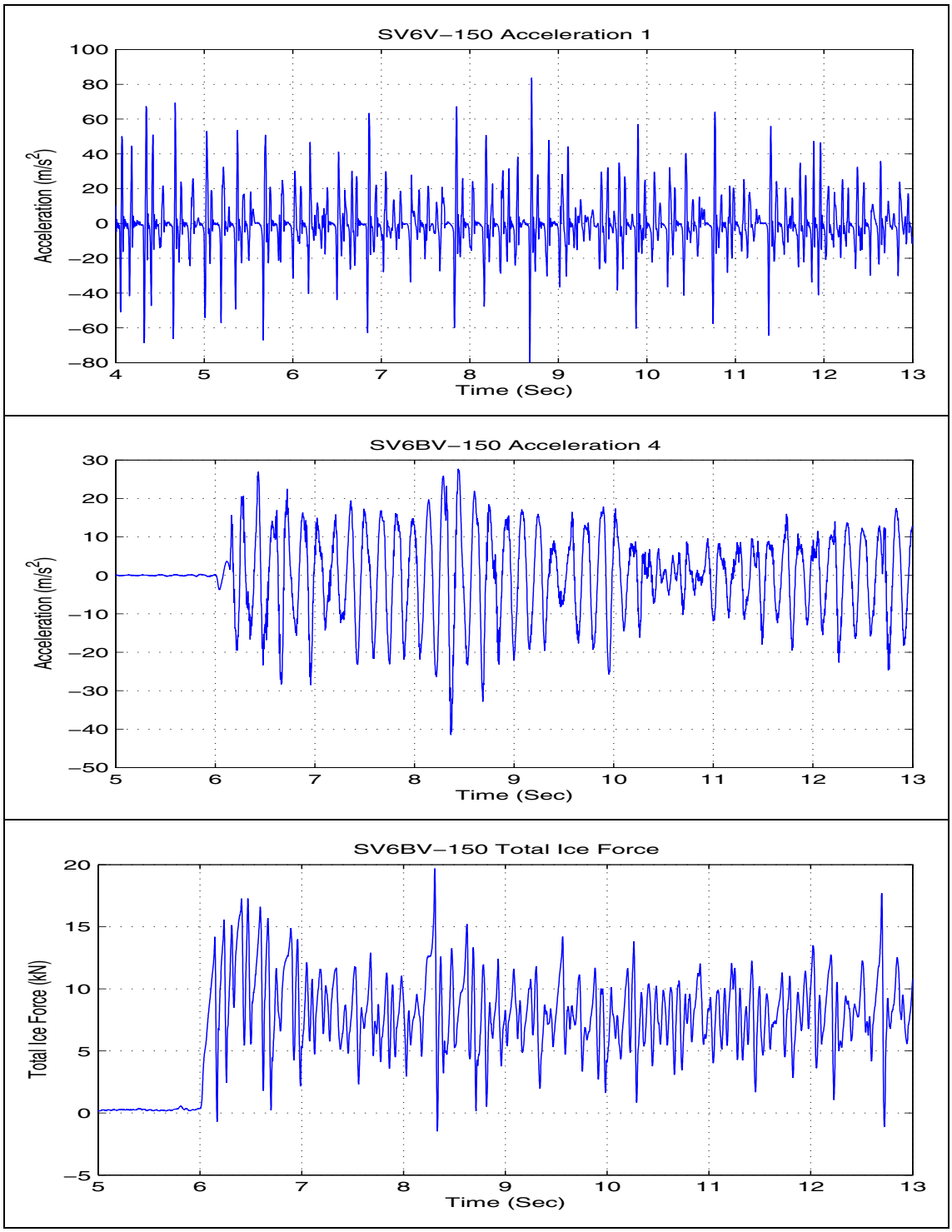

Figure 31. Measured accelerations close to the water level (Acceleration 1) and at the top of the structure (Acceleration 4) at a medium indentation velocity of 150 mm/s.

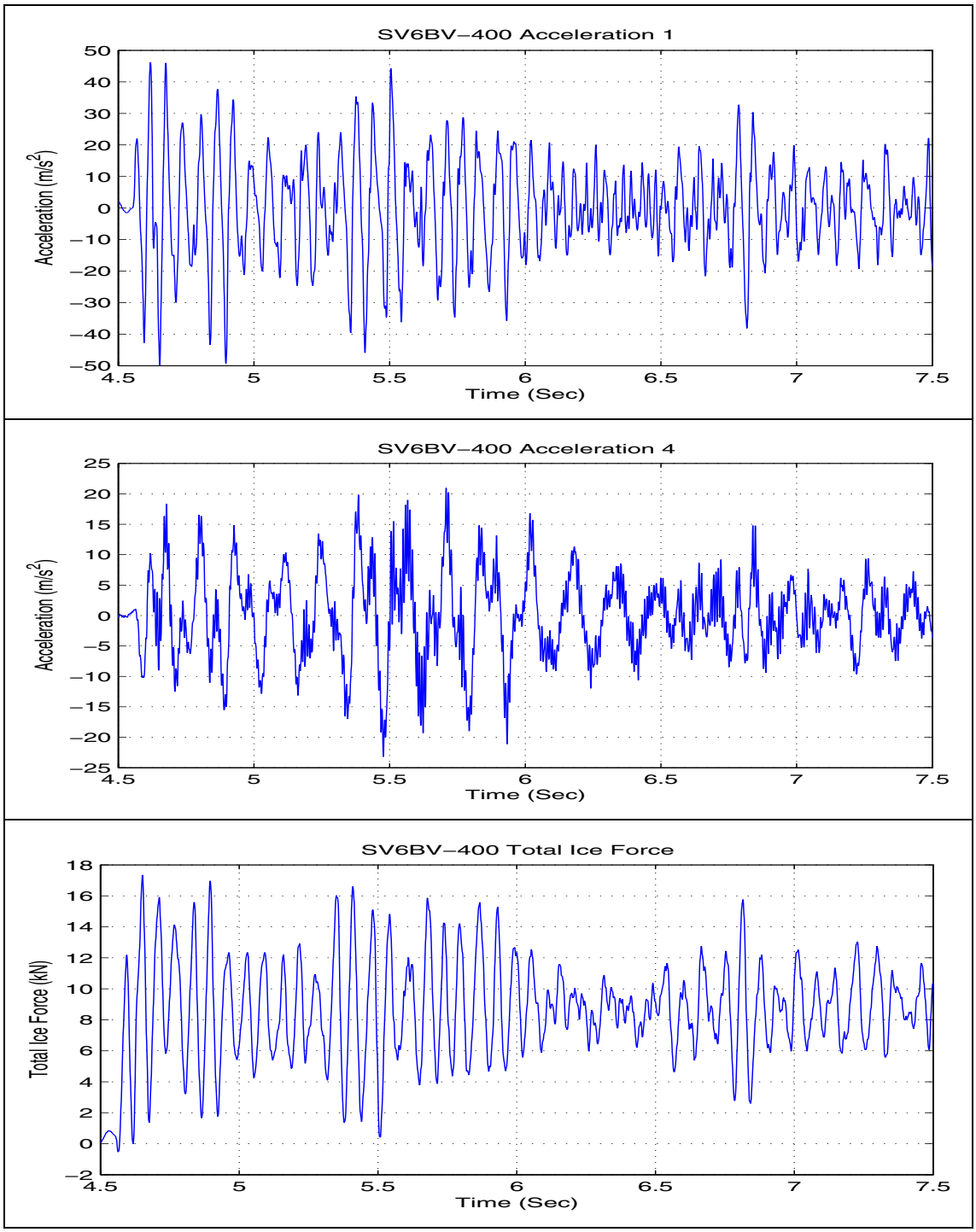

Figure 32. Measured accelerations close to the water level (Acceleration 1) and at the top of the structure (Acceleration 4) at a high indentation velocity of 400 mm/s.

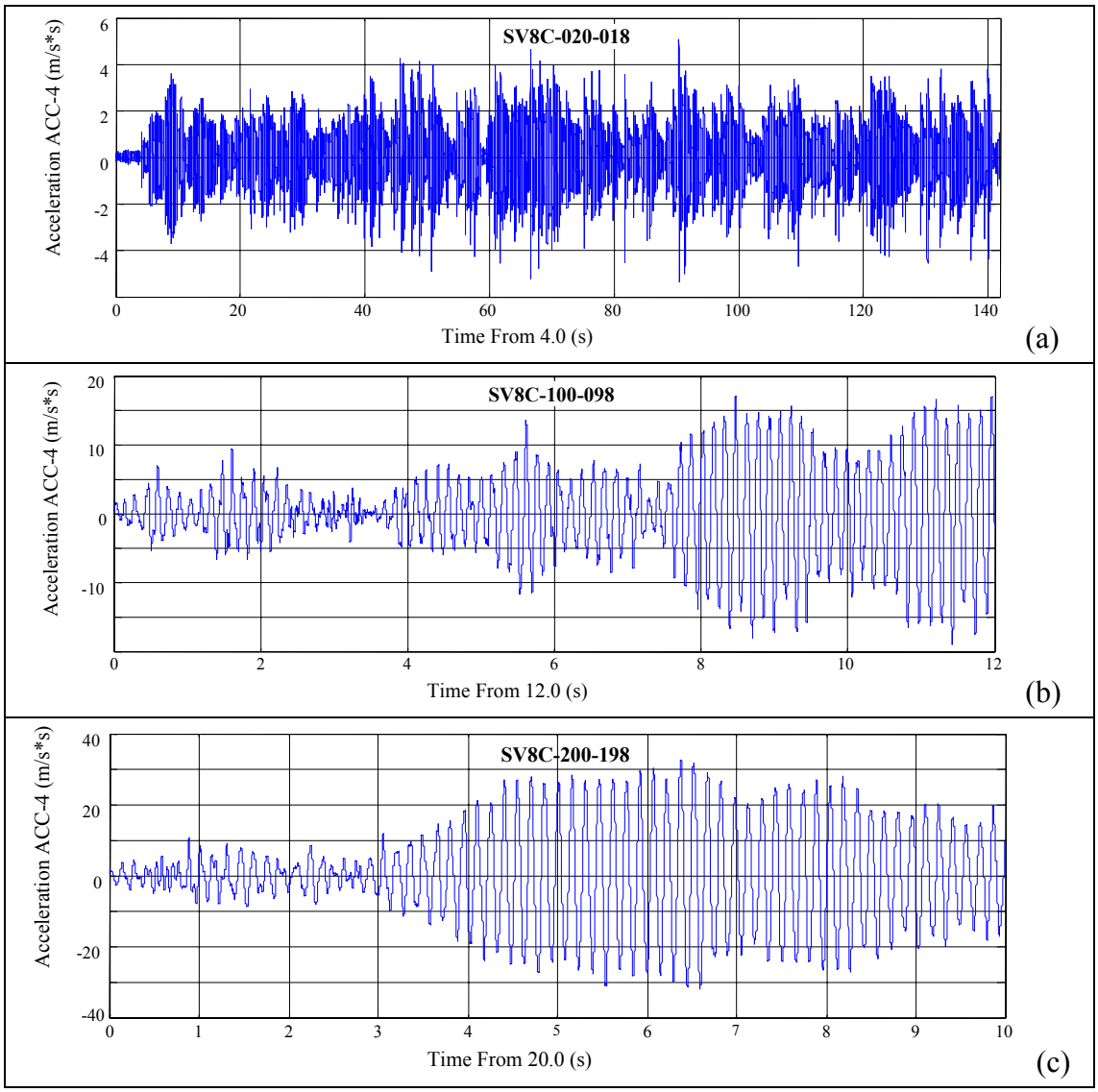

Figure 33. Measured accelerations at the top of the structure at different indentation velocities. The cone was used as the indentor. (a) v = 18 mm/s, (b) v = 98 mm/s, (c) v = 198 mm/s.

Figure 34. Ice failure in front of the inclined indentor.

Figure 35 shows a comparison between the measured response in the two cases where a cylinder and a faceted cone were used as indentors on the same structure. It is commonly deemed that the dynamic response is reduced significantly when the waterline geometry of the structure is inclined instead of vertical. In this test series the cone reduced the maximum response. However, the reduction was only small.

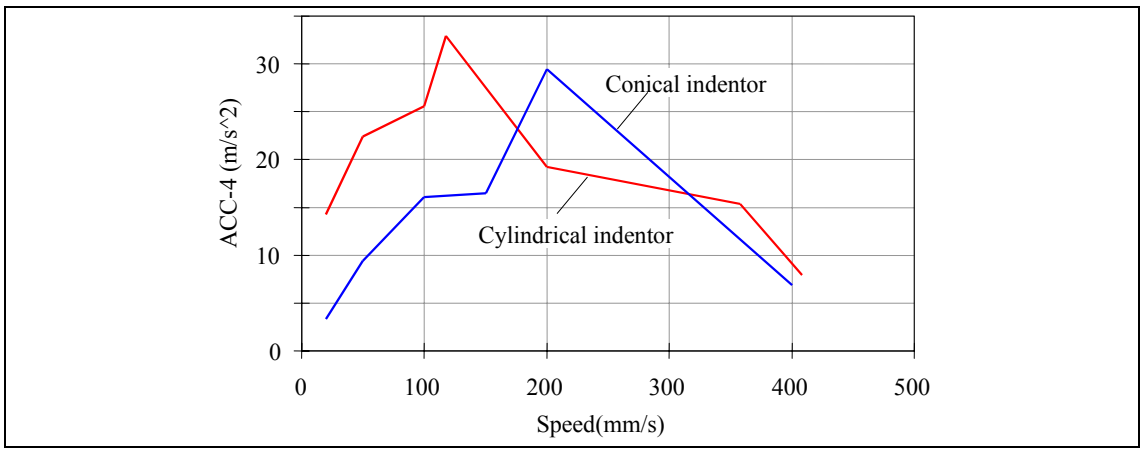

Figure 35. Peak acceleration at the top of the test structure SV8 as a function of indentation velocity.

6. Summary

A series of indentation tests was done using saline columnar grained ice. The dynamic properties of the test structure were varied during the test series. In particular, the stiffness of the structure "as seen by the ice" was varied as well as the structural damping. The present test report describes all the essential details of the tests. All test results are included in three Appendices. Selected results are shown for a structure that had a low structural damping. Steady state vibrations occurred at the lowest natural frequency at some ice velocities when a cylinder was used as an indentor. Heavy vibrations were found also when a faceted cone was used as the indentor. These vibrations were caused by a resonant condition that occurred due to a specific ice failure mode.

Acknowledgements

The research team would like to thank the Hamburg Ship Model Basin (HSVA), especially the ice thank crew, for the hospitality, technical support and professional execution of the test programme in the ARCTECLAB. The research activities carried out at the Major Research Infrastructure ARCTECLAB were financially supported by the Human Potential and Mobility Programme from the European Union through contract HPRI-CT-1999-00035.

References

Peyton, H.R. 1966. Sea ice strength. University of Alaska. Geophysical Institute. Final Report for the Navy Office of Naval Research, Contract Nr 2601(01).

Yue, Q. and Bi, X. 2000. Effect of ice-breaking cones for mitigating ice-induced vibrations. Proc. 15th International Symposium on Ice. Gdansk, Poland, August 28 – September 1, 2000. Pp. 127–133.

APPENDIX A: Compressive strength of the ice sheets

Date	Time	Location	Dimension	Specimen No	Spec. Temp [°C]	Salility [ppt]	Layer	Cross-Head-Speed [mm/s]	Strength [kPa]	mean value [kPa]
23.5.2002	13:00	55m	40x80x160mm	55_1	-3.3		0-40mm	2	198	
				55-2	-3.5				243	
				55_3	-3.4				220	
				55_4	-3.2				183	
				55_5	-3.1				159	201
23.5.2002	14:00	55m	30x60x120	55_6	-4.1		total thickness	2	160	
				55_7					147	
				55_8	-3.3				121	143
23.5.2002	17:00	55m	40x80x160mm	55_9	-4.4		0-40mm	2	574	
				55_10					427	
				55_11	-3.8				551	517
23.5.2002	15:30	22m	40x80x160mm	22_2	-3.2		0-40mm	2	266	
				22_3	-3.3				240	
				22_4	-2.3				277	
				22_5	-2.0				326	277
24.5.2002	8:00	22m	40x80x160mm	22_21	-4.9		0-40mm	2	439	
				22_22	-3.8		0-40mm		431	
				22_23	-3.0		40-80mm		265	
				22_24	-3.9		0-40mm		629	
				22_25	-3.2		40-80mm		326	418

24.5.2002	10:00	55m	40x80x160mm	55_31	-5.3	0-40mm	2	865	
				55_33	-4.3	0-40mm		760	
				55_34	-3.5	40-80mm		682	
				55_35	-4.2	0-40mm		285	
				55_36	-4.2	40-80mm		314	581
29.5.2002	8:30	38m	40x80x160mm	38_1	-4.9	0-40mm	2	392	
				38_2	-4.6			493	
				38_3	-4.6			498	
				38_4	-3.6			292	
				38_5	-3.0			375	410
29.5.2002	9:00	22m	40x80x160mm	22_31	-3.8	0-40mm	2	535	
				22_32	-4.1			449	
				22_33	-4.0			554	
				22_34	-4.0			481	
				22_35	-3.9			686	541
30.5.2002	18:00	38m	40x80x160mm	38_6	-5.0	0-40mm	2	958	
				38_7	-4.5	40-80mm		601	
				38_8	-4.7	0-40mm		718	
				38_9	-4.8	0-40mm		578	
				38_10	-4.3	40-80mm		989	769
30.5.2002	18:45	55m	40x80x160mm	55_41	-5.0	0-40mm	2	933	
				55_42	-3.5	40-80mm		935	
				55_43	-4.4	0-40mm		346	
				55_44	-3.0	40-80mm		570	
				55_45	-5.0	0-40mm		631	683

A2

5.6.2002	10:45	22m	40x80x160mm	22_41	-4.1	3.4	0-40mm	2	698	
				22_42	-4.4	4.3			513	
				22_43	-4.1	4.1			513	
				22_44	-4.8	4.1			437	
				22_45	-3.8	4.6			396	511
5.6.2002	10:00	55m	40x80x160mm	55_51	-4.1	4.3	0-40mm	2	647	
				55_52	-4.4	4.3			560	
				55_53	-3.7	4.6			350	
				55_54	-4.3	4.4			383	
				55_55	-4.1	4.4			347	457
6.6.2002	9:45	55m	40x80x160mm	55_61	-3.1	2.4	40-80mm	2	296	
				55_62	-3.0	4.1	0-40mm		274	
				55_63	-2.3	2.7	40-80mm		248	
				55_64	-3.2	4.0	0-40mm		273	
				55_65	-3.1	2.4	40-80mm		365	
				55_66	-2.9	4.0	0-40mm		317	
				55_67	-2.5	2.5	40-80mm		499	325

APPENDIX B: Bending strength of the ice sheets

Versuchsserie:		VTT-1000		Abschaltdaten:		22.5.02 5:30	
Datum Uhrzeit: 22.5.02 7:40	lfd. Nr.:	Kraft [N]	Länge [mm]	Breite [mm]	Dicke [mm]	Sigma [kPa]	Mittelwerte
Position: [Tm] 22 / 7	2	5.0	235.0	82.0	37.5	61.1	
	3	4.5	232.0	83.0	37.5	53.7	
	4	5.1	230.0	78.0	37.5	64.2	
Mittelwerte:		4.9	232.3	81.0	37.5	59.7	1. Messreihe
Position: [Tm] 38 / 7	5	5.8	234.0	82.0	38.0	68.8	
	6	8.2	235.0	82.0	38.0	97.6	72.5
	7	6.0	227.0	81.0	38.0	69.9	
Mittelwerte:		6.7	232.0	81.7	38.0	78.8	[kPa]
Position: [Tm] 55 / 7	8	7.0	235.0	87.0	38.0	78.6	
	9	6.9	237.0	80.0	38.0	84.9	
	10	6.2	230.0	80.0	38.0	74.1	Dateien:
Mittelwerte:		6.7	234.0	82.3	38.0	79.2	M020522A-C
Datum Uhrzeit: 22.5.02 11:40	lfd. Nr.:	Kraft [N]	Länge [mm]	Breite [mm]	Dicke [mm]	Sigma [kPa]	
Position: [Tm] 22 / 7	11	5.0	235.0	75.0	39.0	61.8	
	12	5.0	235.0	76.0	39.0	61.0	
	13	5.0	225.0	80.0	39.0	55.5	
Mittelwerte:		5.0	231.7	77.0	39.0	59.4	2. Messreihe
Position: [Tm] 38 / 7	14	7.0	235.0	80.0	40.0	77.1	
	15	7.5	231.0	82.0	40.0	79.2	66.8
	16	6.0	235.0	80.0	40.0	66.1	
Mittelwerte:		6.8	233.7	80.7	40.0	74.1	[kPa]
Position: [Tm] 55 / 7	17	5.5	235.0	75.0	40.0	64.6	
	18	6.5	231.0	79.0	40.0	71.3	
	19	6.2	227.0	82.0	40.0	64.4	Dateien:
Mittelwerte:		6.1	231.0	78.7	40.0	66.8	M020522D-F
						Δ-Sigma/h:	-1
Datum Uhrzeit: 23.5.02 8:55	lfd. Nr.:	Kraft [N]	Länge [mm]	Breite [mm]	Dicke [mm]	Sigma [kPa]	
Position: [Tm] Feld 2	2	20.0	335.0	125.0	52.5	116.7	
	3	21.0	300.0	109.0	52.0	128.3	
	4	18.7	303.0	105.0	52.0	119.7	
Mittelwerte:		19.9	312.7	113.0	52.2	121.6	3. Messreihe
Position: [Tm] Feld 5	5	16.5	297.0	95.0	53.0	110.2	
	6	18.8	288.0	105.0	53.0	110.1	127.6
	7	20.0	295.0	98.0	53.0	128.6	
Mittelwerte:		18.4	293.3	99.3	53.0	116.3	[kPa]
Position: [Tm] Feld 8	8	23.0	295.0	100.0	52.0	150.6	
	9	20.0	292.0	94.0	52.0	137.9	
	10	24.0	280.0	102.0	52.0	146.2	Dateien:
Mittelwerte:		22.3	289.0	98.7	52.0	144.9	M020523A-E
						Δ-Sigma/h:	2.861365501

Versuchsserie:		VTT-2000		Abschaltdaten:		29.05.2002 06:30	
Datum Uhrzeit: 29.5.02 6:30	lfd. Nr.:	Kraft [N]	Länge [mm]	Breite [mm]	Dicke [mm]	Sigma [kPa]	Mittelwerte
Position: [Tm]	2	19.0	557.0	153.0	71.0	82.3	
22 / 7	3	15.0	552.0	138.0	71.0	71.4	
	4	18.0	546.0	146.0	71.0	80.1	
Mittelwerte:		17.3	551.7	145.7	71.0	78.0	1. Messreihe
Position: [Tm]	5	23.0	538.0	147.0	75.5	88.6	
38 / 7	6	23.0	540.0	150.0	75.0	88.3	80.6
	7	18.0	542.0	141.0	75.5	72.8	
Mittelwerte:		21.3	540.0	146.0	75.3	83.3	[kPa]

Versuchsserie:		VTT-3000		Abschaltdaten:		05.06.2002 08:15	
Datum Uhrzeit: 5.6.02 8:15	lfd. Nr.:	Kraft [N]	Länge [mm]	Breite [mm]	Dicke [mm]	Sigma [kPa]	Mittelwerte
Position: [Tm]	2	27.3	460.0	180.0	78.5	67.9	
22 / 7	3	39.2	457.0	195.0	72.5	104.9	
	4	40.9	421.0	204.0	74.5	91.2	
Mittelwerte:		35.8	446.0	193.0	75.2	88.0	1. Messreihe
Position: [Tm]	5	0.0	0.0	0.0	0.0		
55 / 7	6	32.3	526.0	218.0	76.5	79.9	89.2
	7	35.7	522.0	192.0	76.0	100.8	
Mittelwerte:		22.7	349.3	136.7	50.8	90.4	[kPa]
Position: [Tm]	8						
Feld 8	9						
	10						Dateien:
Mittelwerte:							M020605A-C

Datum Uhrzeit: 6.6.02 7:45	lfd. Nr.:	Kraft [N]	Länge [mm]	Breite [mm]	Dicke [mm]	Sigma [kPa]	
Position: [Tm]	12	26.0	555.0	174.0	87.5	65.0	
22 / 7	13	24.0	580.0	190.0	83.0	63.8	
	14	22.7	560.0	175.0	84.5	61.0	
Mittelwerte:		24.2	565.0	179.7	85.0	63.3	2. Messreihe
Position: [Tm]	15	33.9	580.0	170.0	87.0	91.7	
55 / 7	16	31.0	582.0	175.0	83.0	89.8	73.7
	17	30.2	607.0	192.0	90.0	70.7	
Mittelwerte:		31.7	589.7	179.0	86.7	84.1	[kPa]

Appendix C:

Time histories of representative indentation tests. The following time signal are shown for each test case on two pages.

- Acceleration 1
- Acceleration 2
- Acceleration 3
- Acceleration 4
- Displacement 1
- Displacement 2
- Carriage speed
- Total ice force

The displacement signals contain occasional noise, which was caused by the crushed ice impacting on the displacement measuring systems.

Test SV6V-010

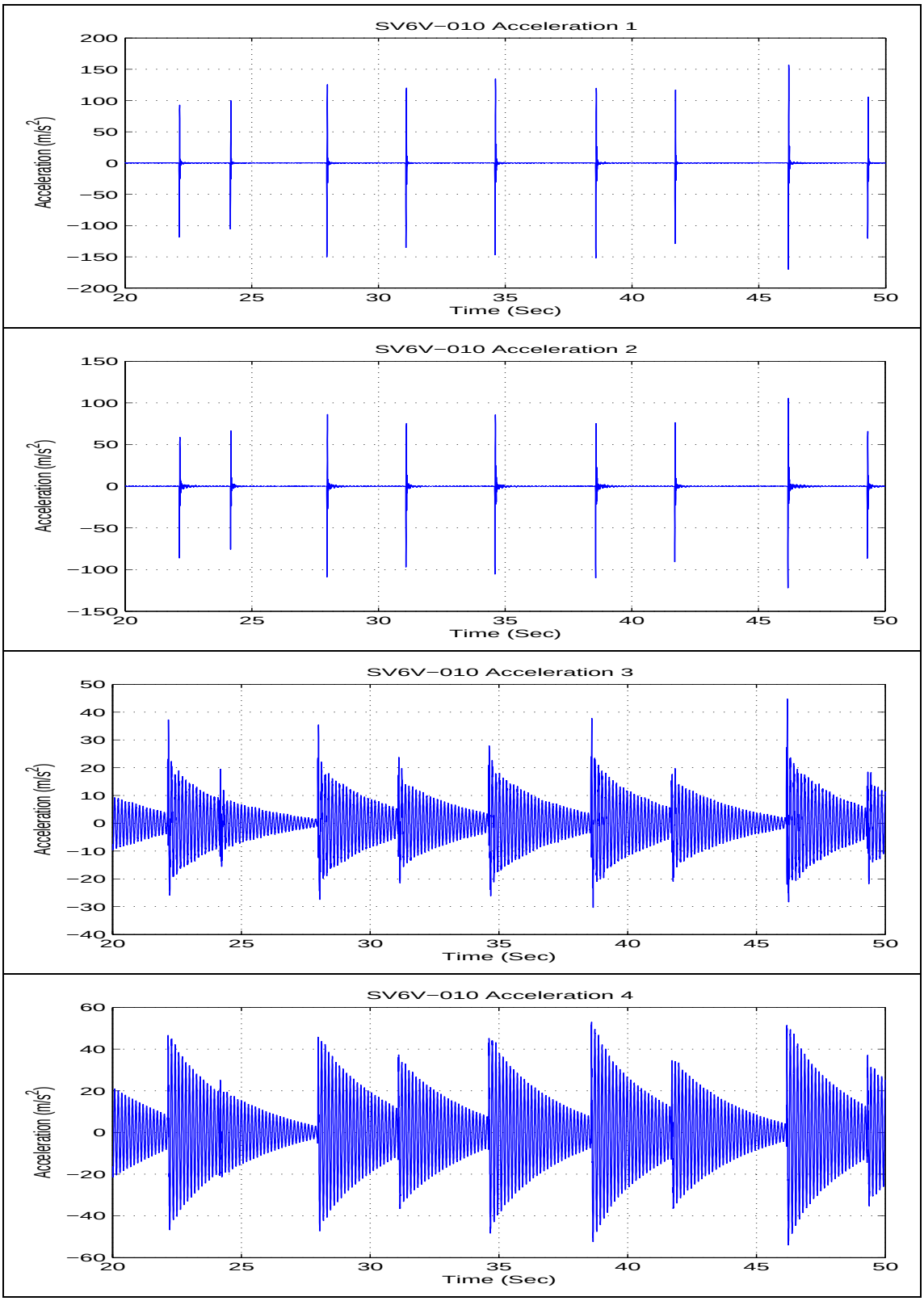

Test SV6V-010

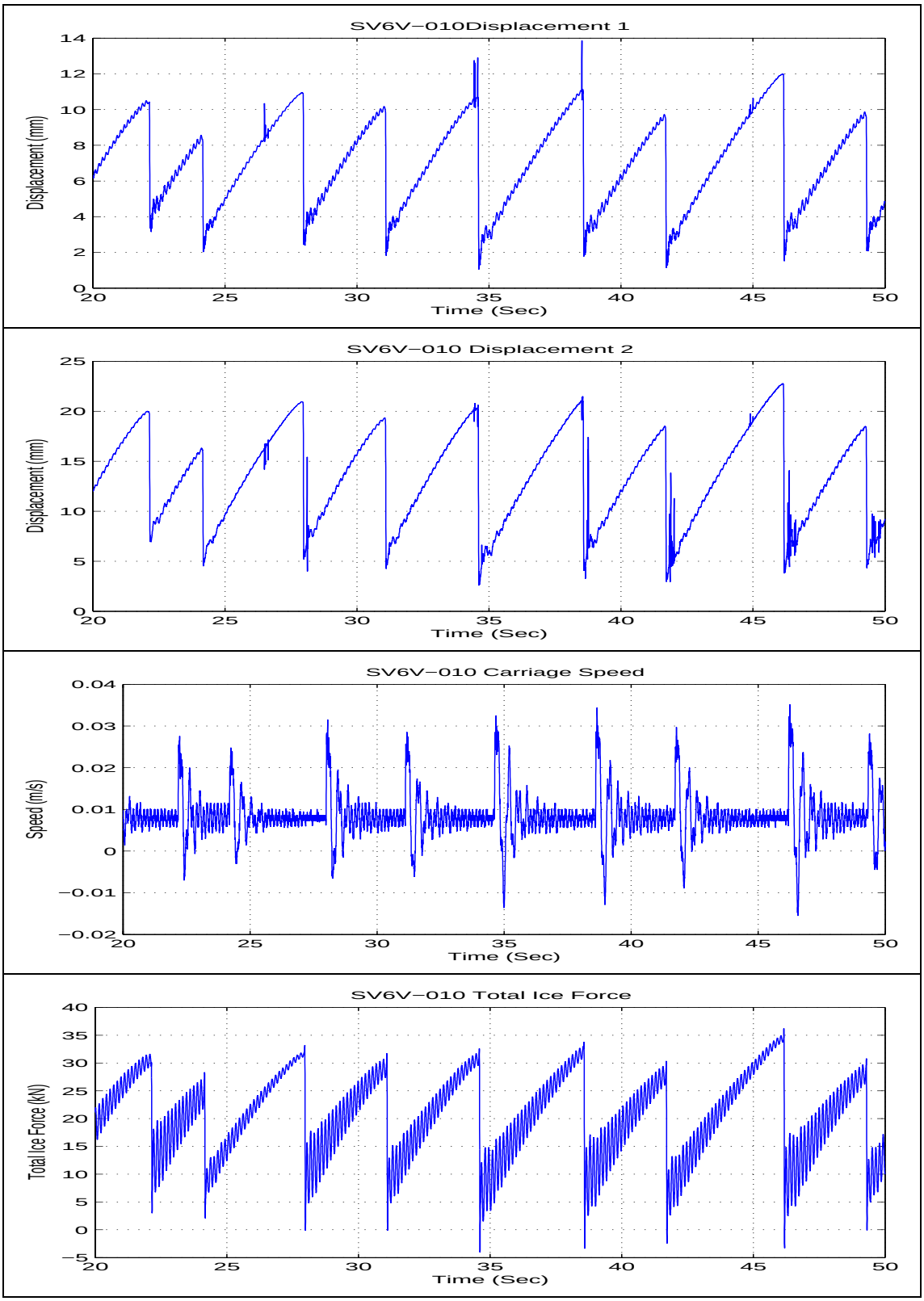

Test SV6V-020

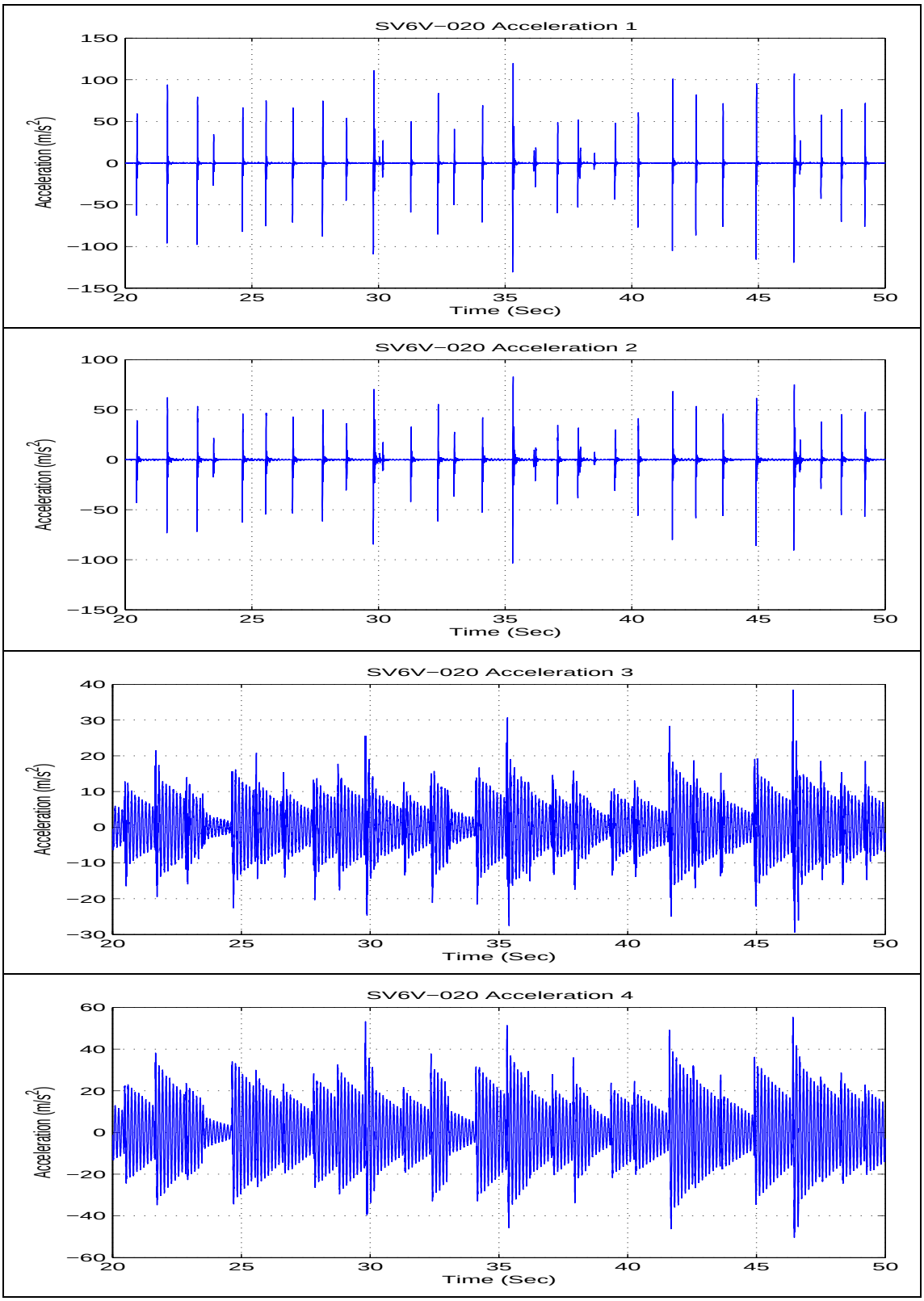

Test SV6V-020

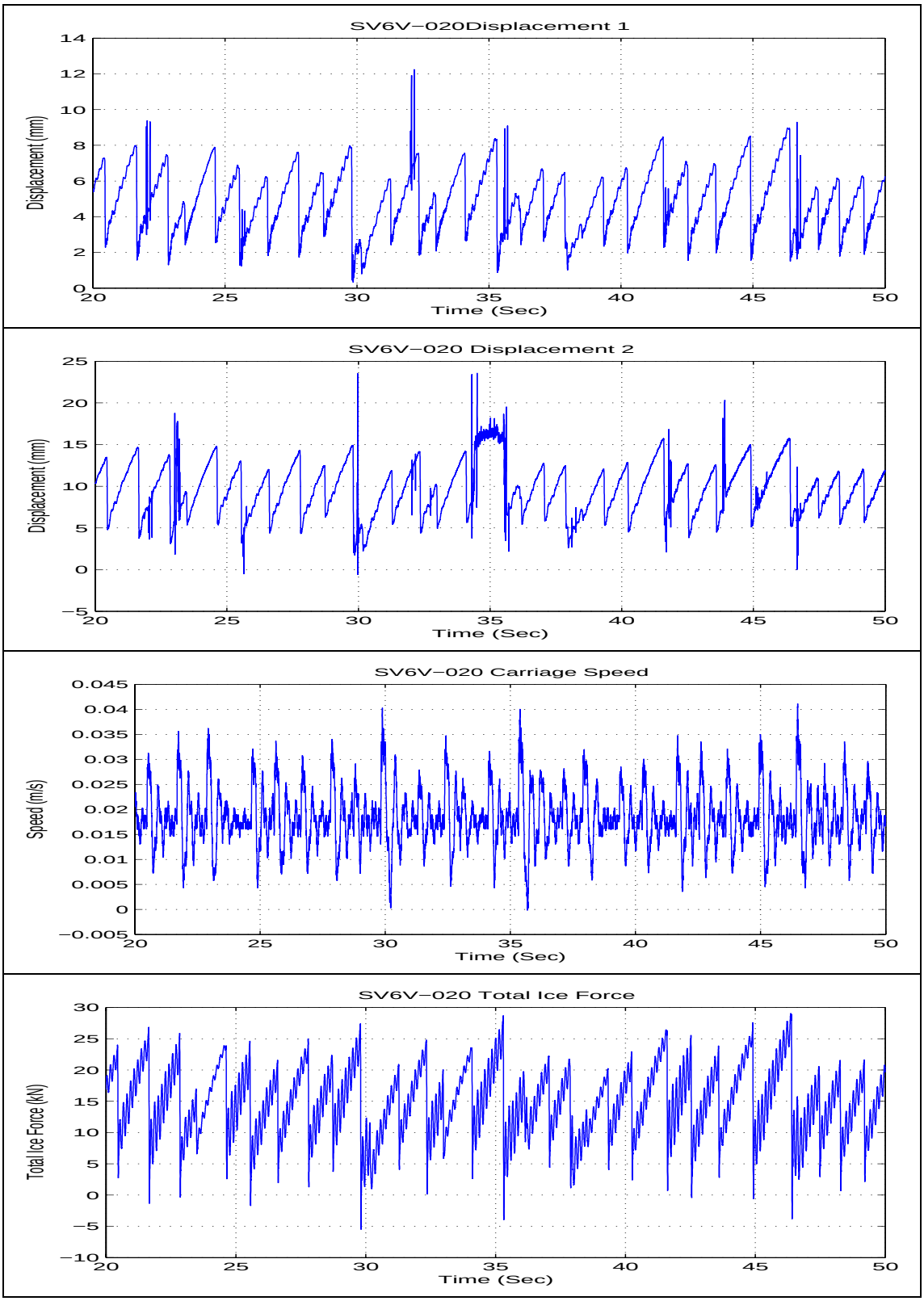

Test SV6V-040

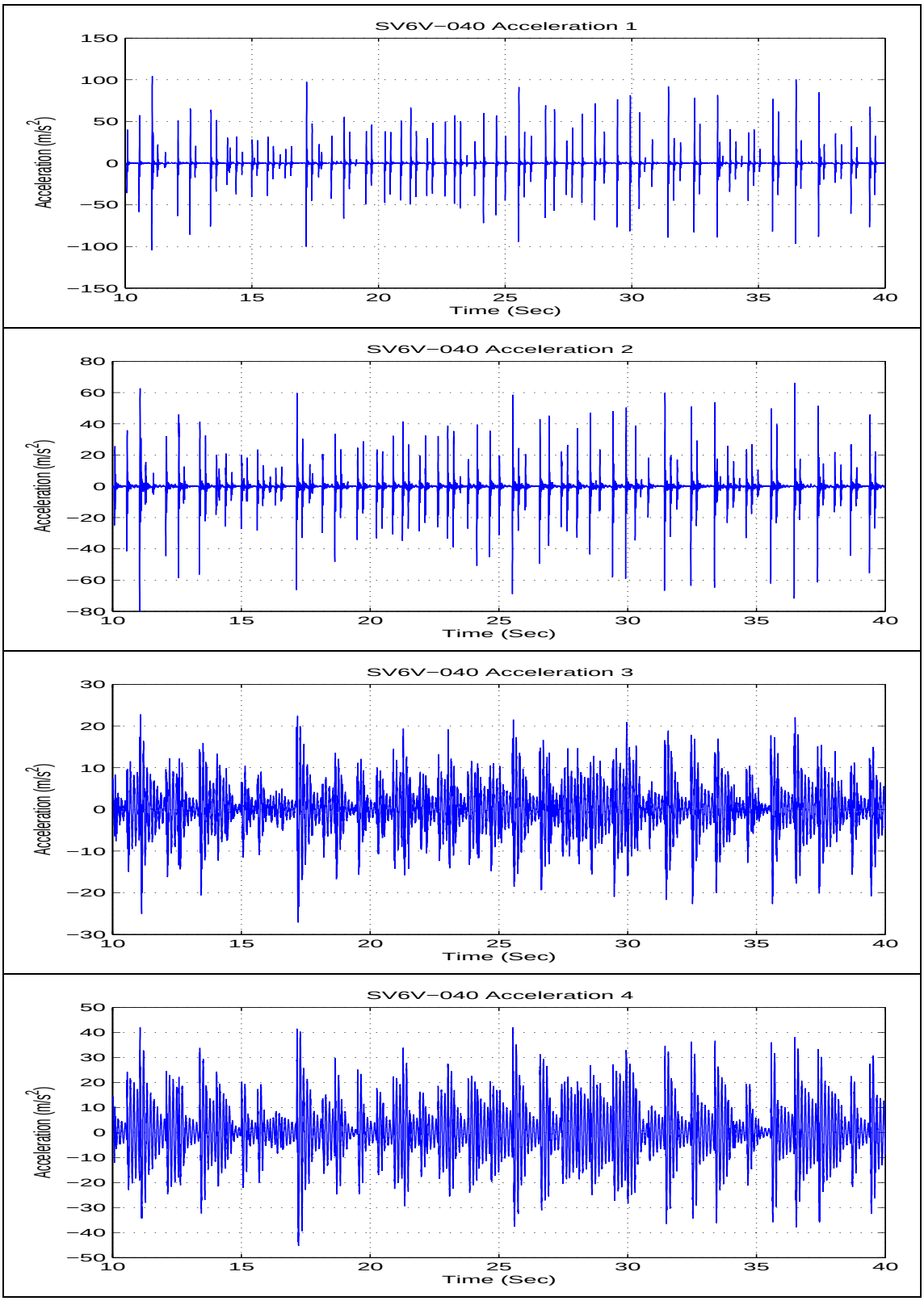

Test SV6V-040

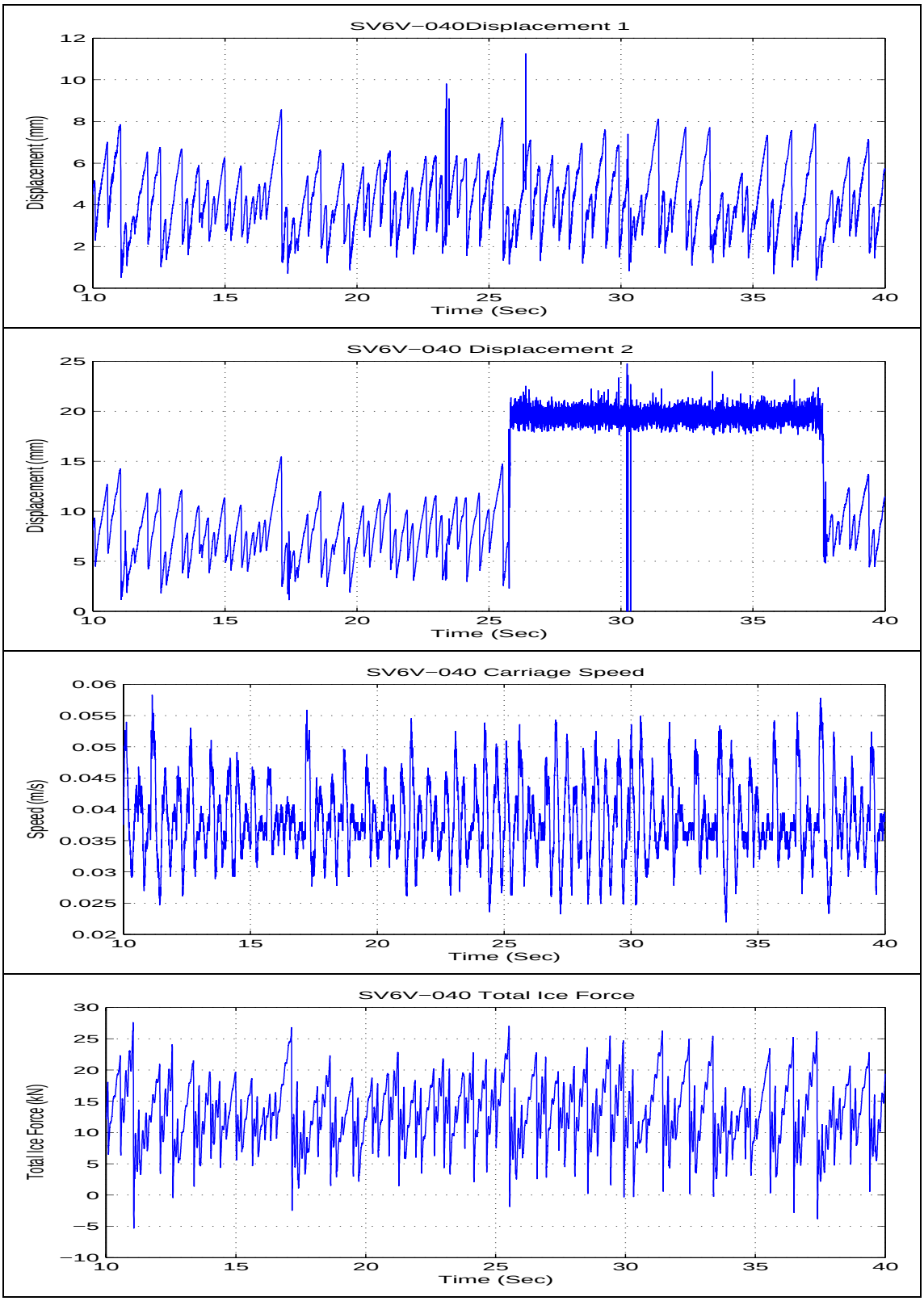

Test SV6V-100

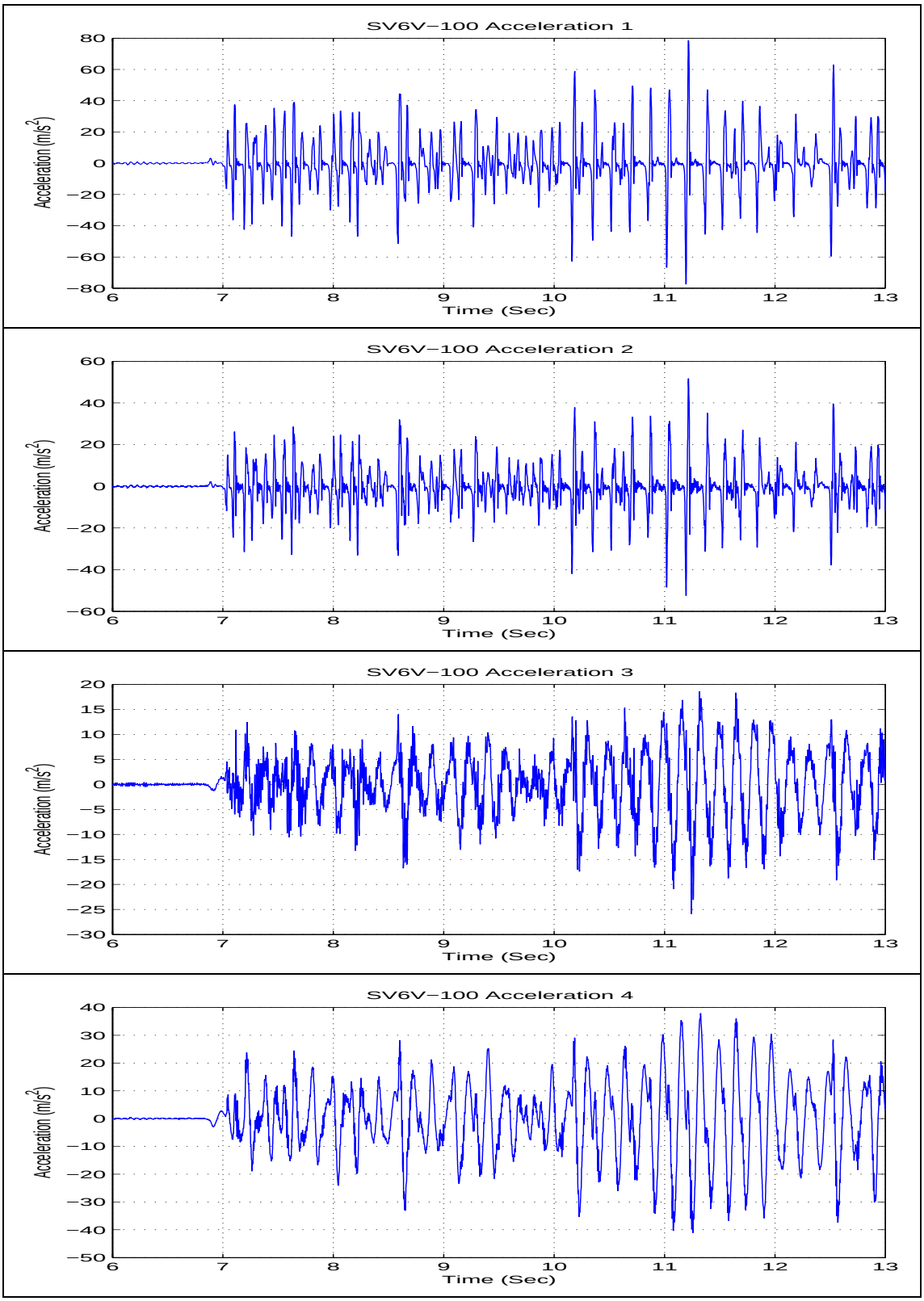

Test SV6V-100

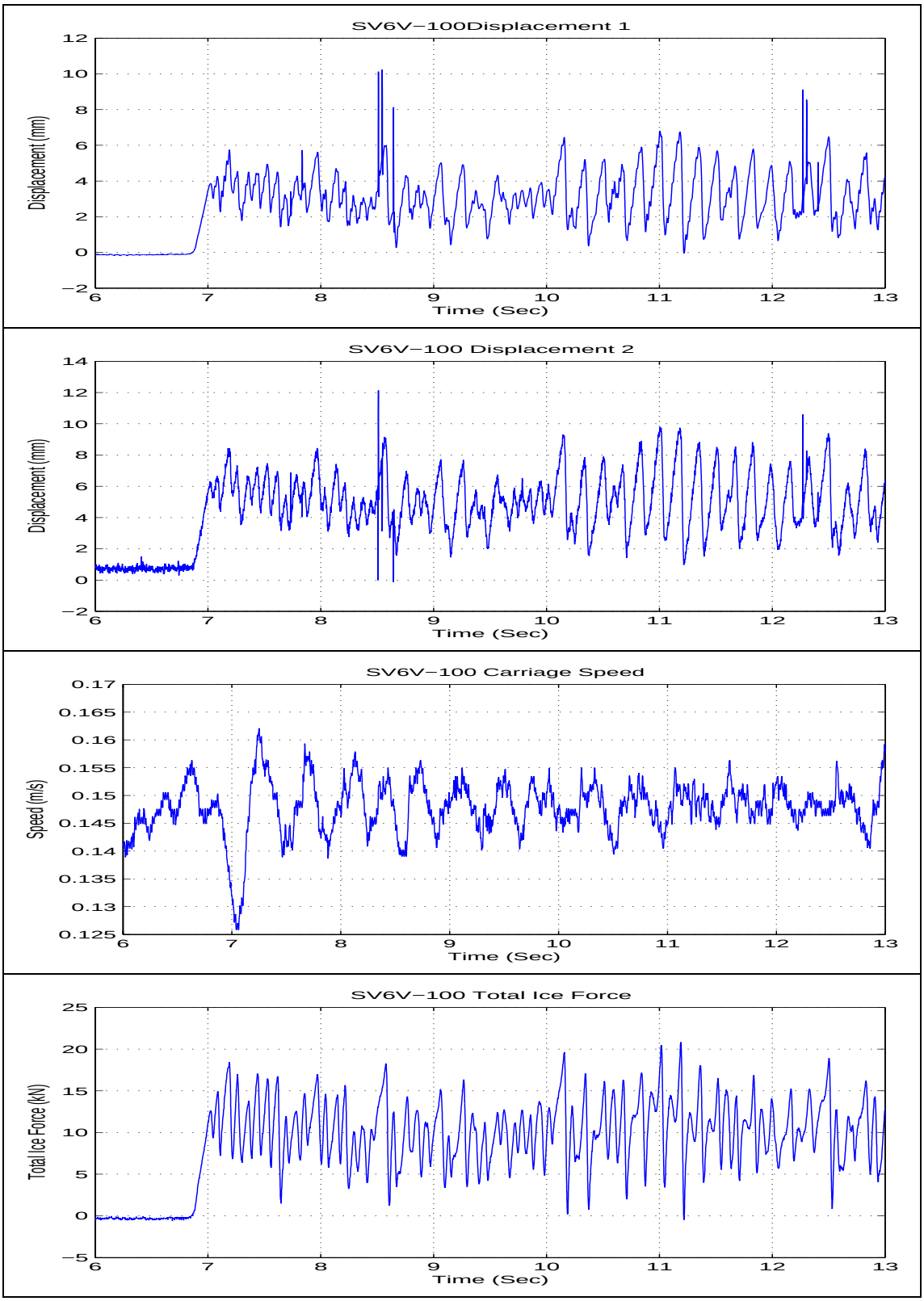

Test SV6V-150

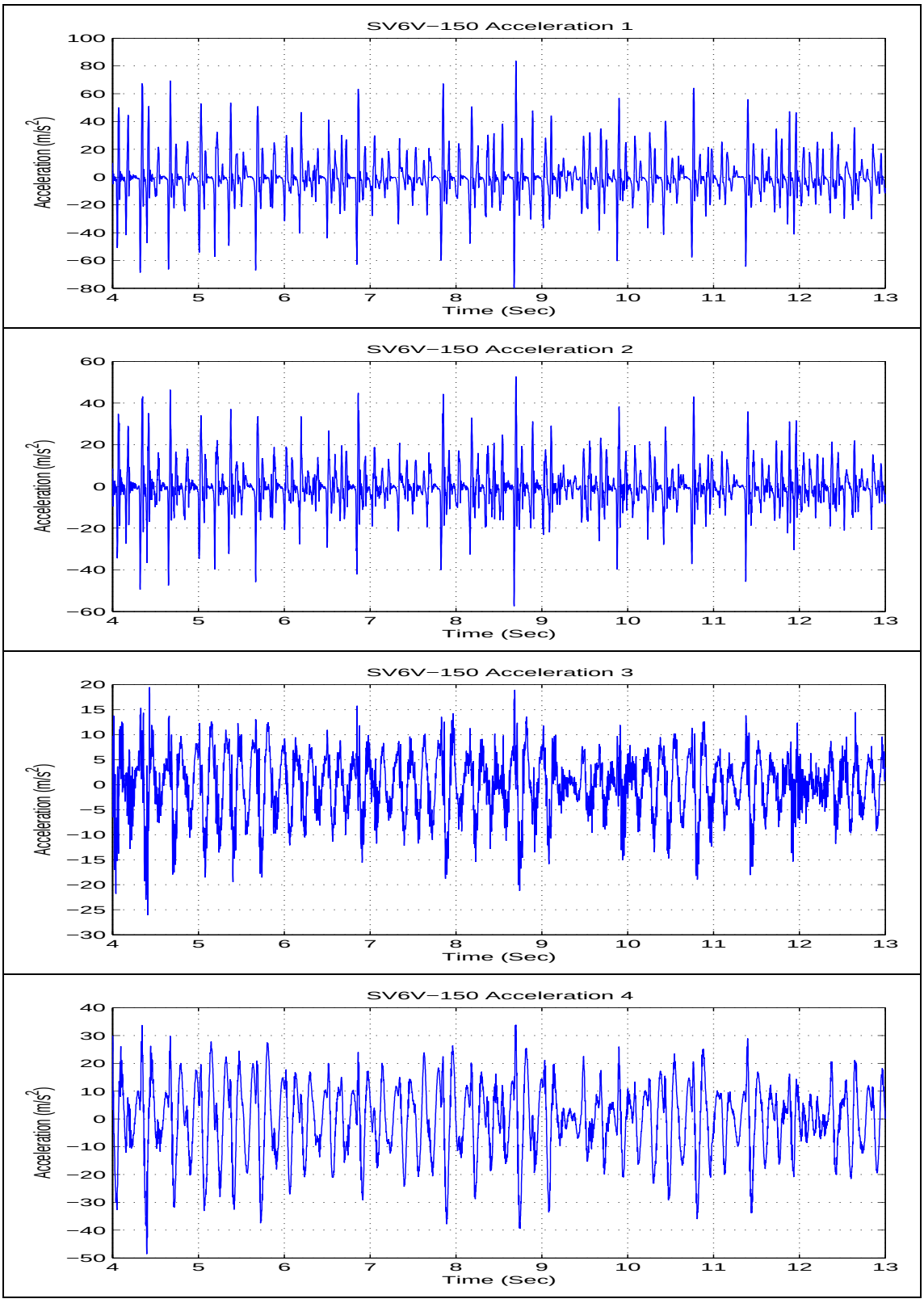

Test SV6V-150

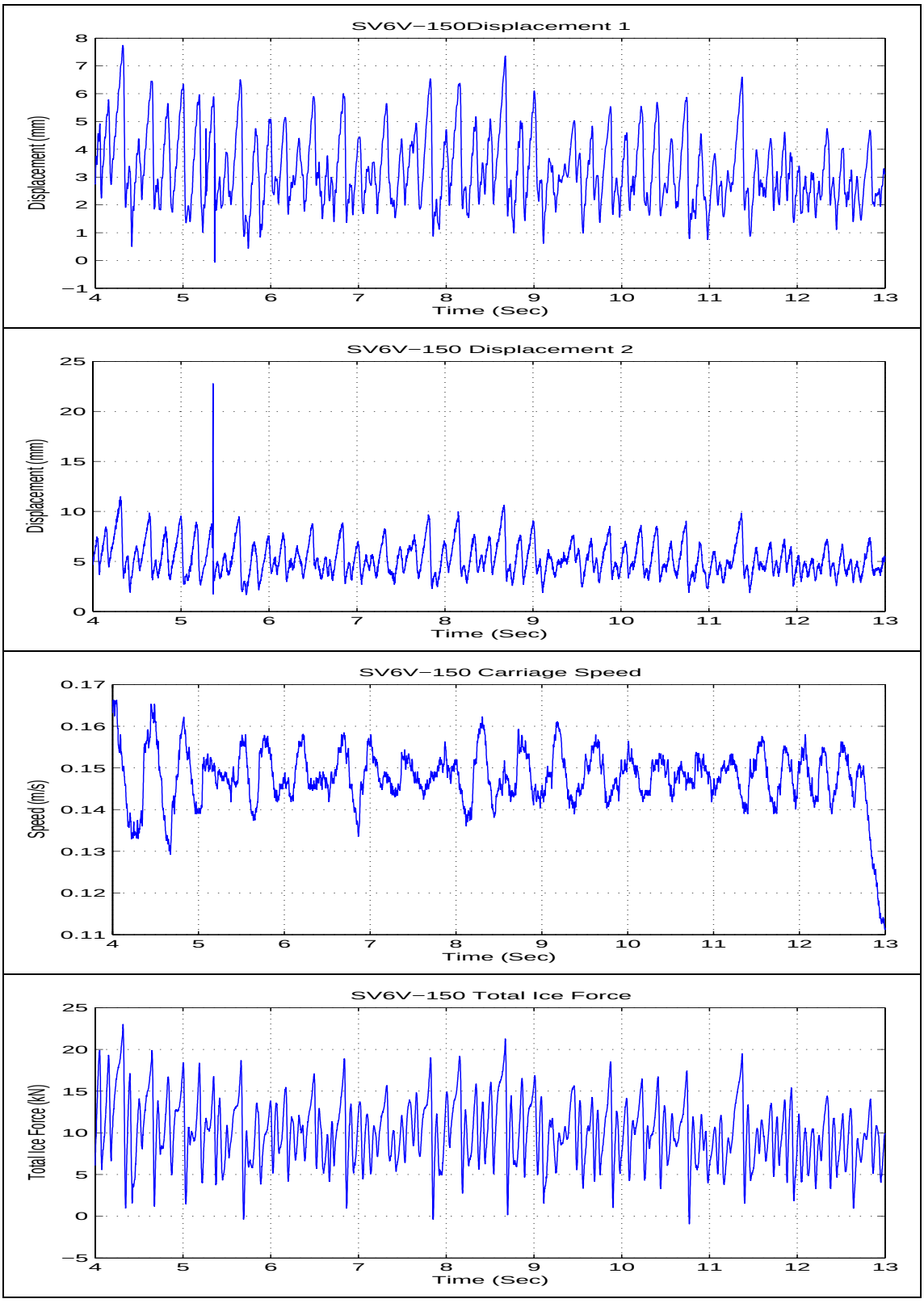

Test SV6V-200

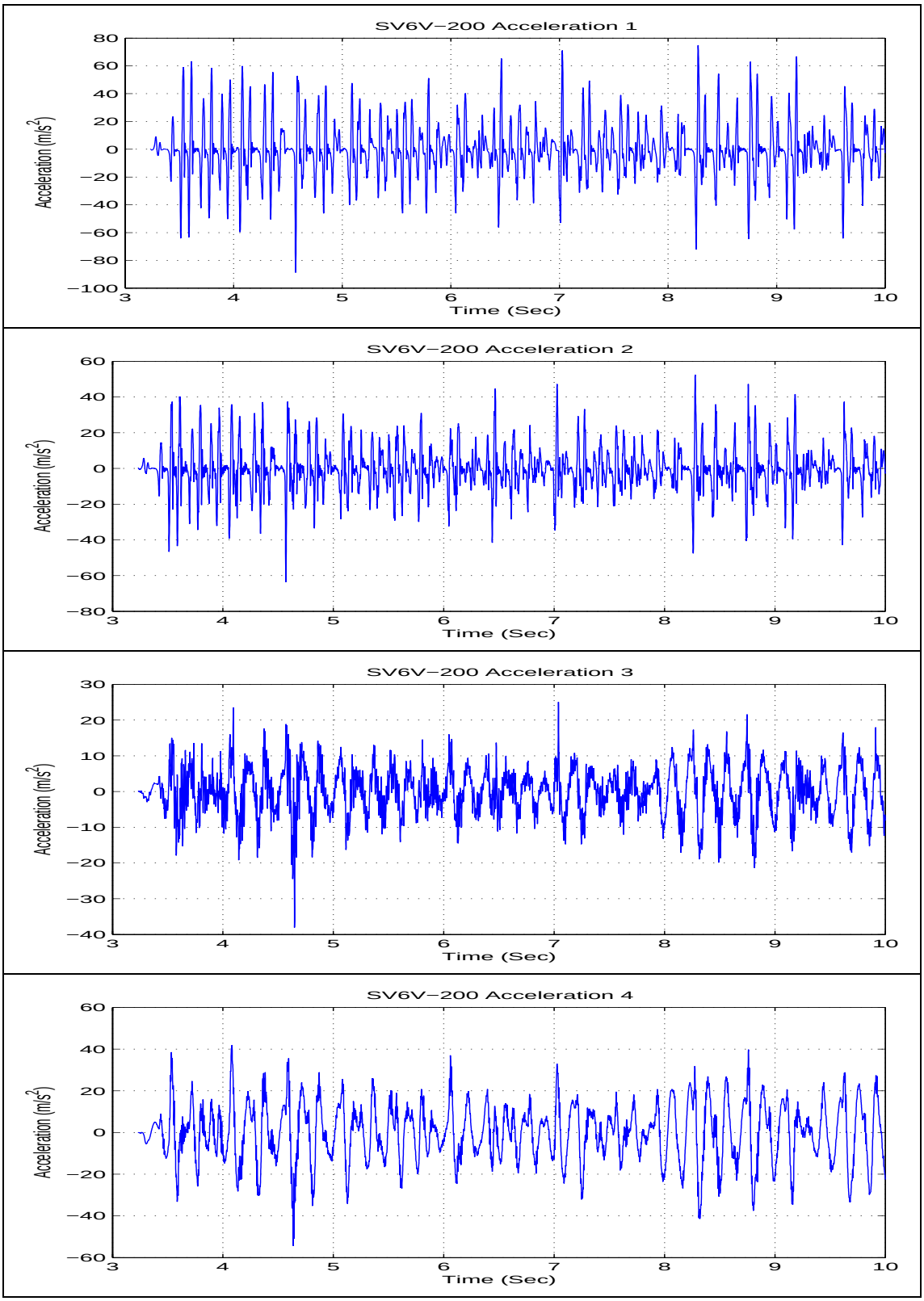

Test SV6V-200

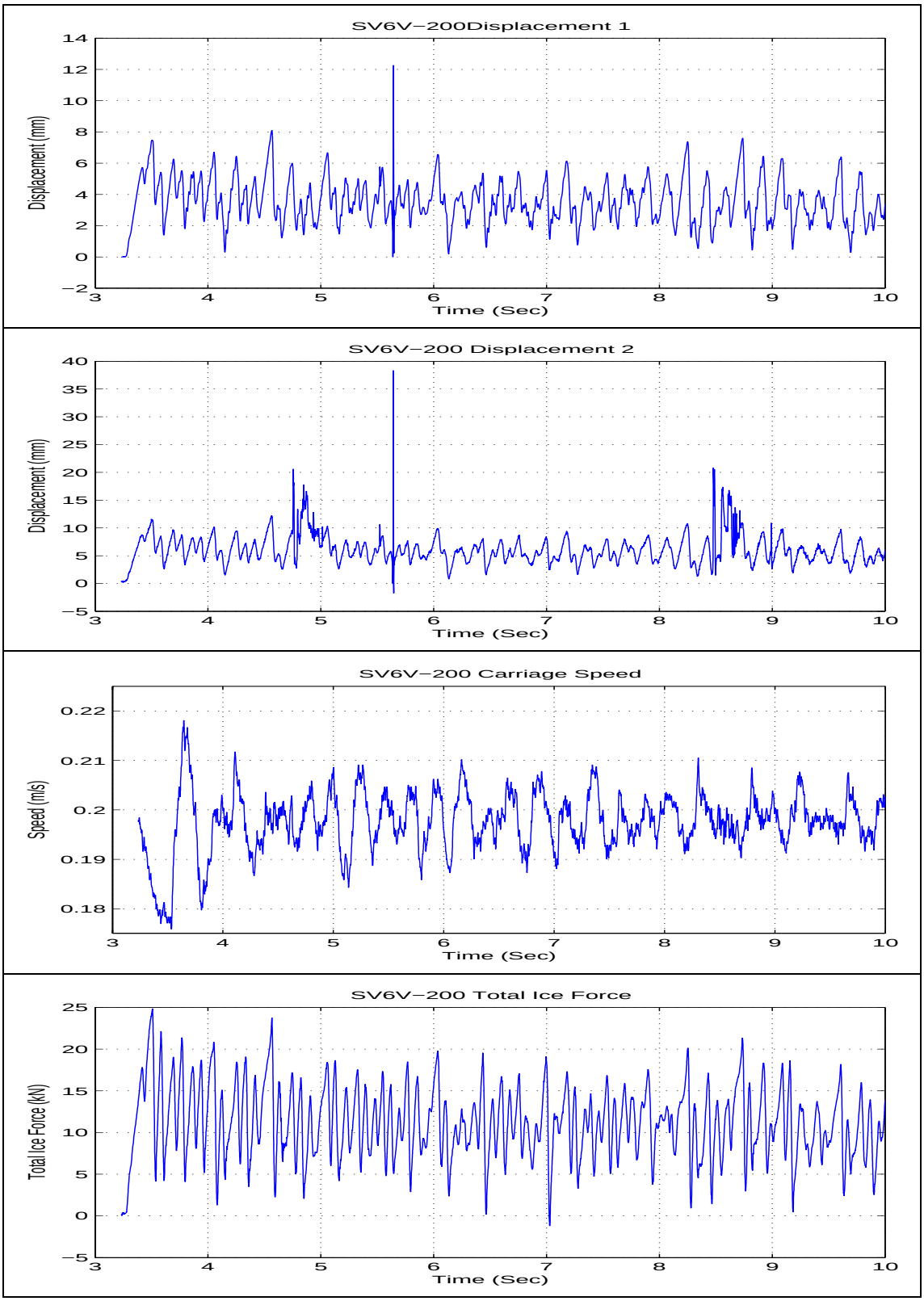

Test SV6BV-100

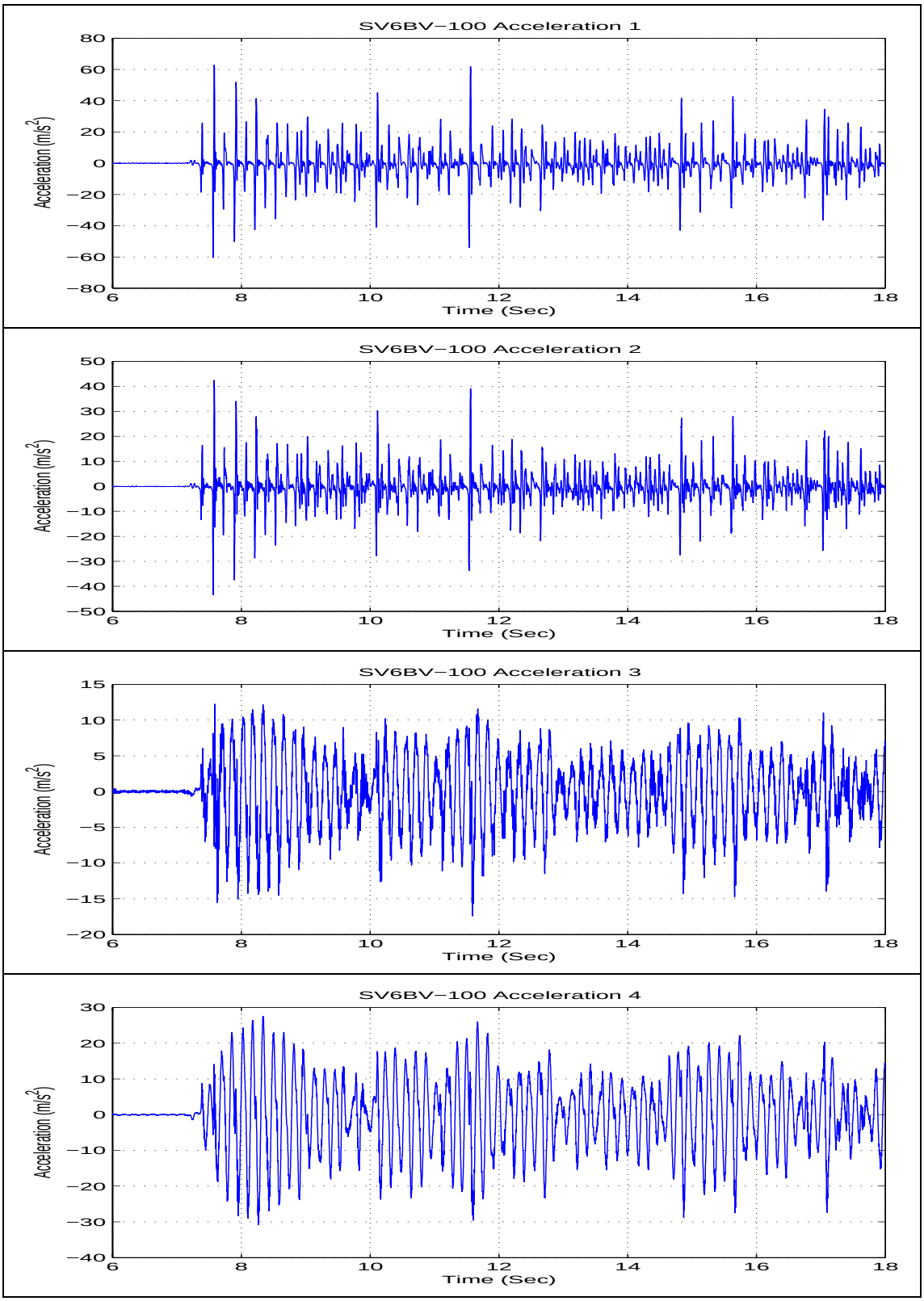

Test SV6BV-100

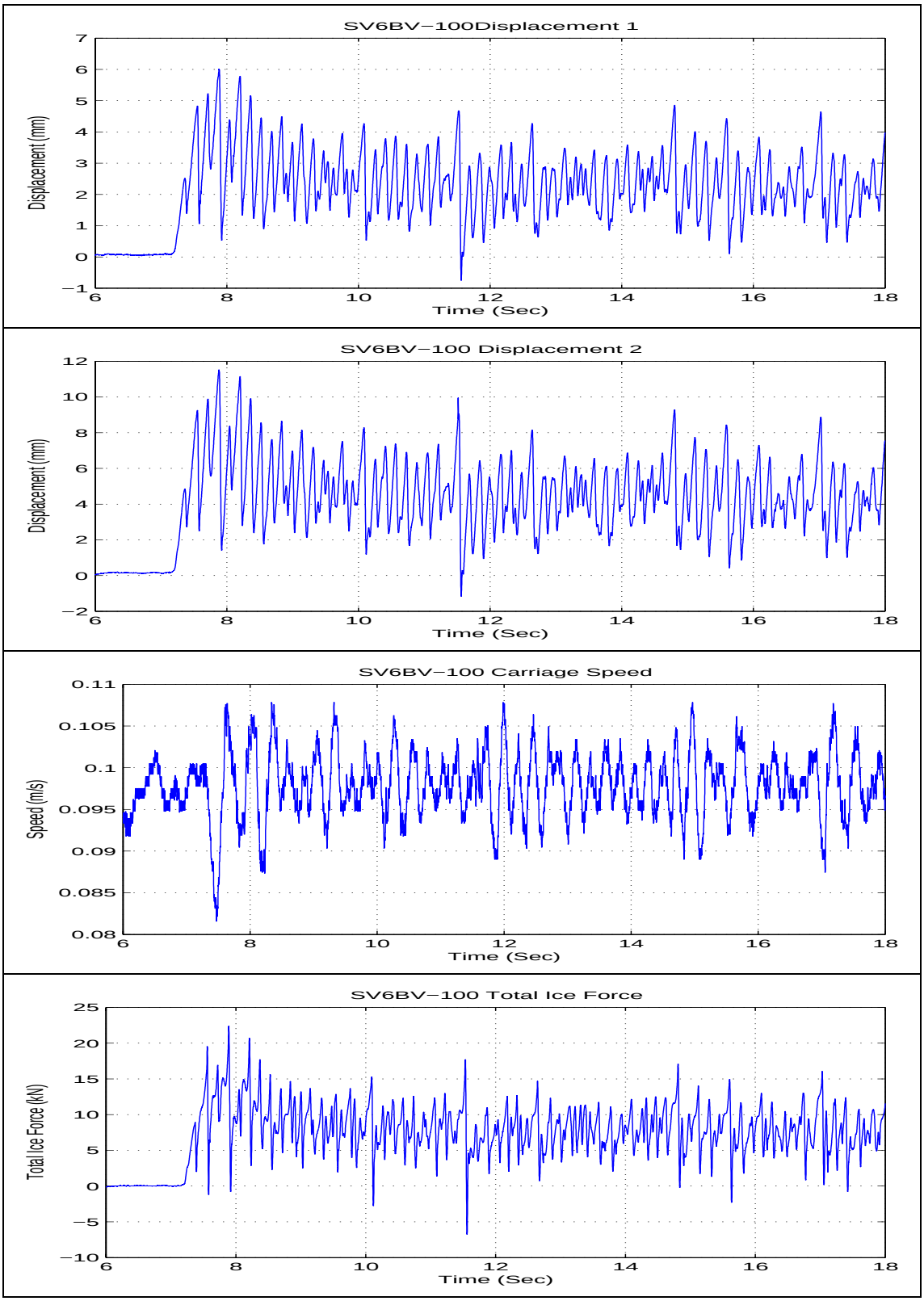

Test SV6BV-150

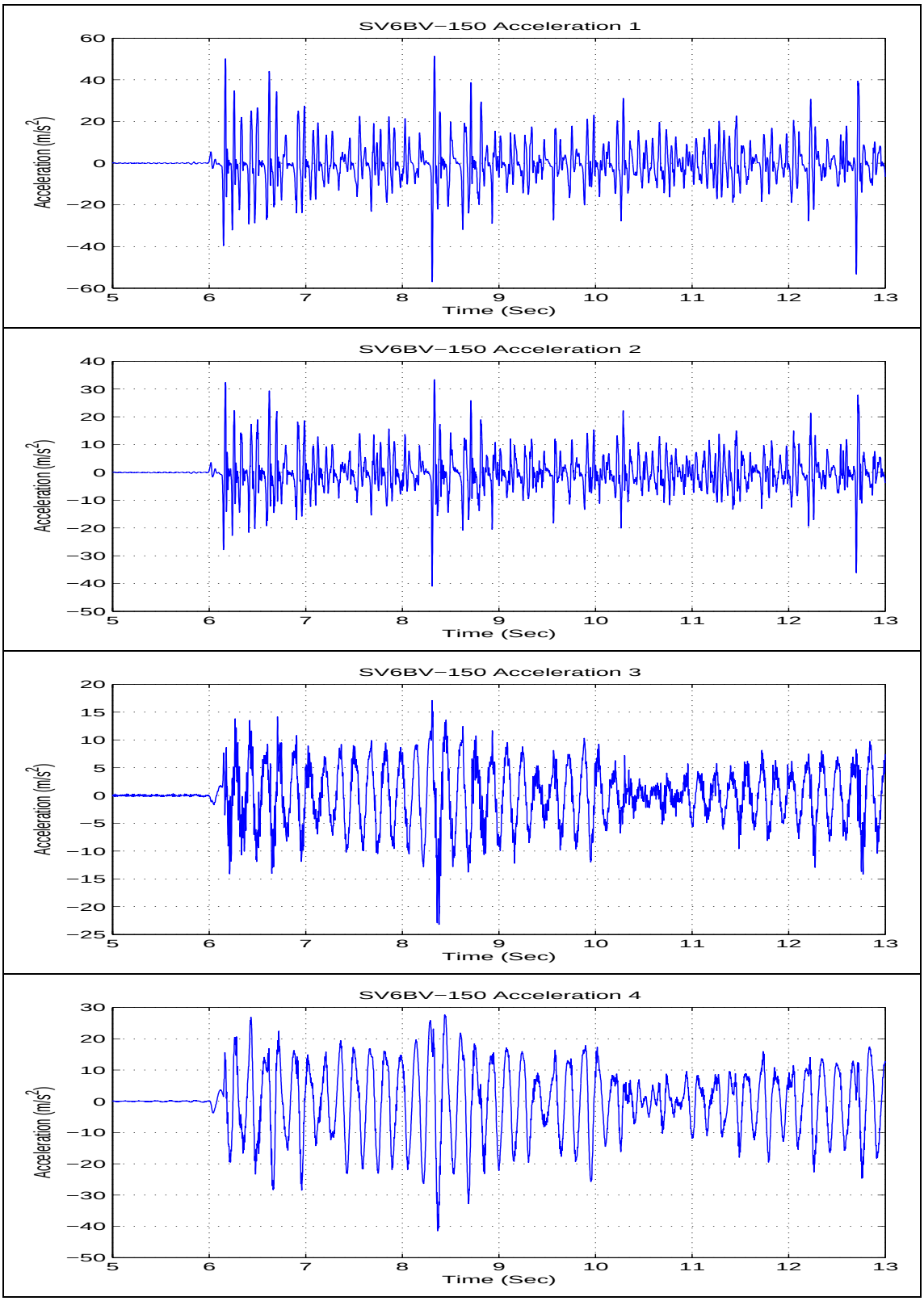

Test SV6BV-150

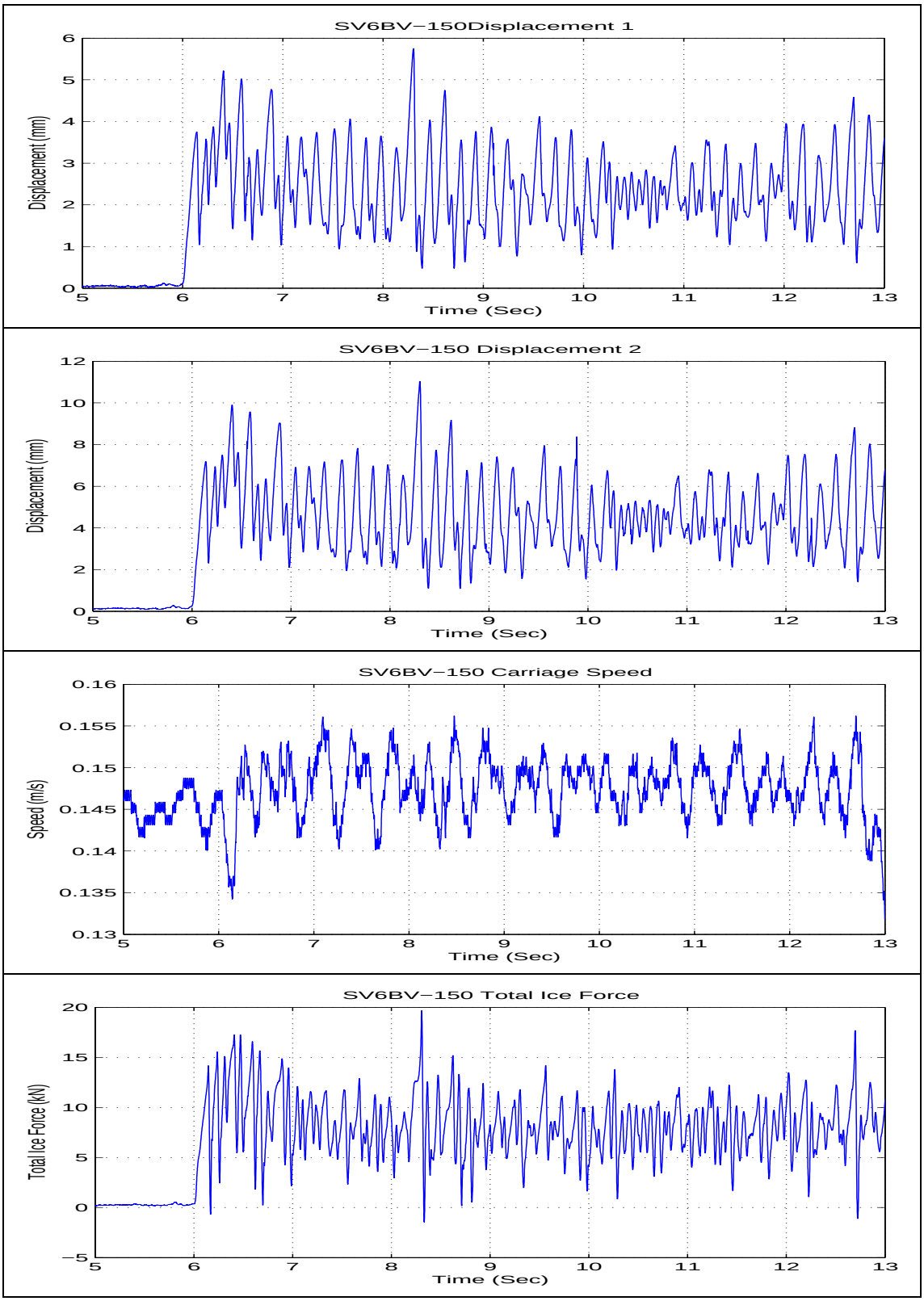

Test SV6BV-200

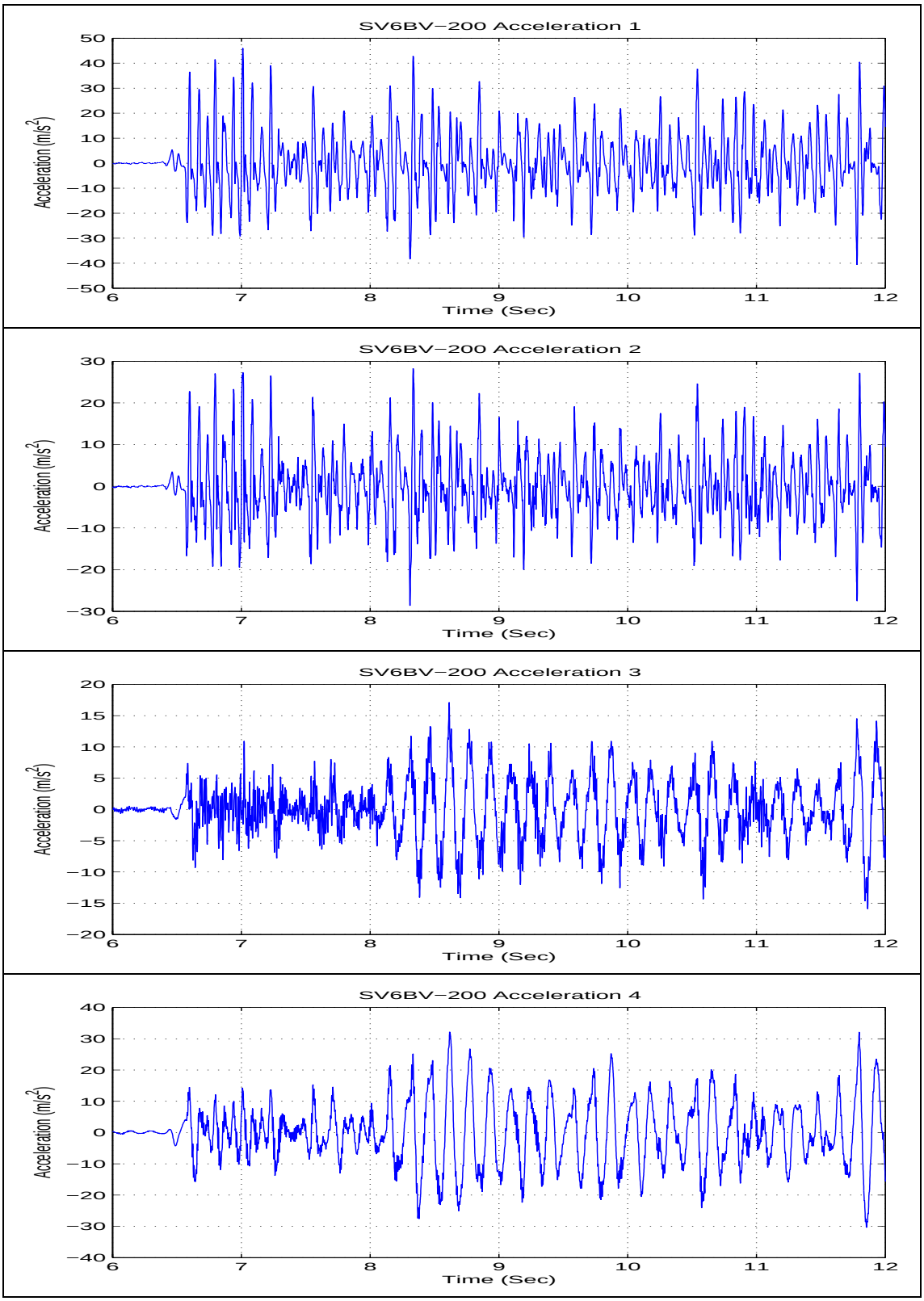

Test SV6BV-200

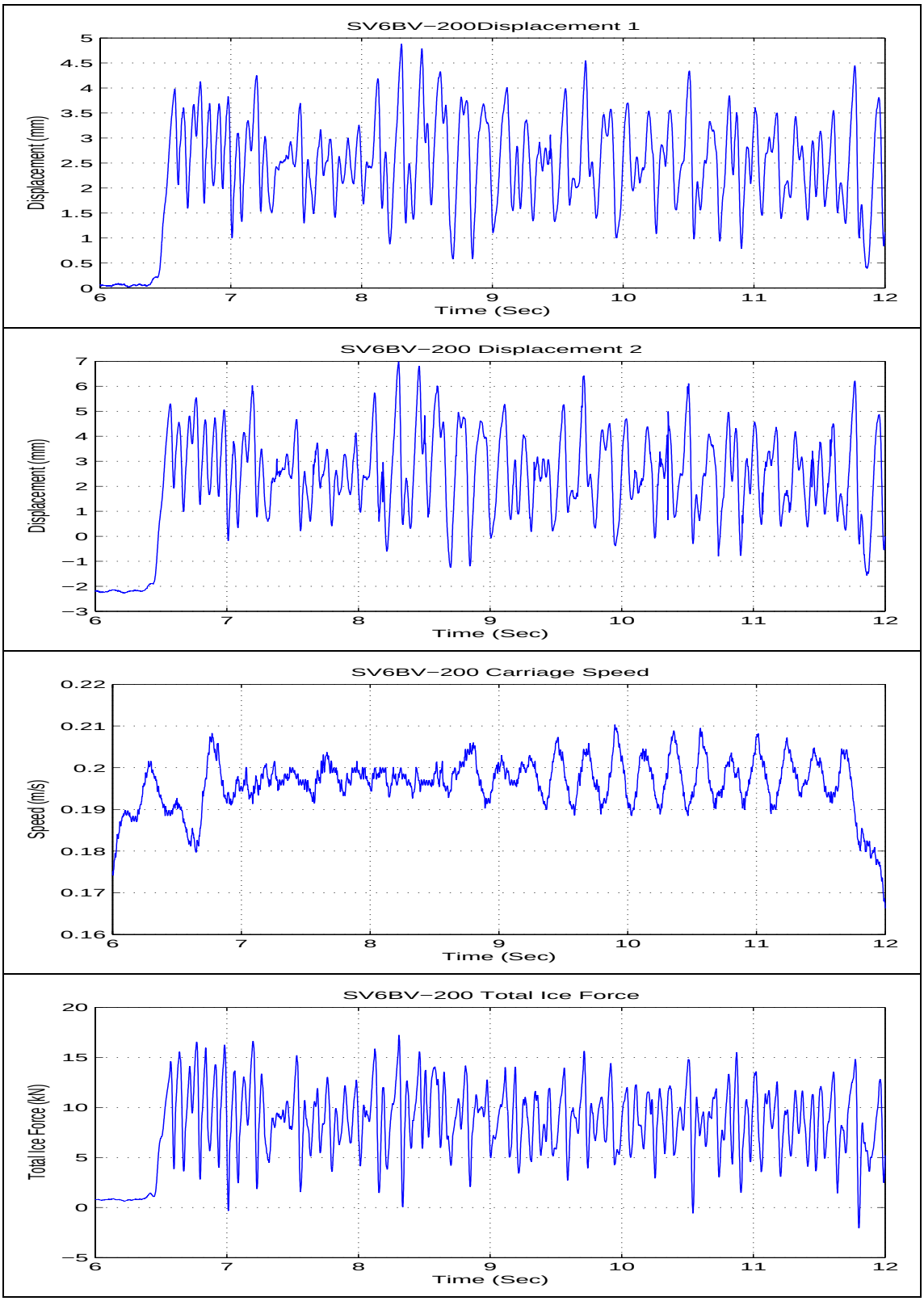

Test SV6BV-250

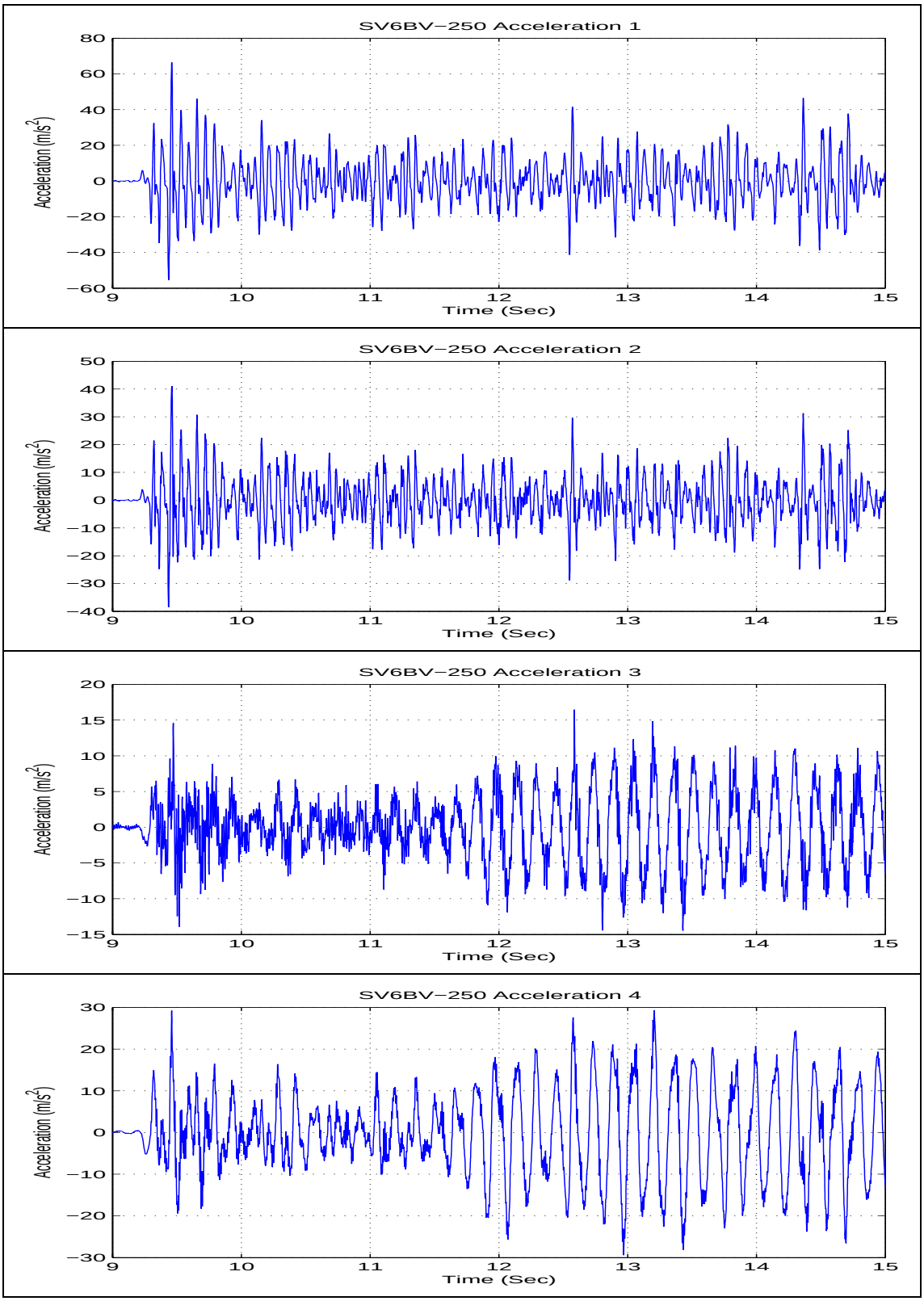

Test SV6BV-250

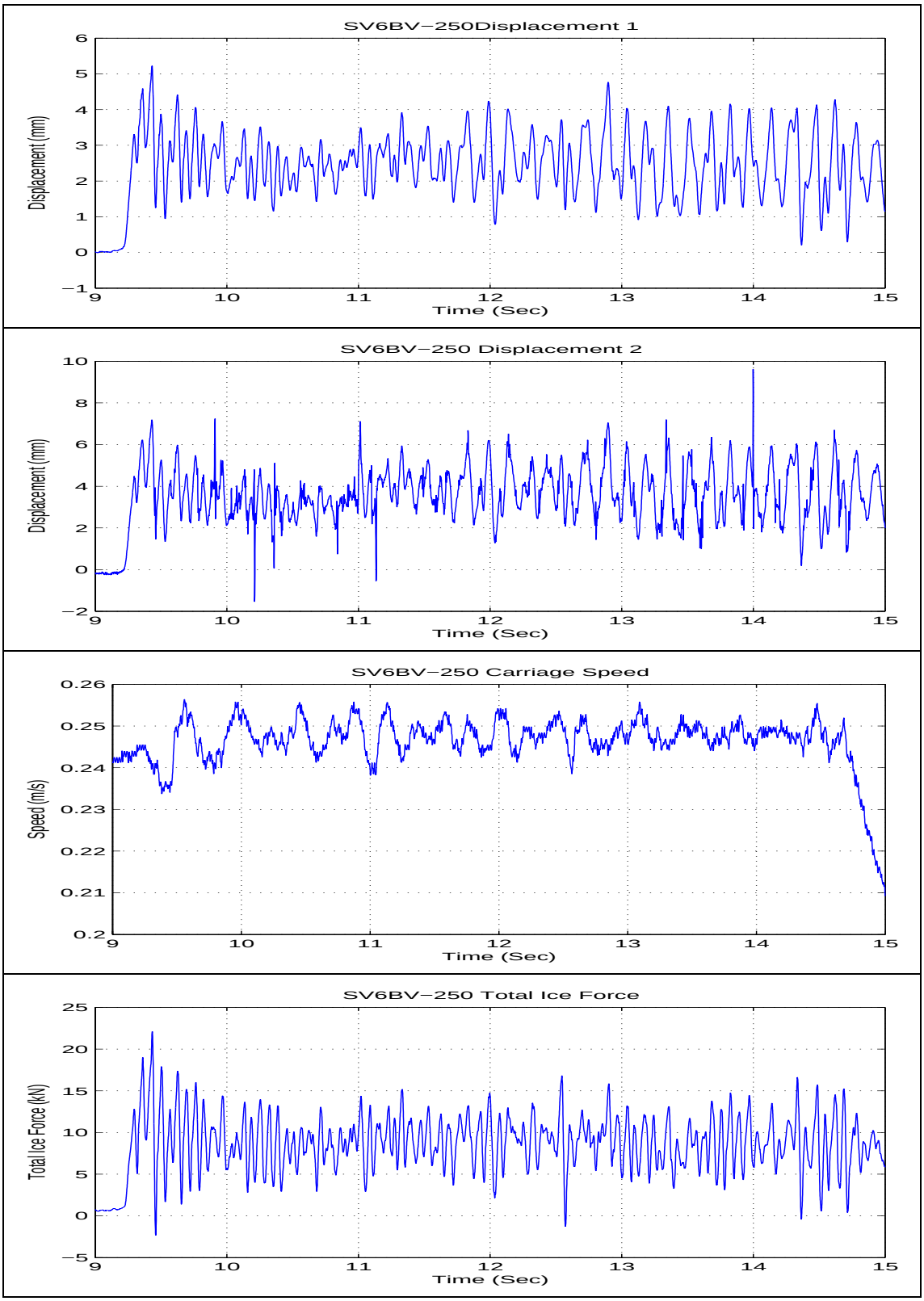

Test SV6BV-300

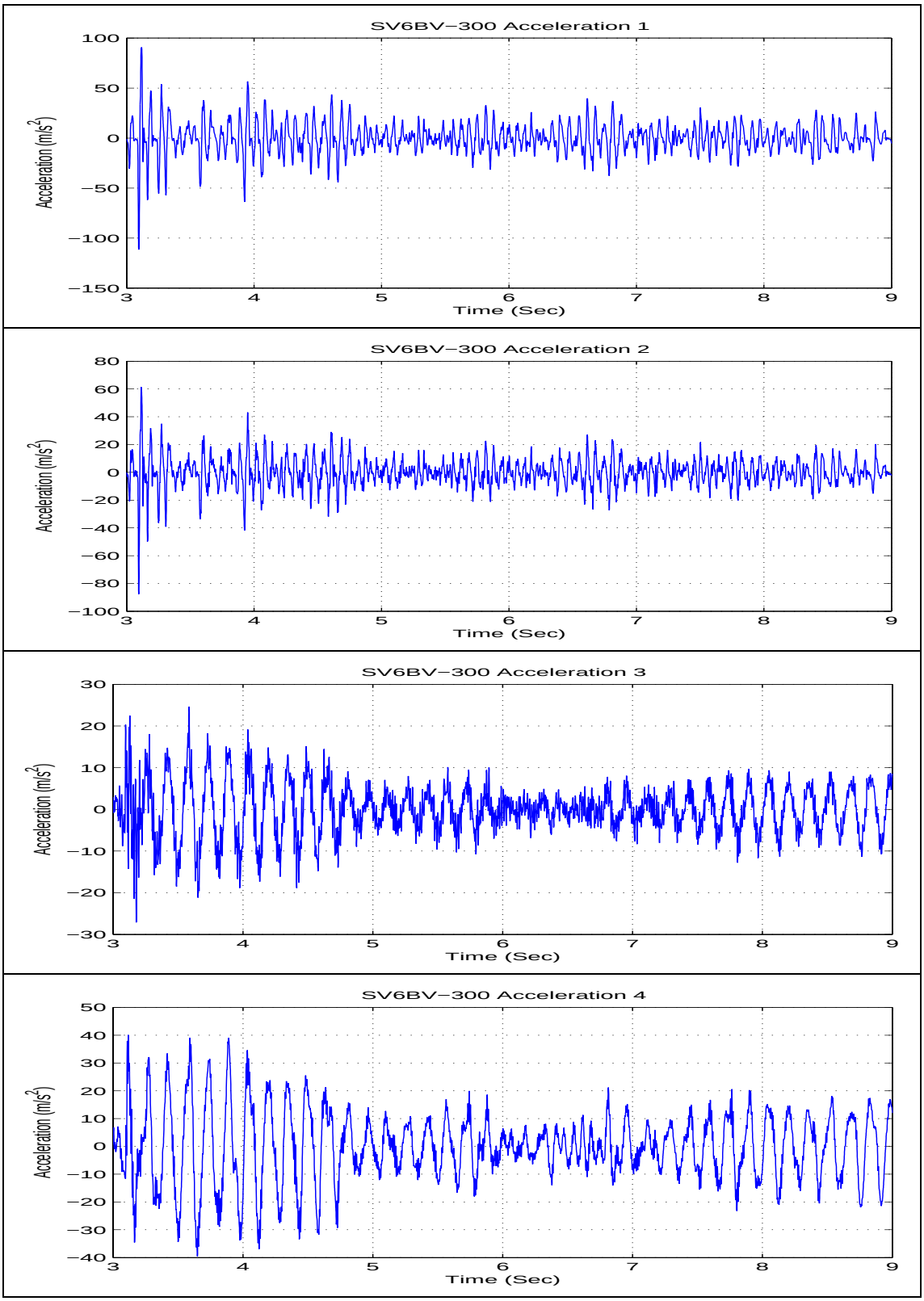

Test SV6BV-300

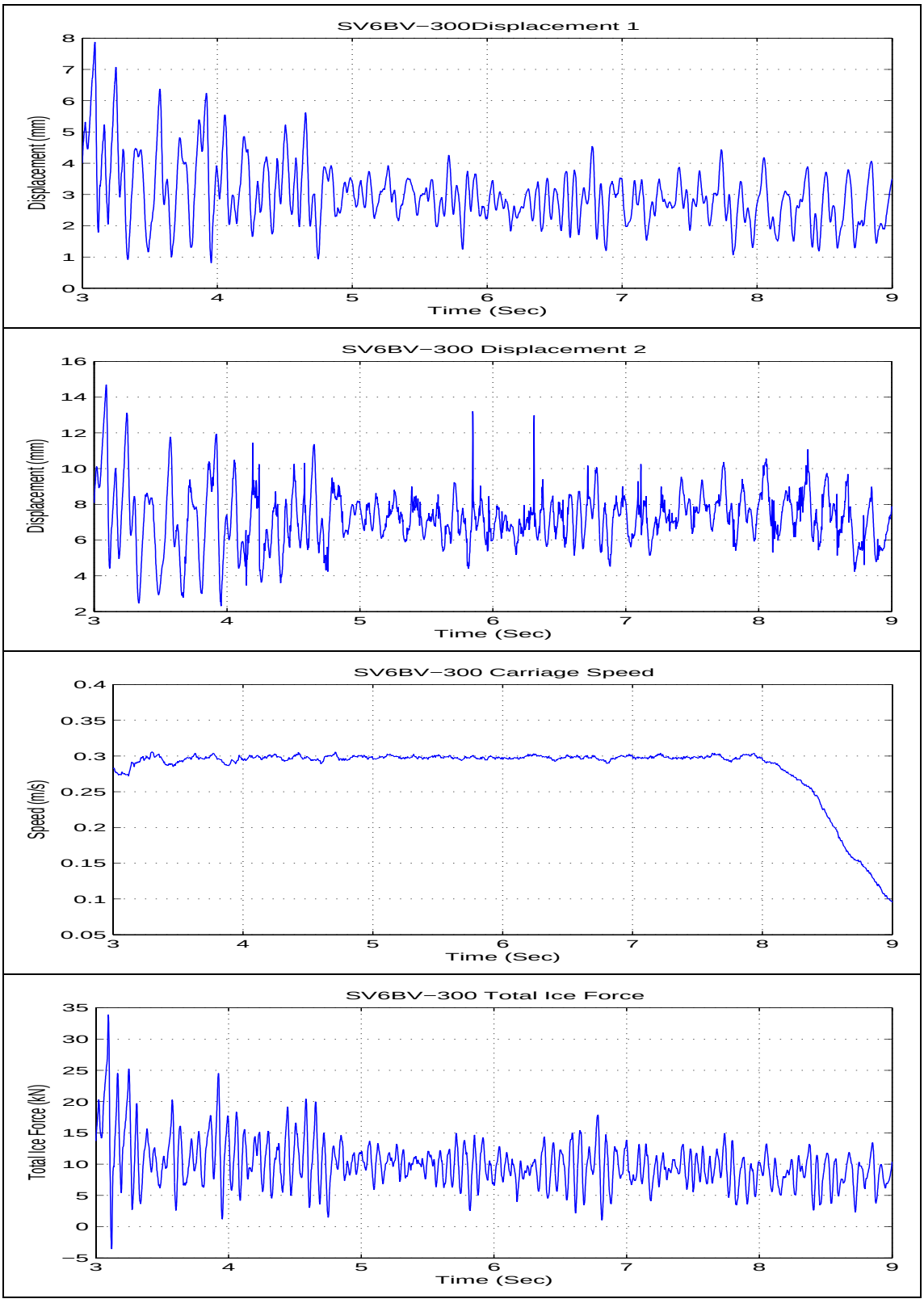

Test SV6BV-350

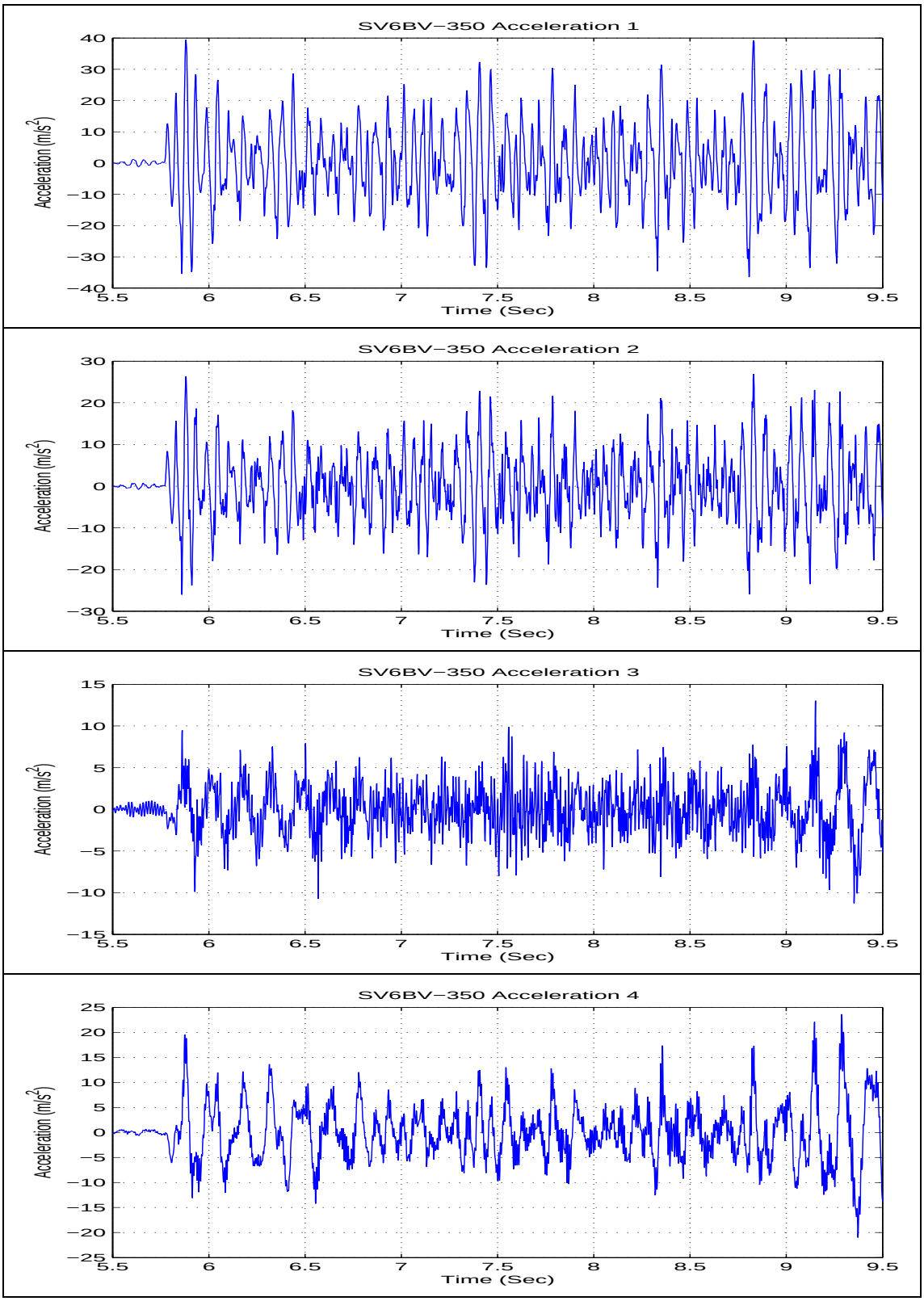

Test SV6BV-350

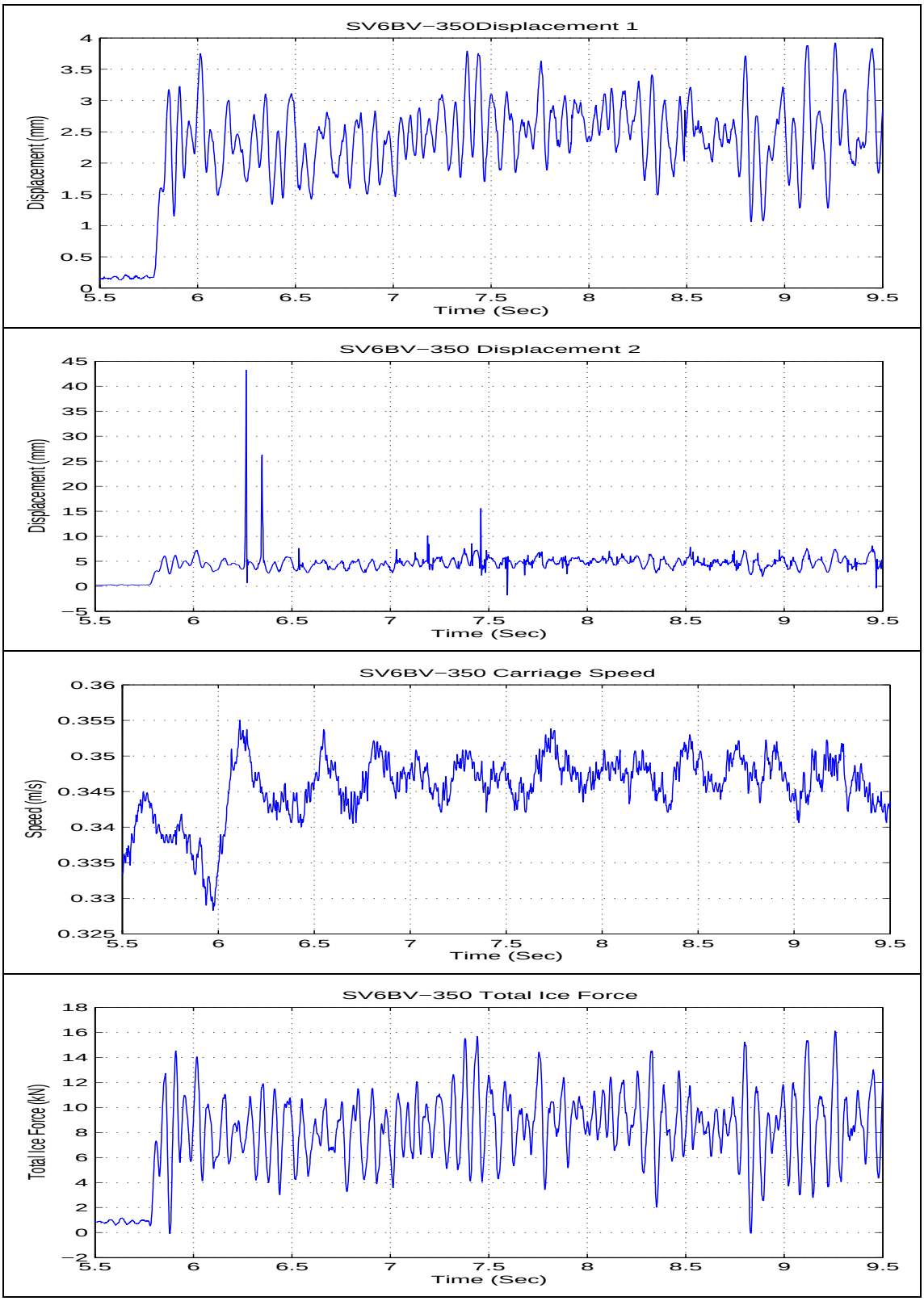

Test SV6BV-400

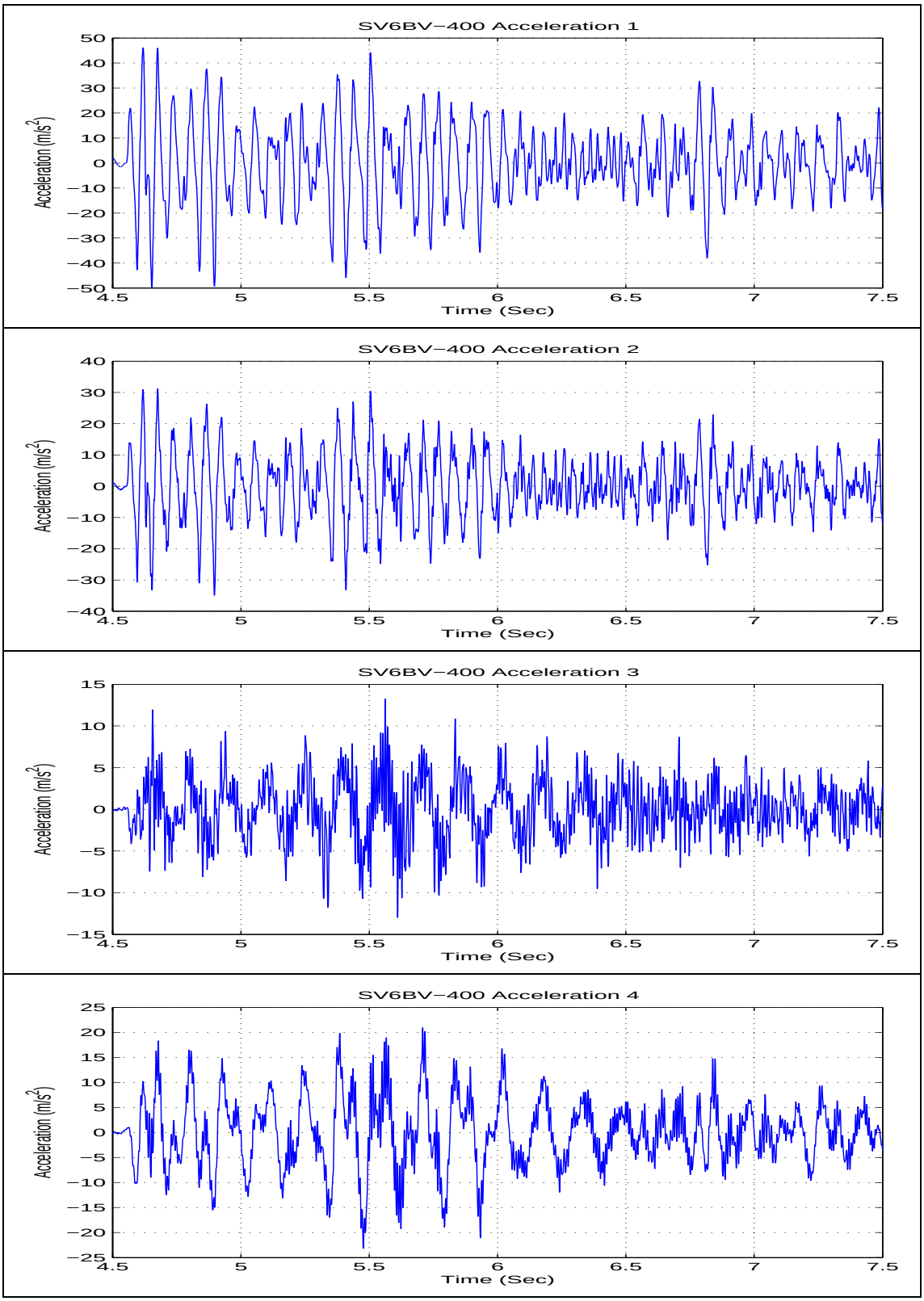

Test SV6BV-400

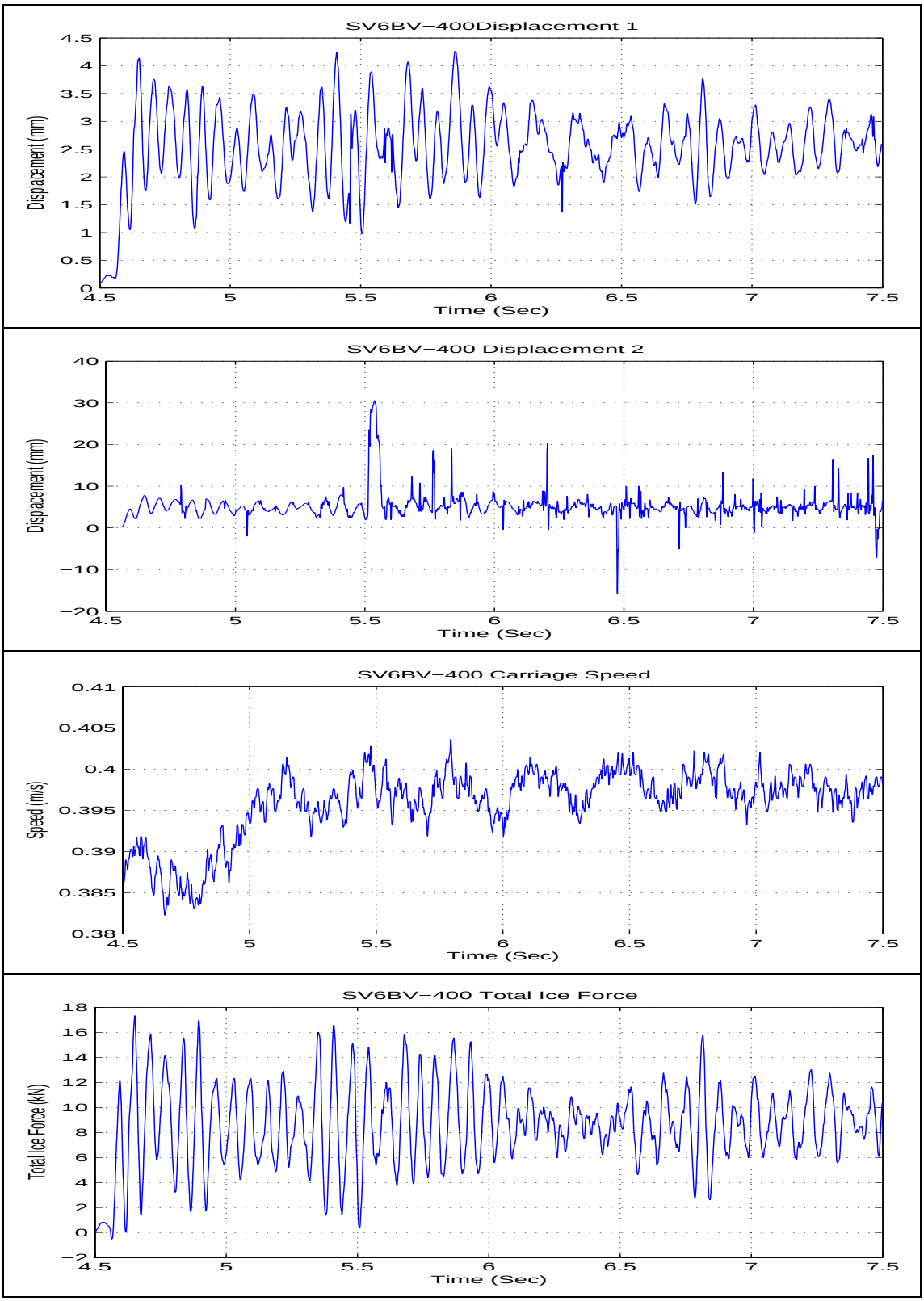

Test SV6BV-450

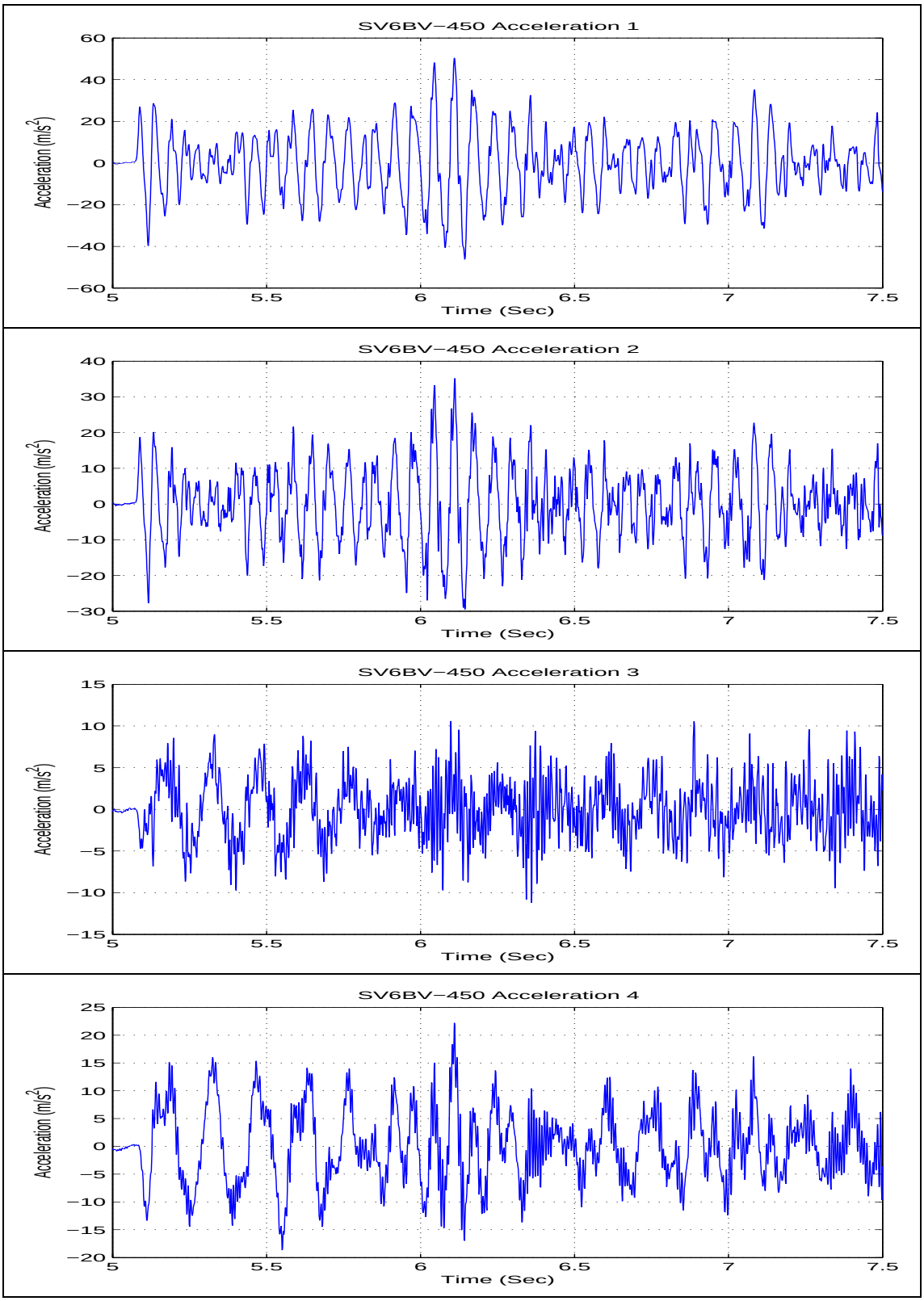

Test SV6BV-450

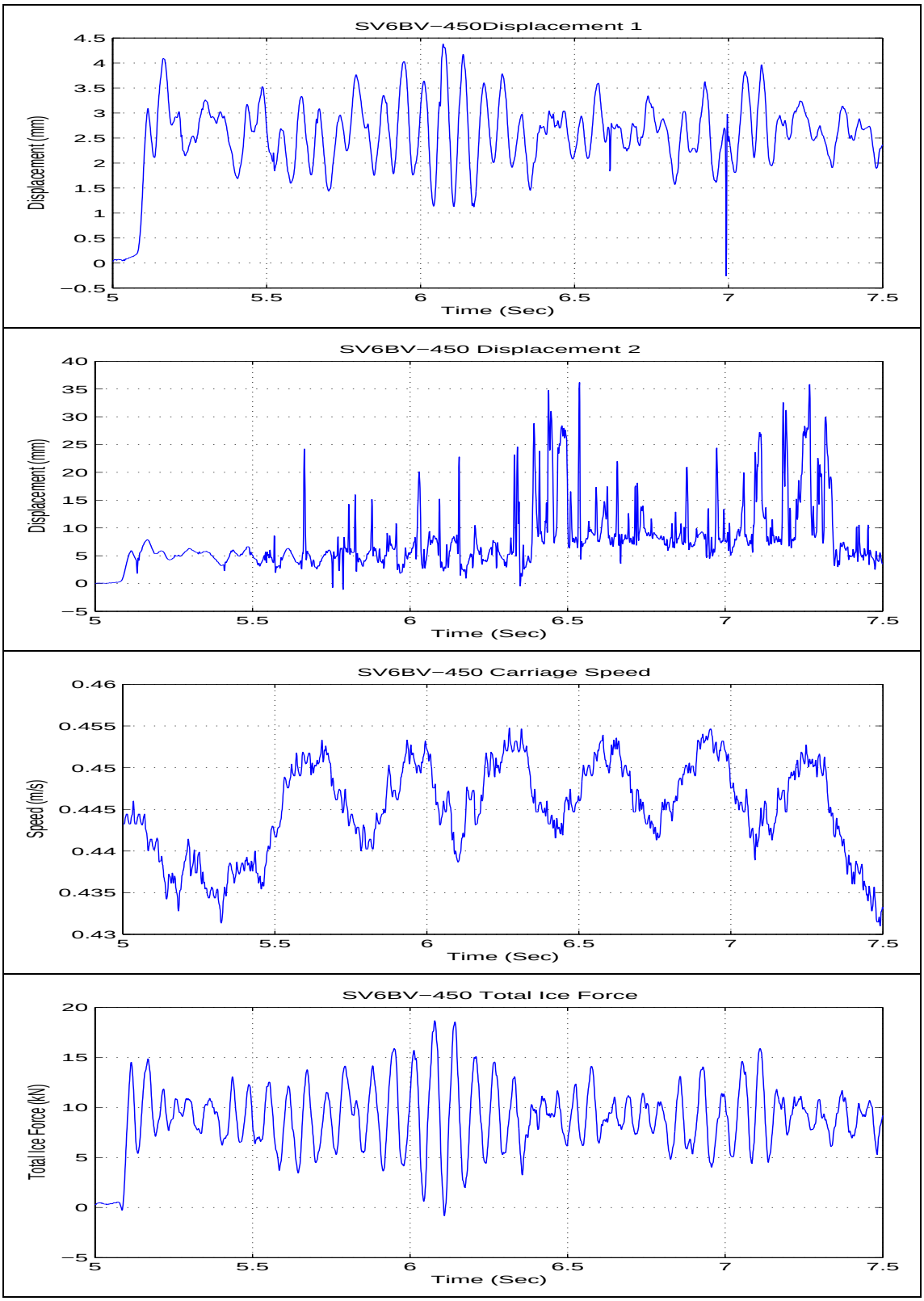

Test SV6BV-500

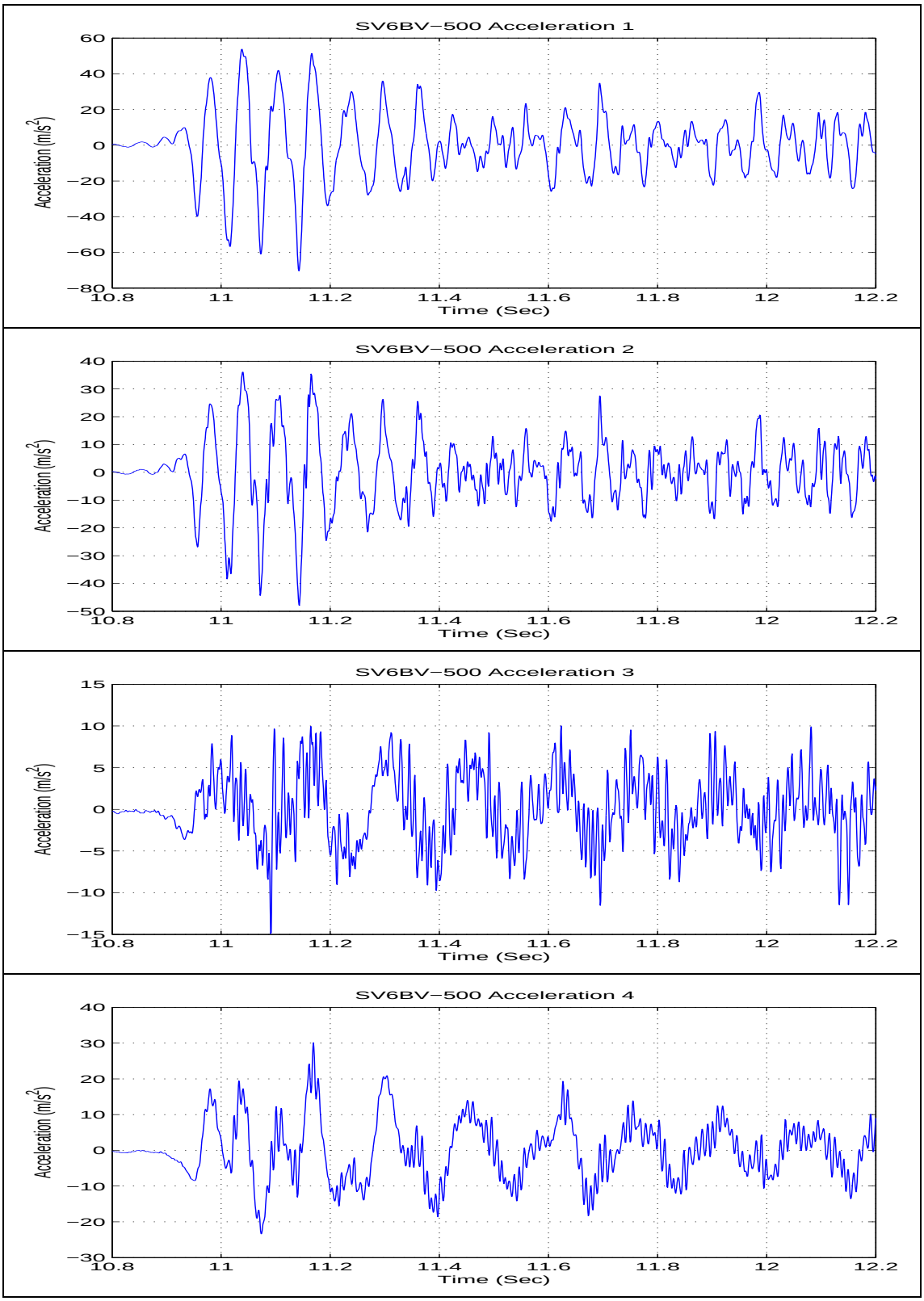

Test SV6BV-500

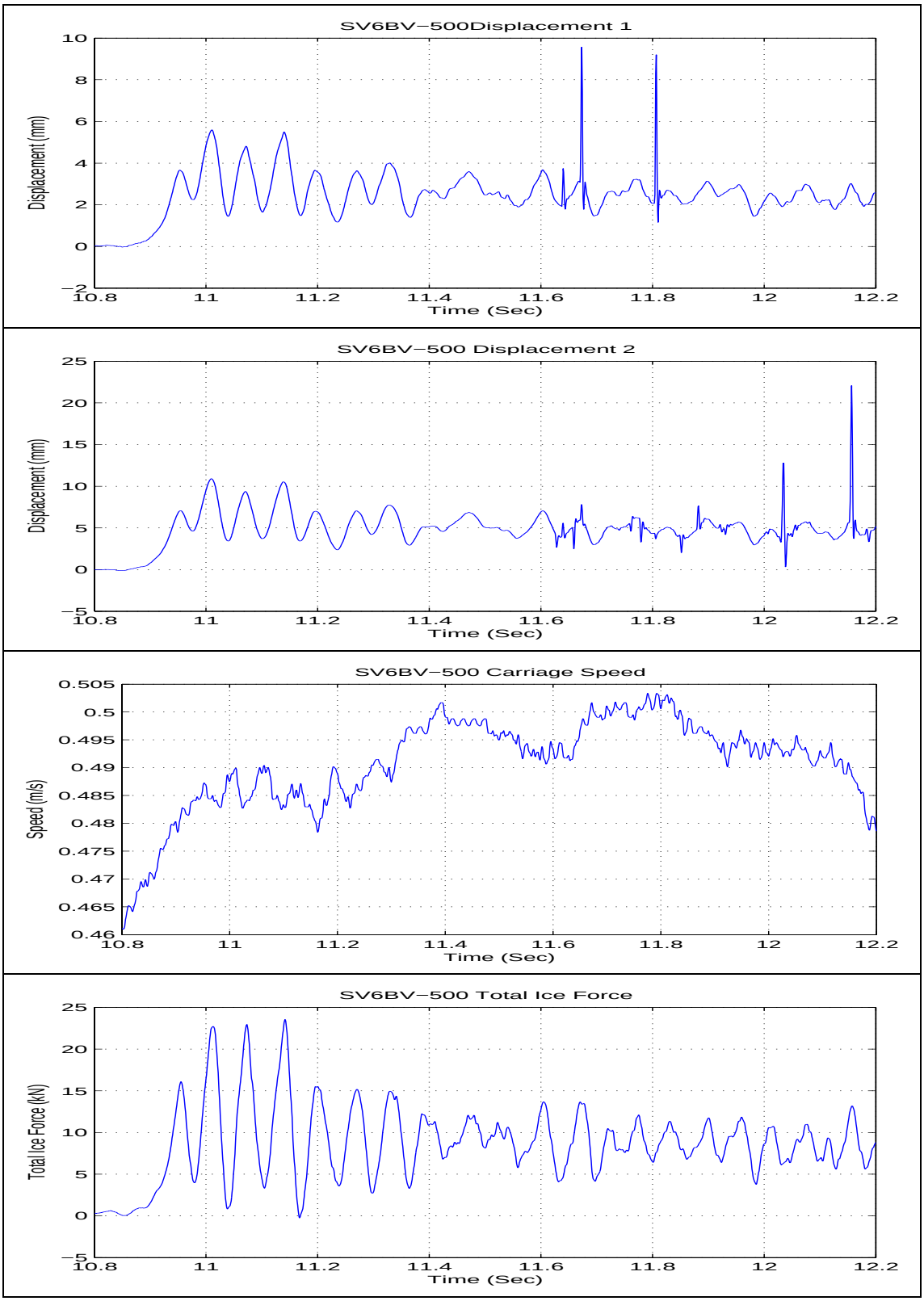

Test SV6BV-600

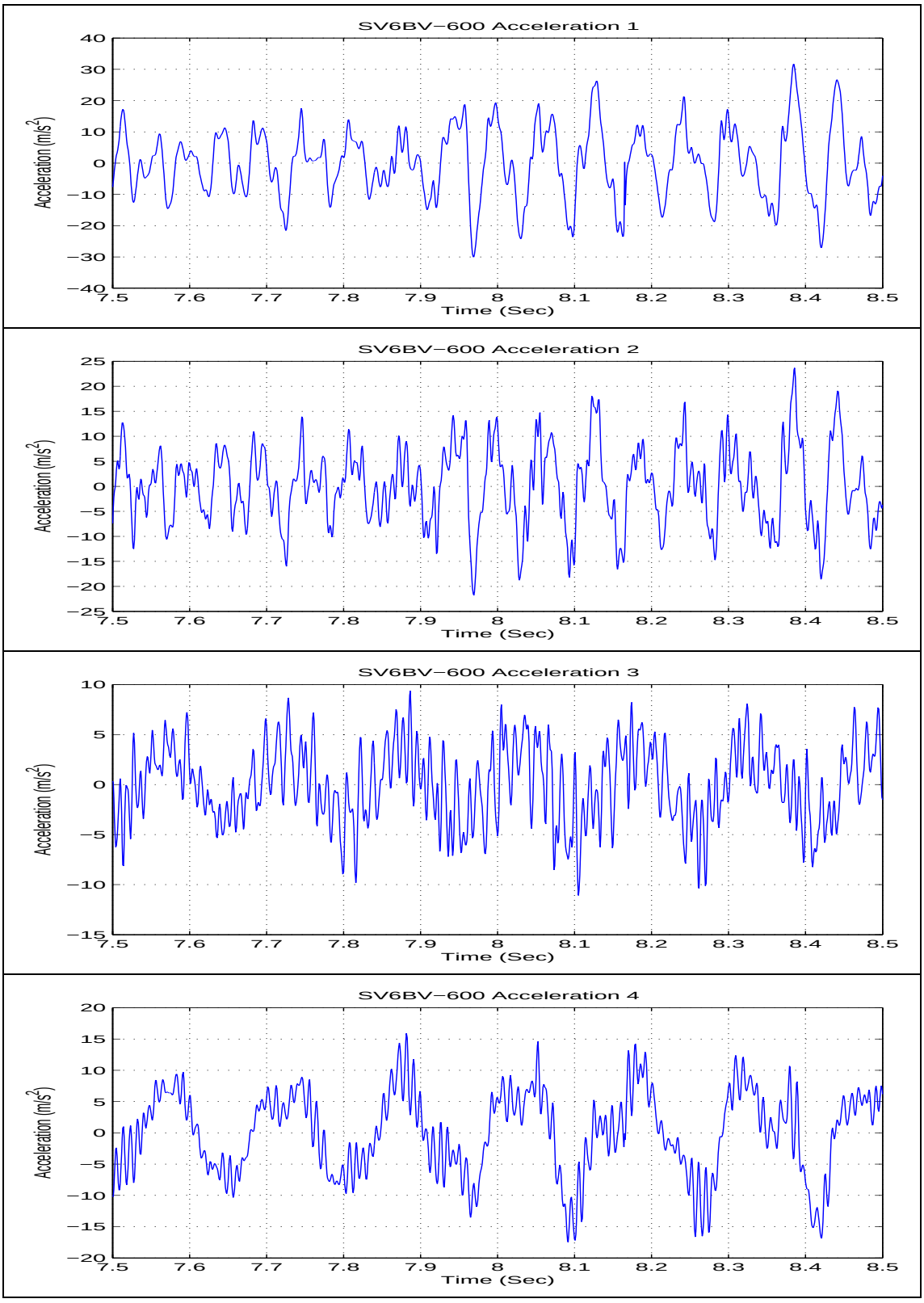

Test SV6BV-600

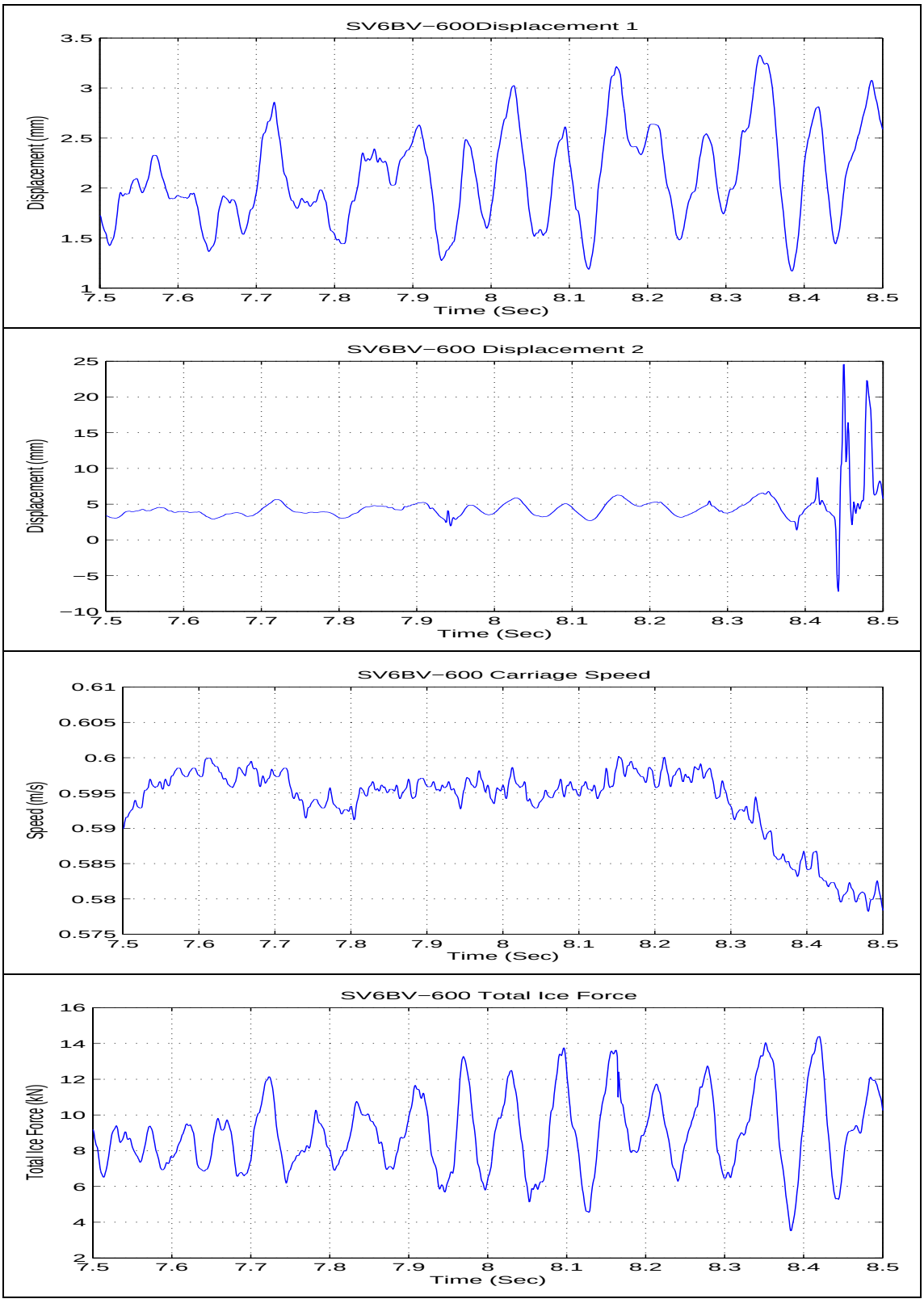

Test SV7V-SW1-048

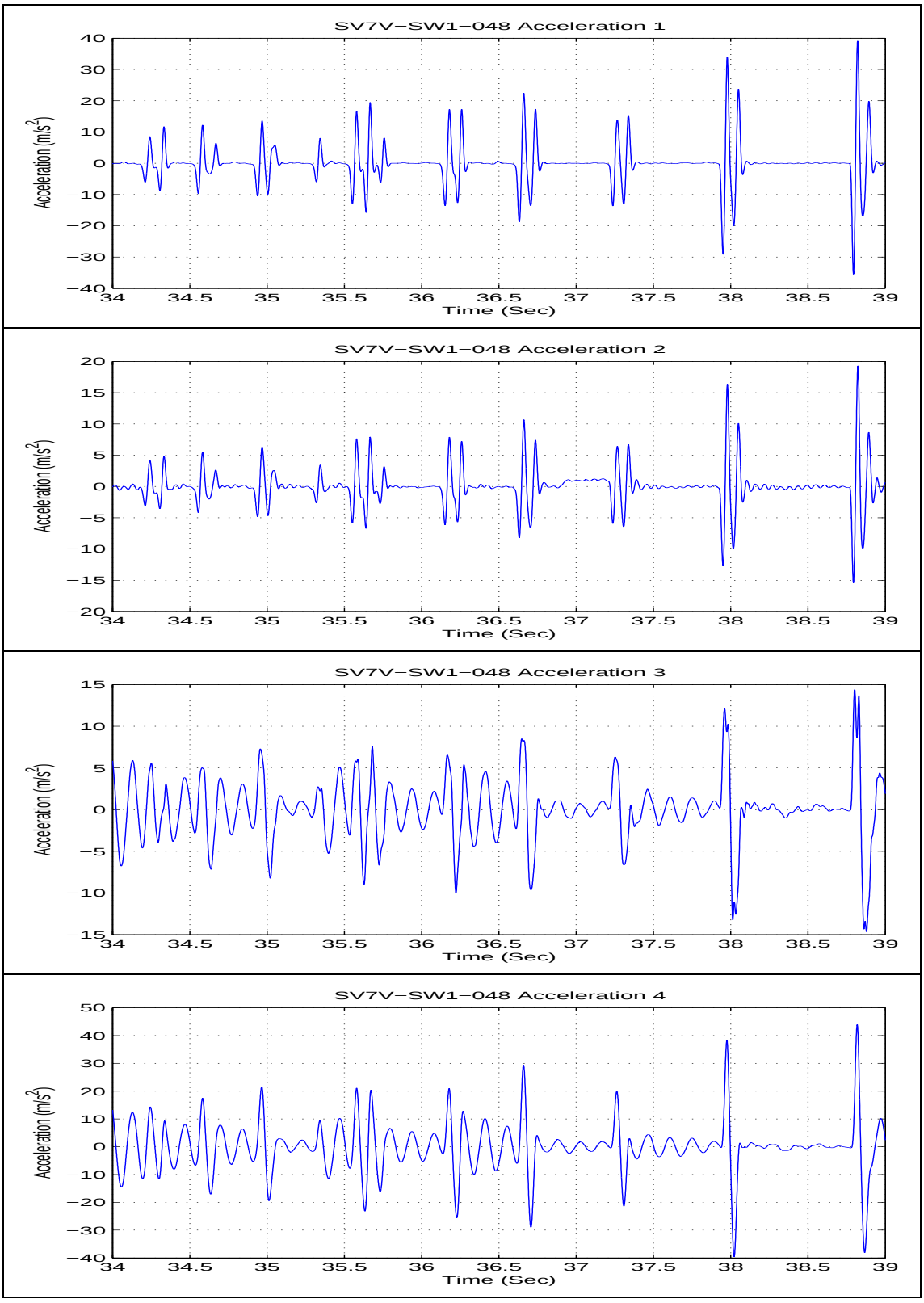

Test SV7V-SW1-048

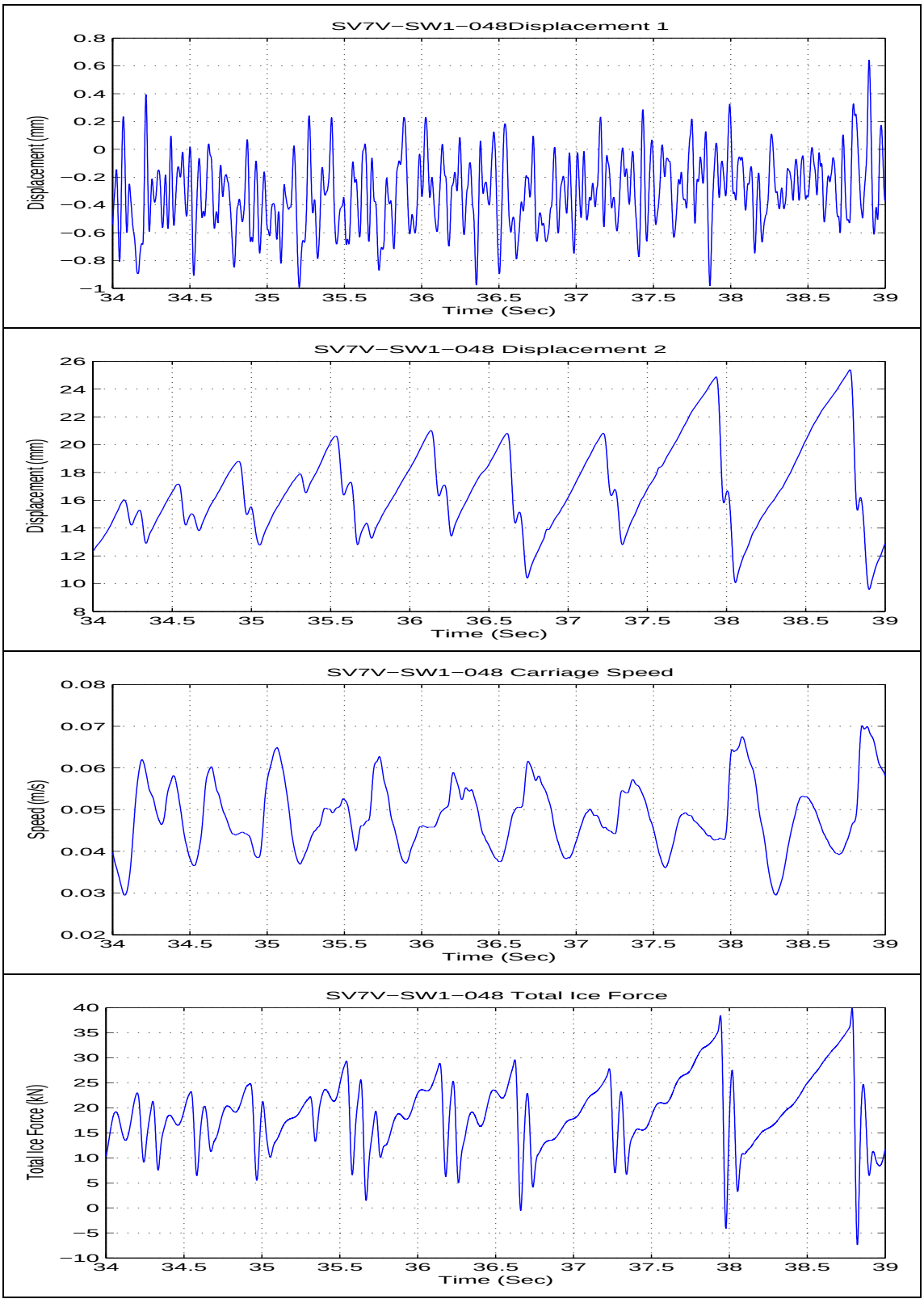

Test SV7V-SW1-108

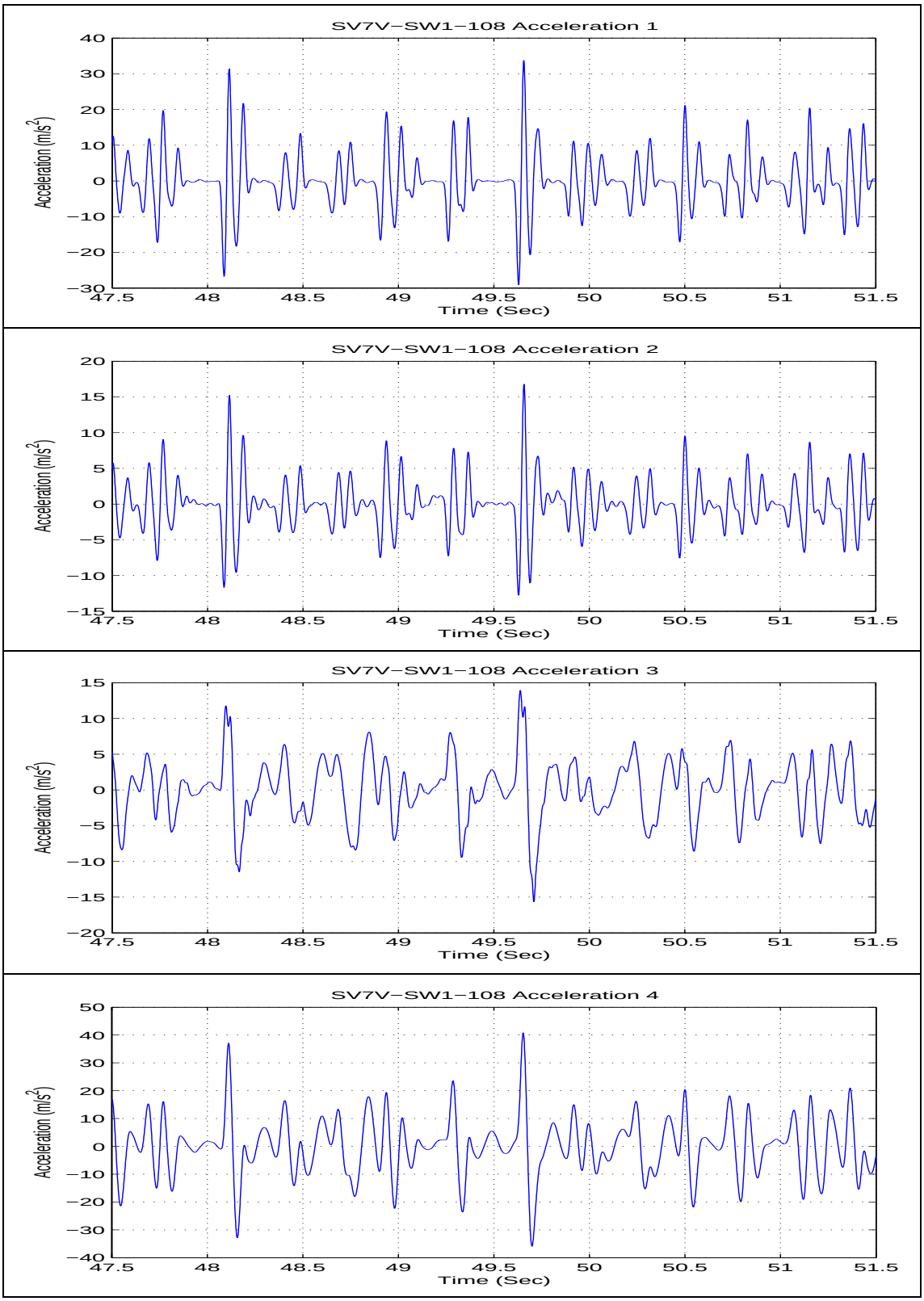

Test SV7V-SW1-108

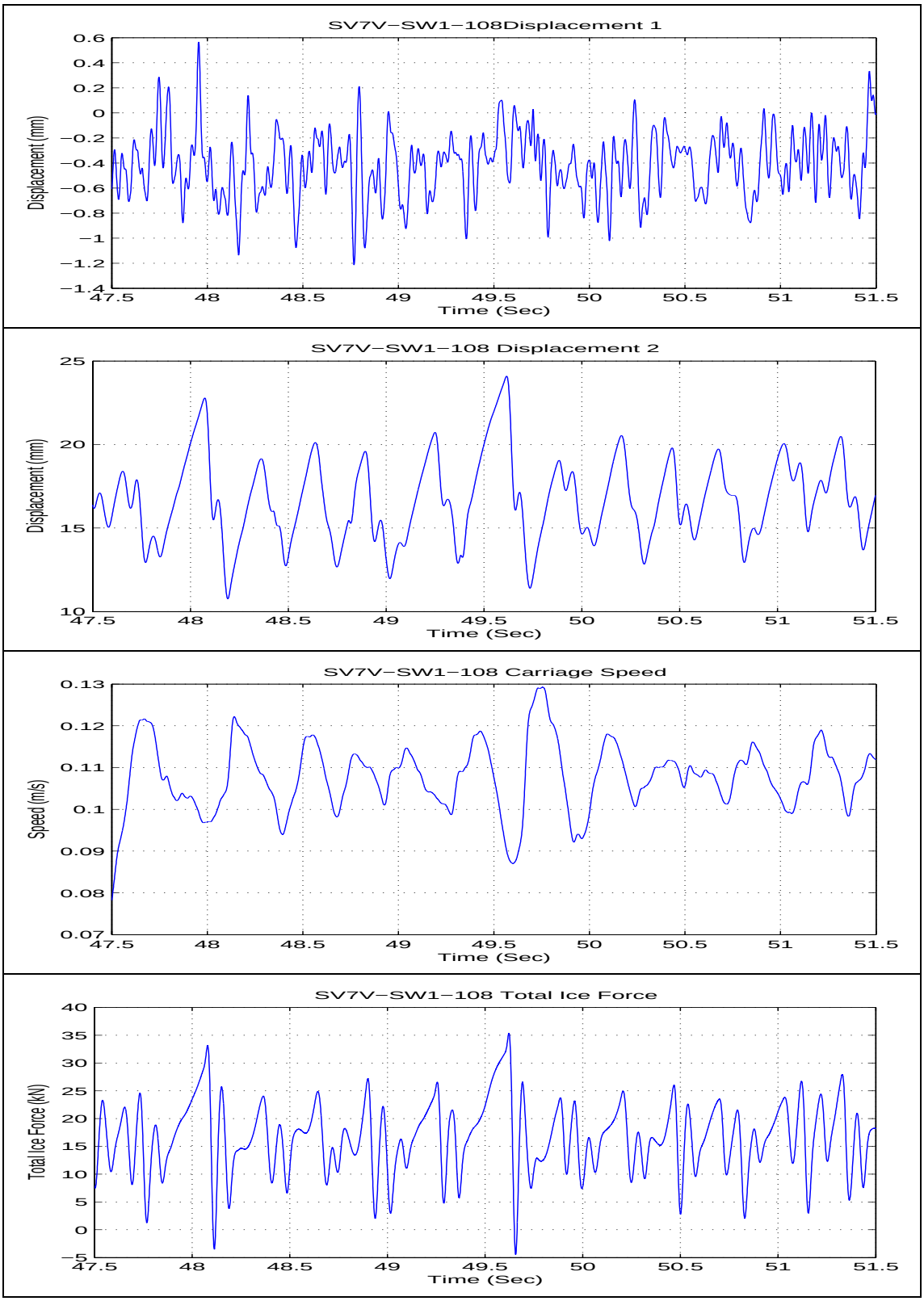

Test SV7V-SW2-168

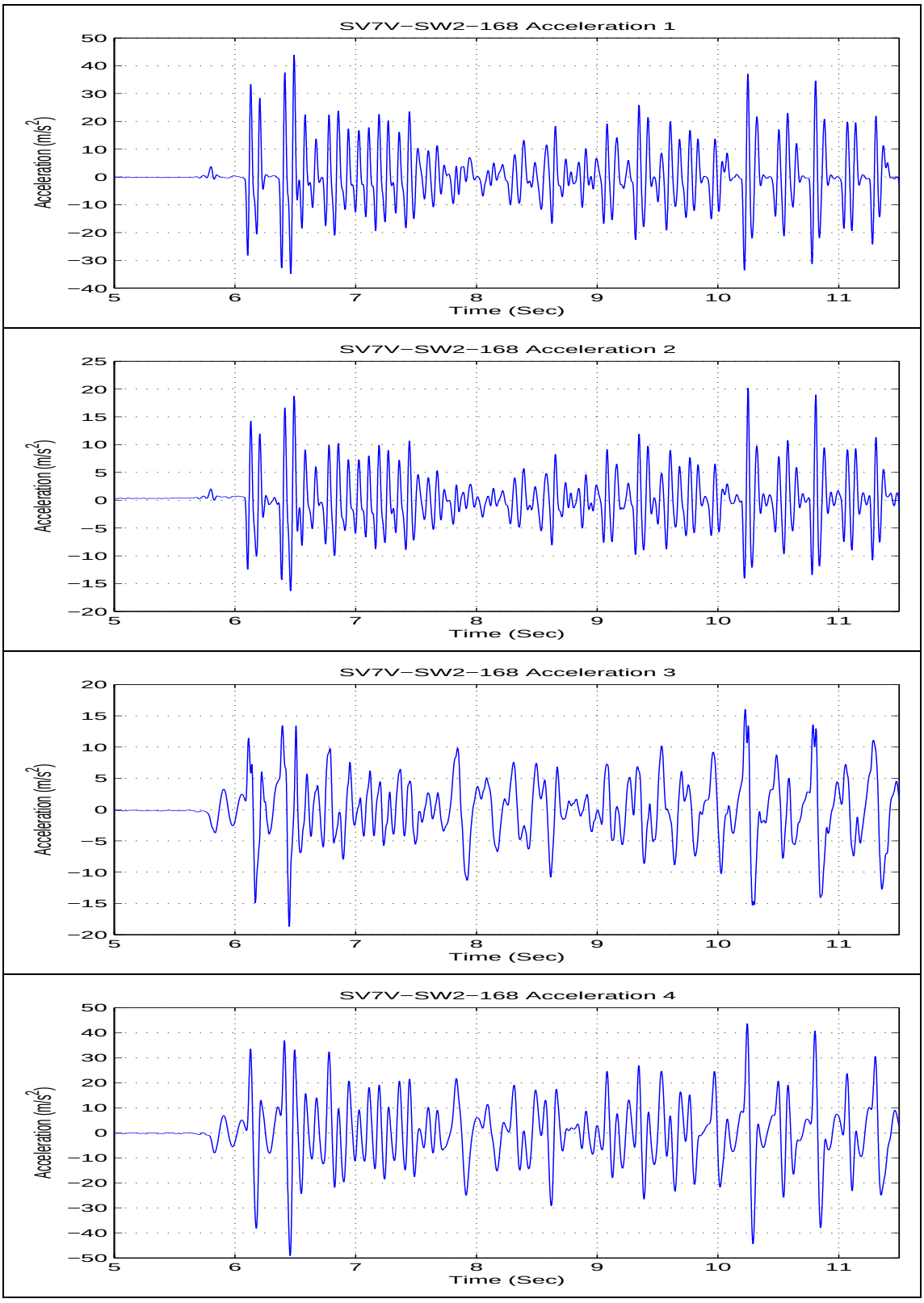

Test SV7V-SW2-168

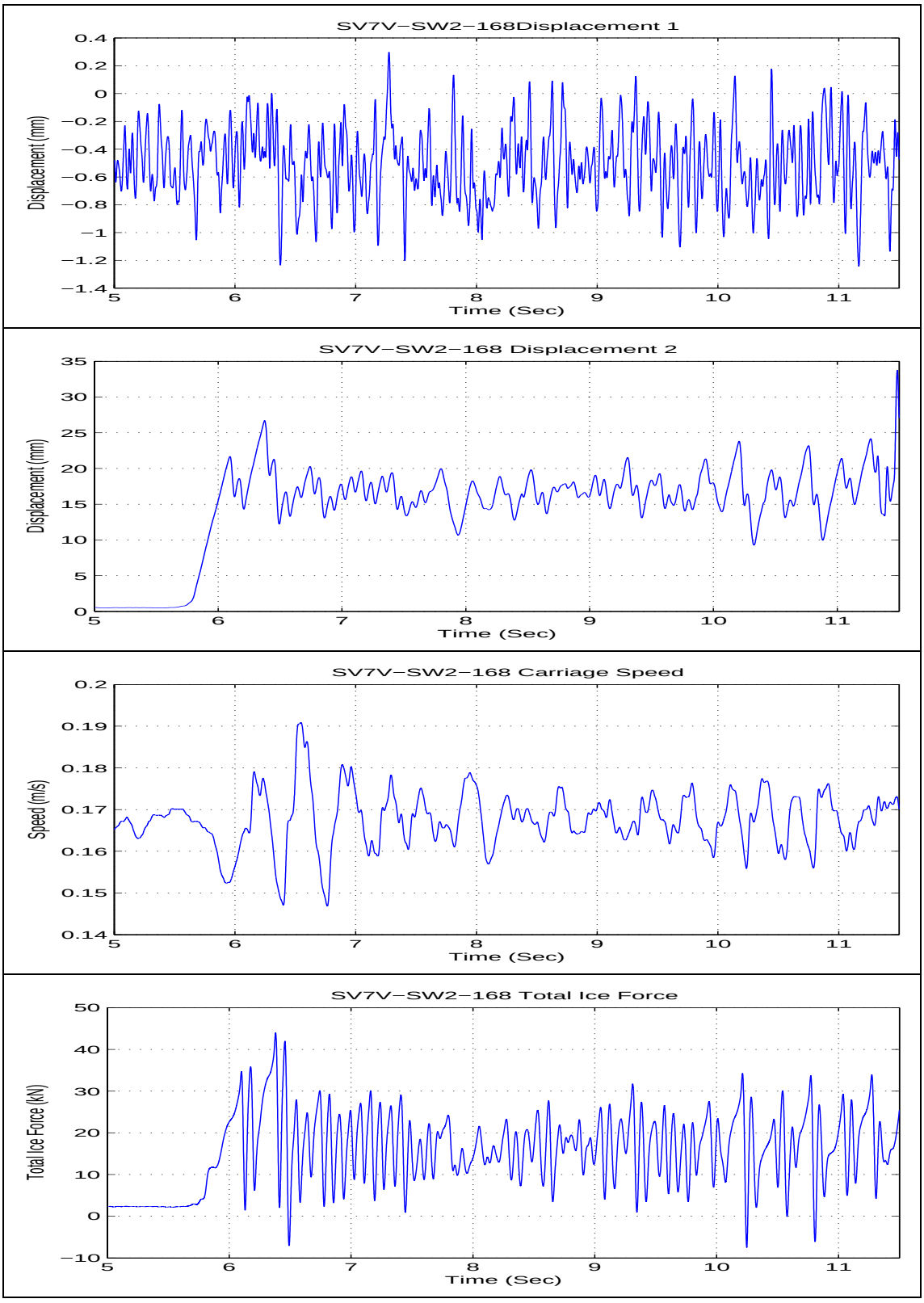

Test SV7V-SW2-228

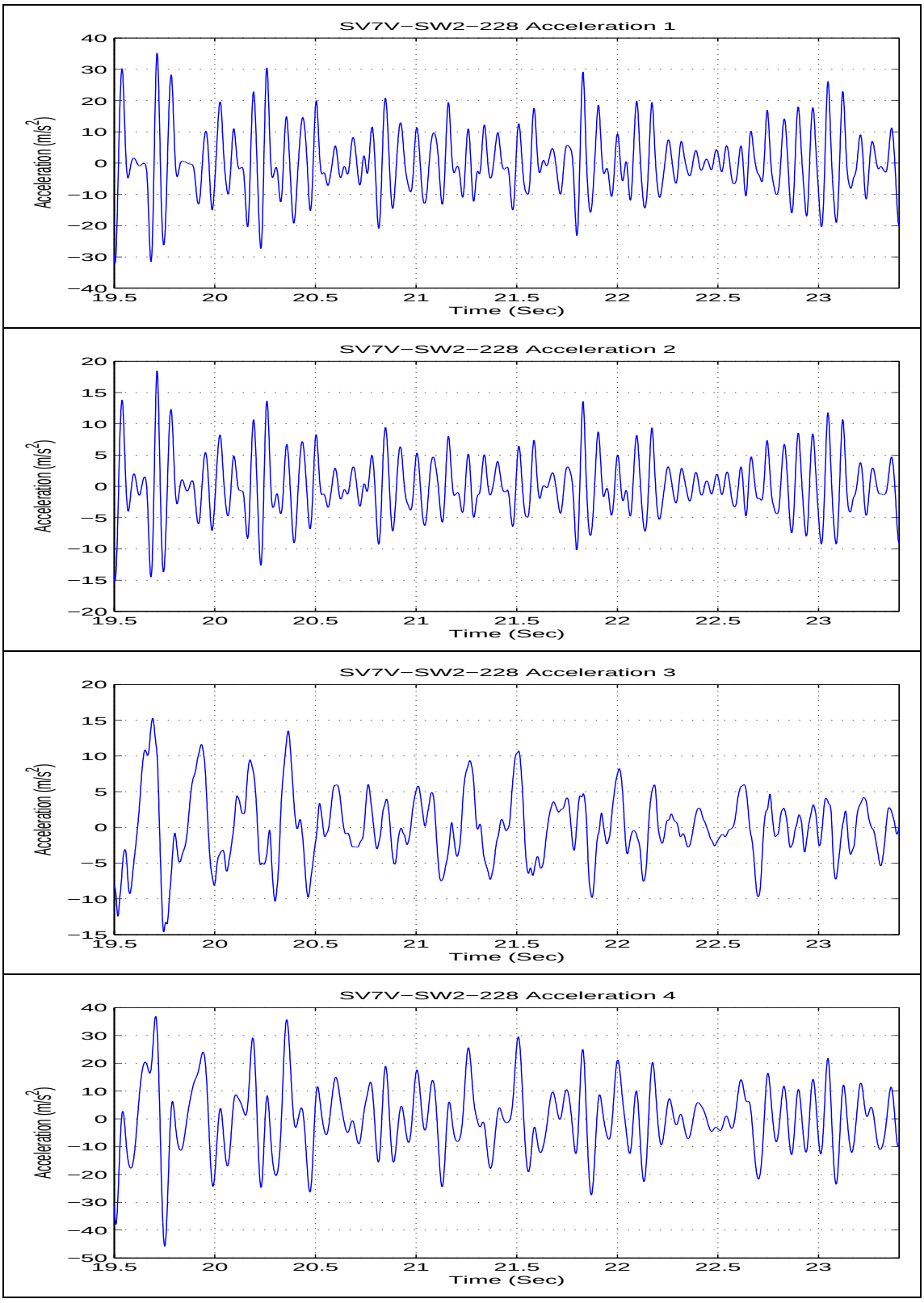

Test SV7V-SW2-228

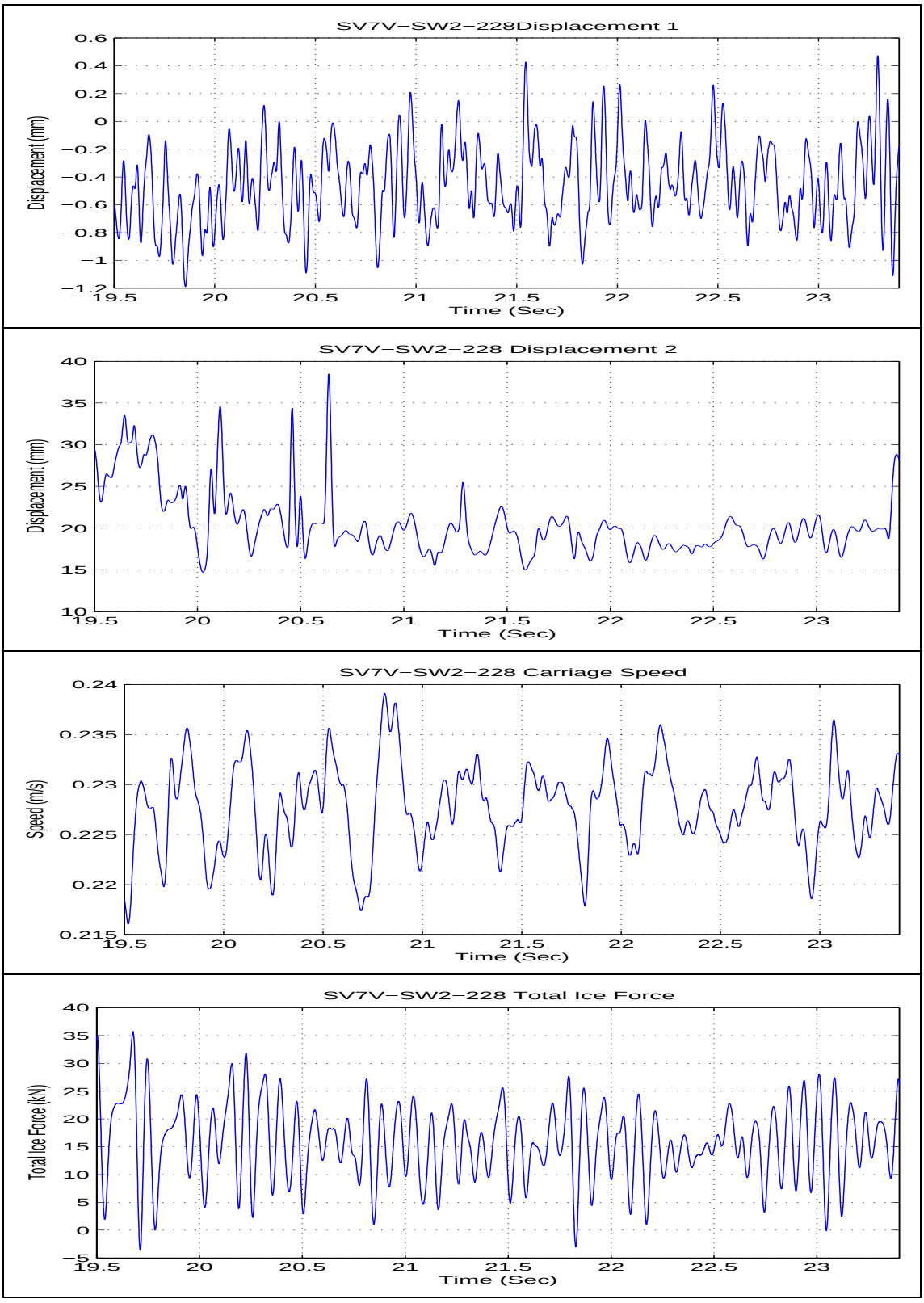

Test SV7V-SW3-298

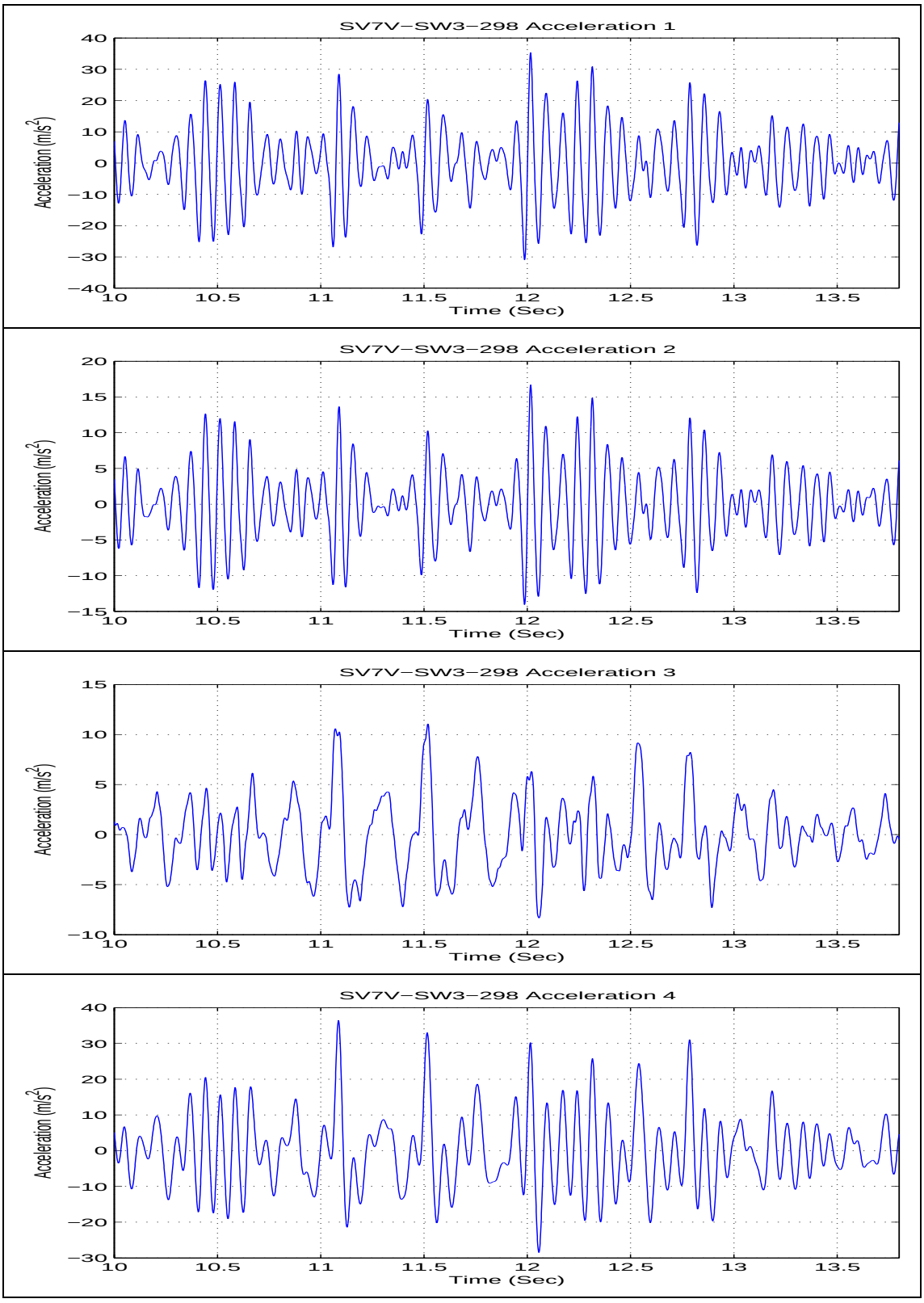

Test SV7V-SW3-298

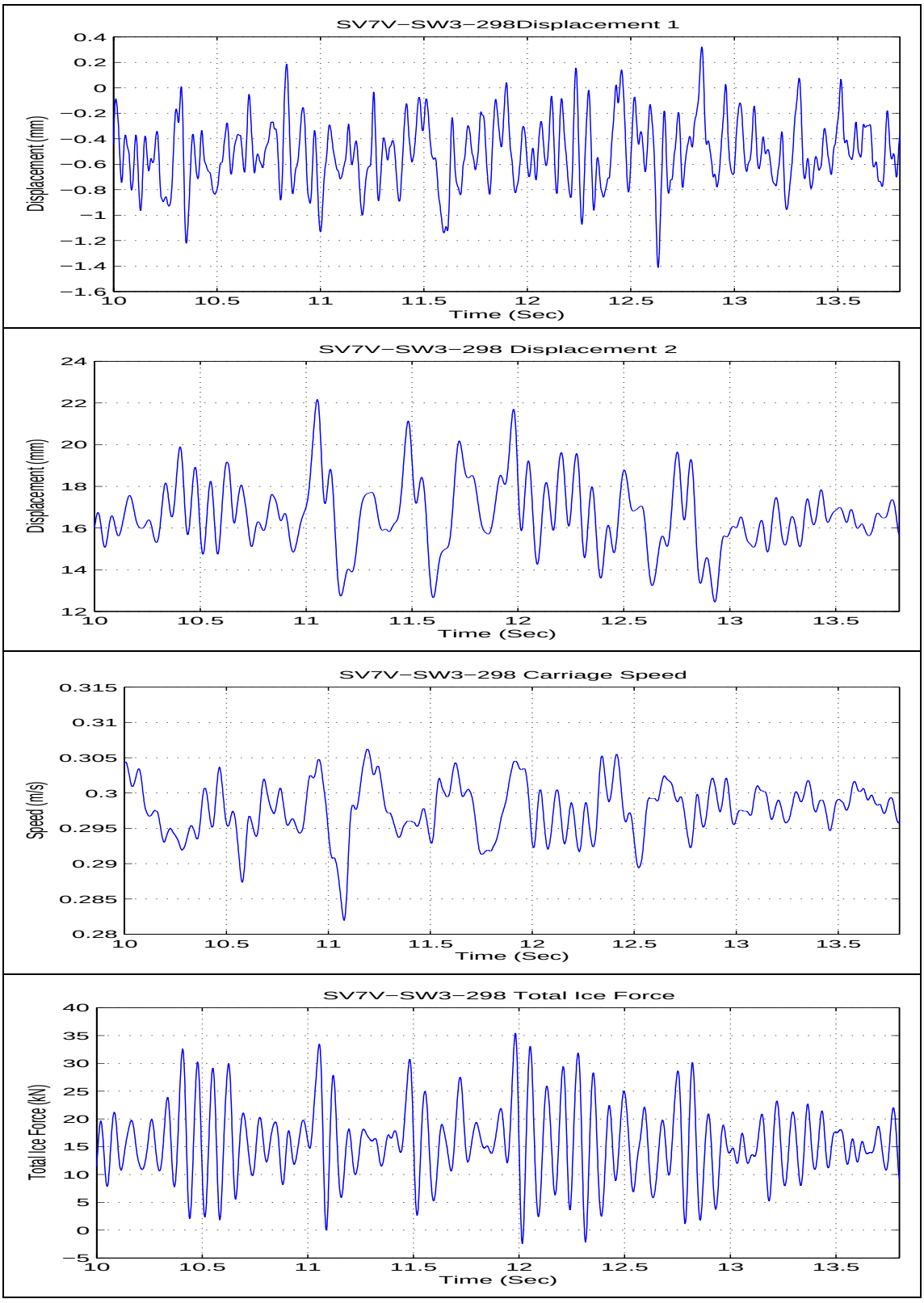

Test SV7V-SW4-398

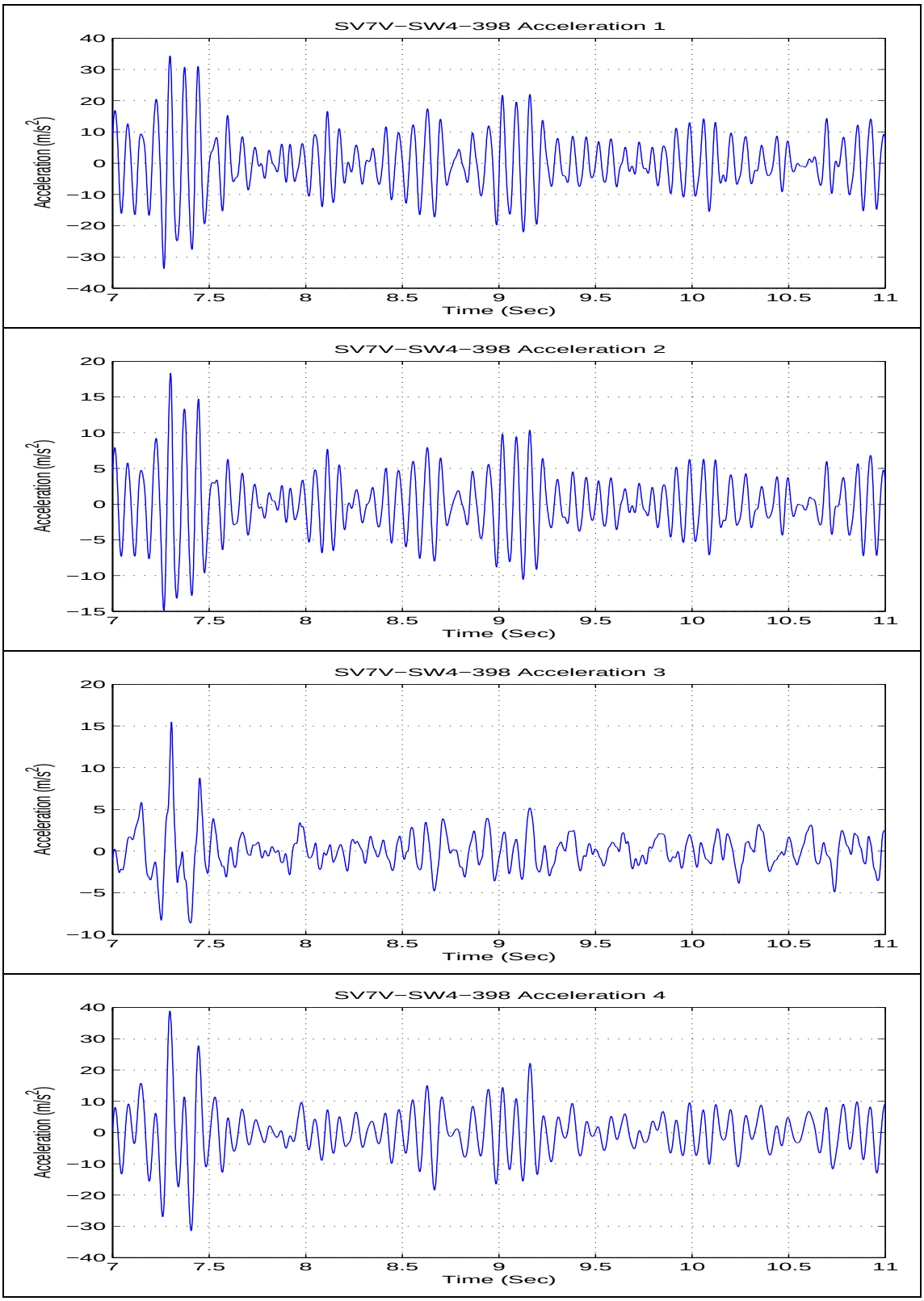

Test SV7V-SW4-398

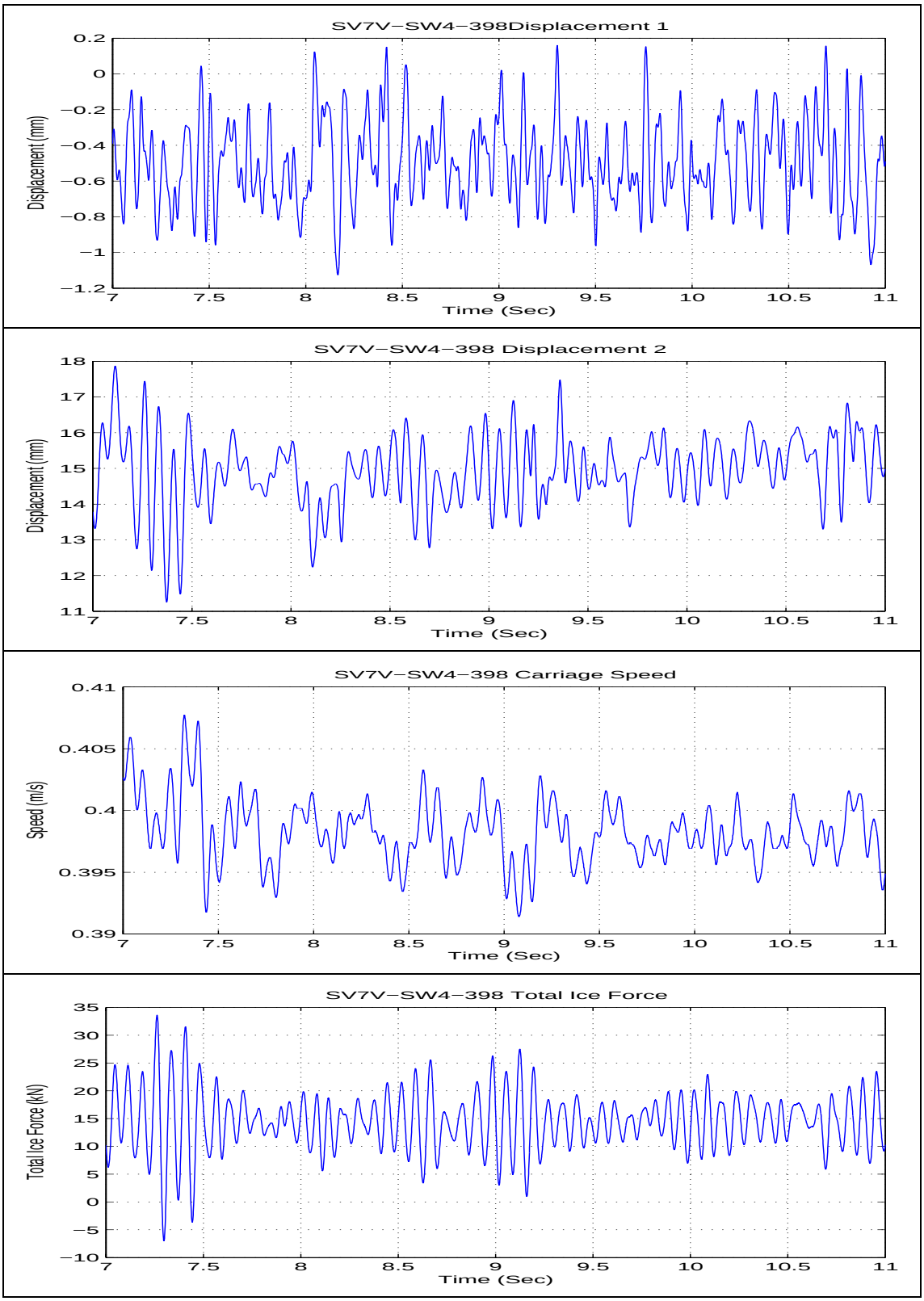

Test SV7V-SW5-238

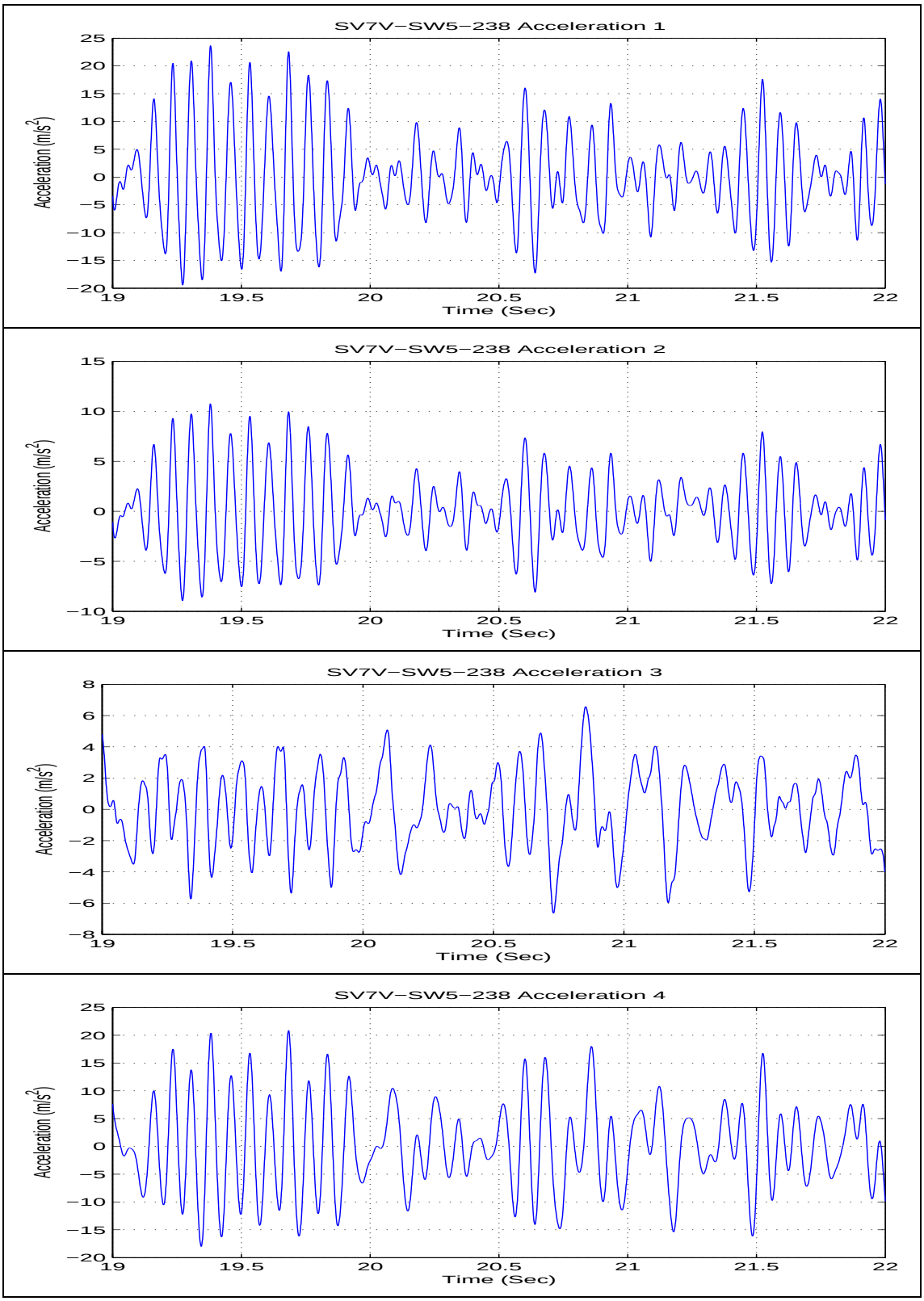

Test SV7V-SW5-238

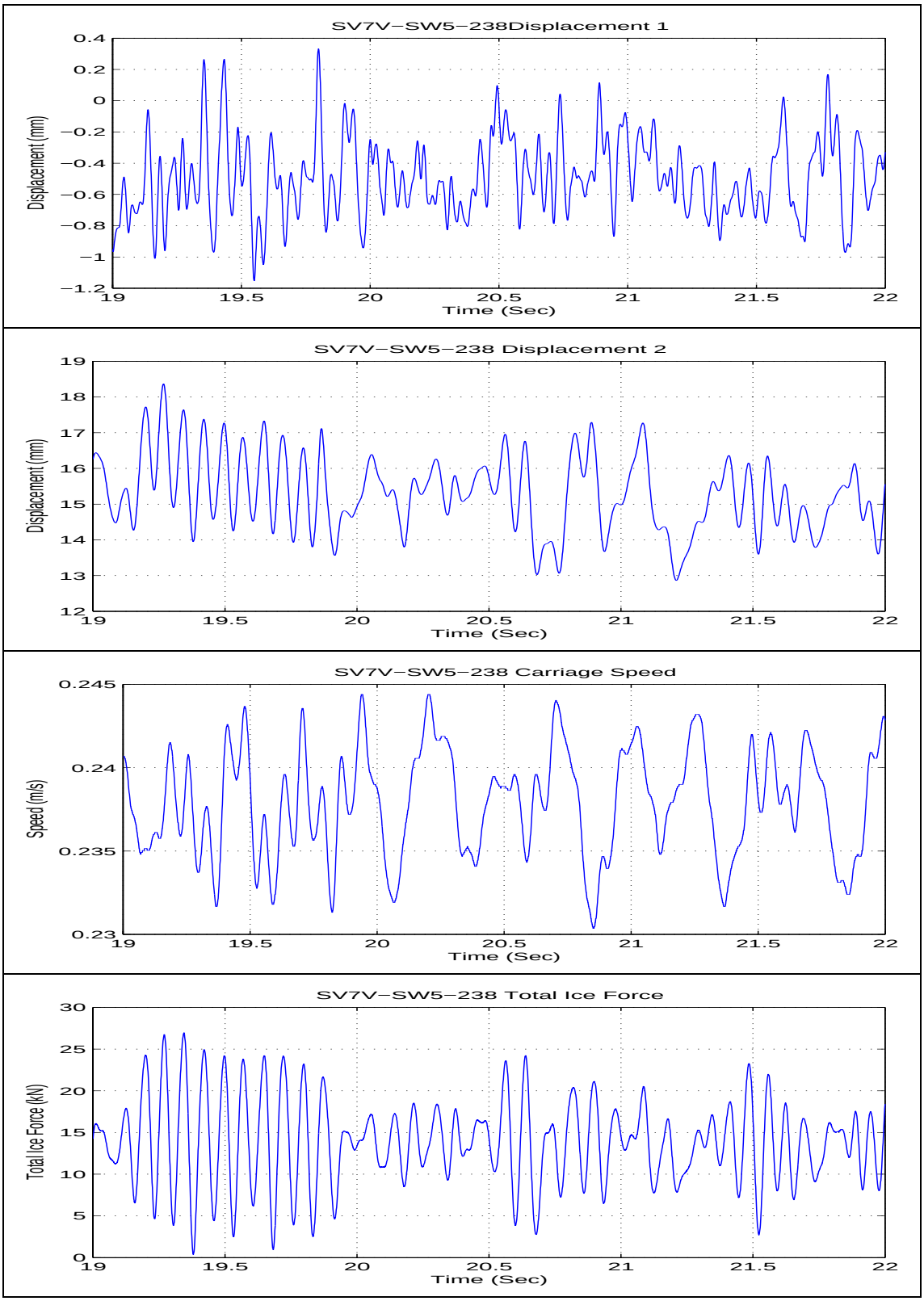

Test SV8V-SW1-008

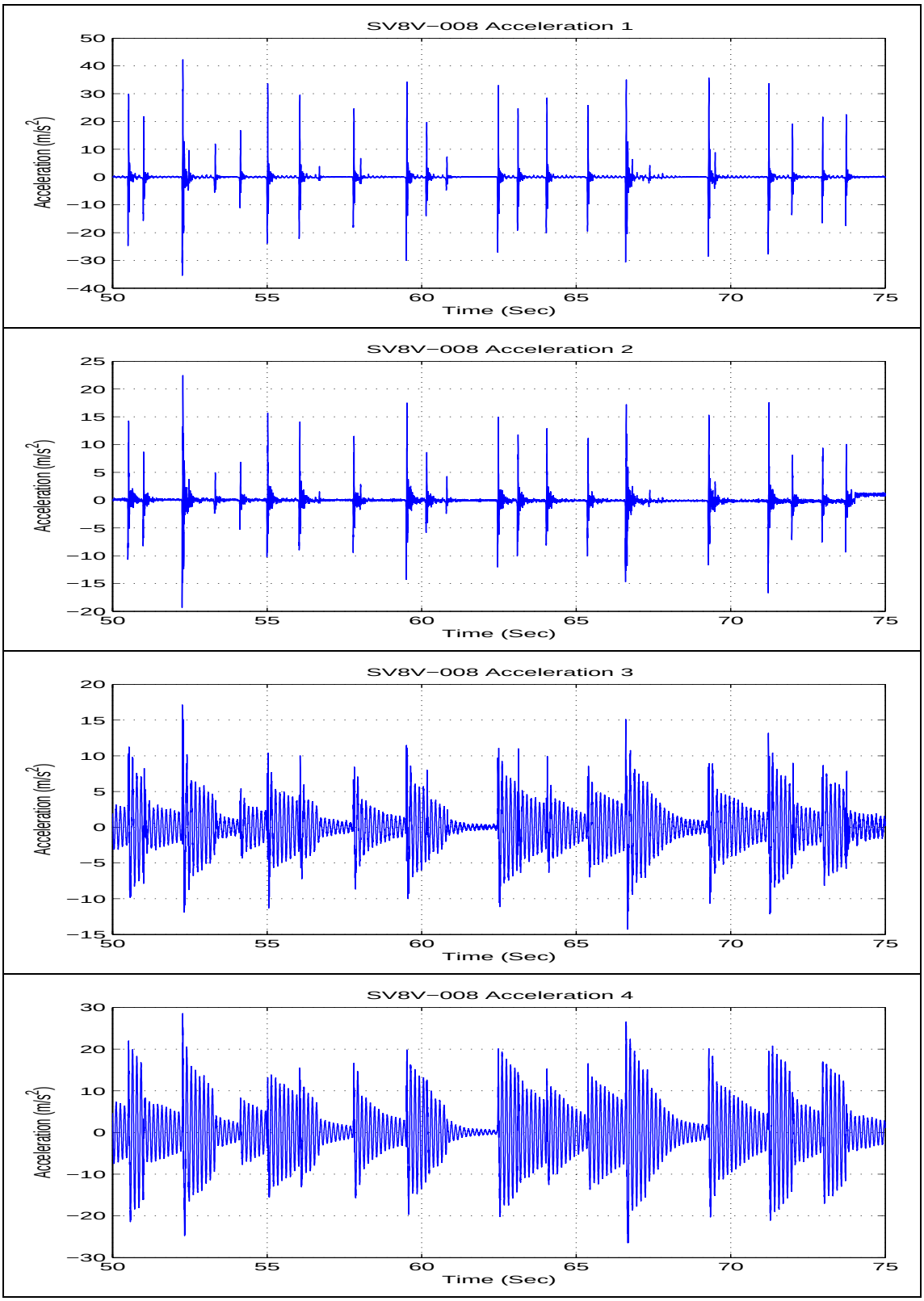

Test SV8V-SW1-008

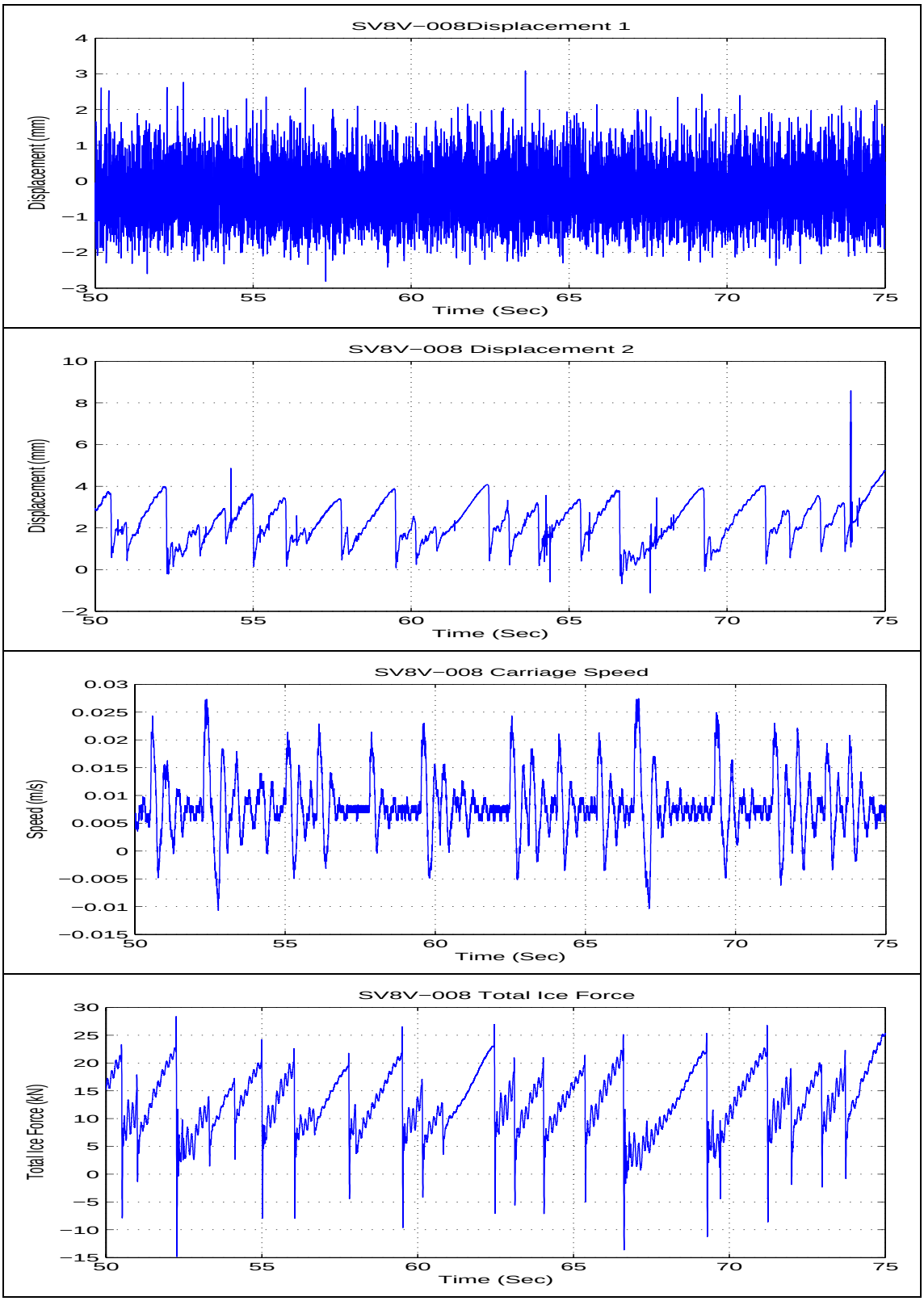

Test SV8V-SW2-018

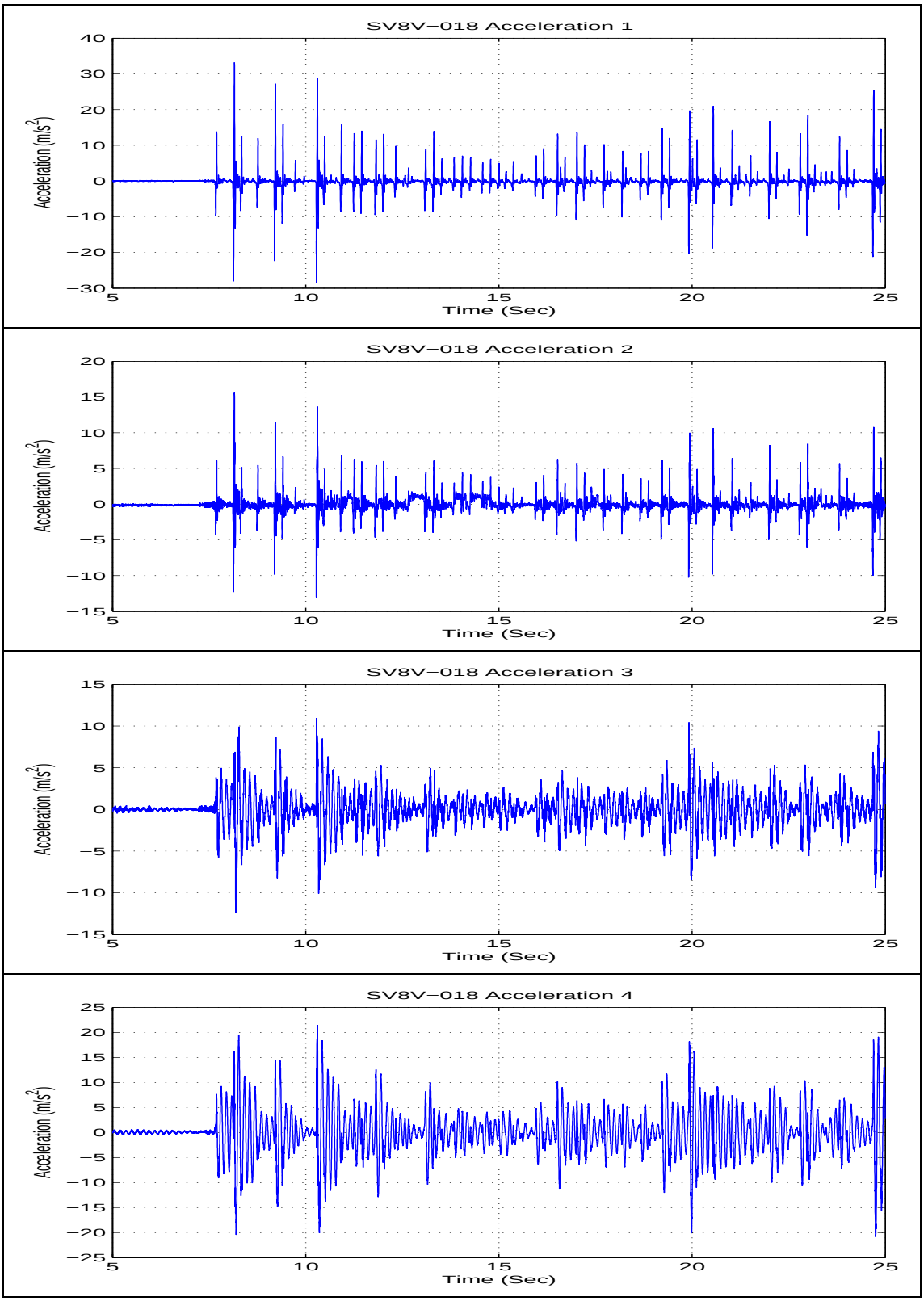

Test SV8V-SW2-018

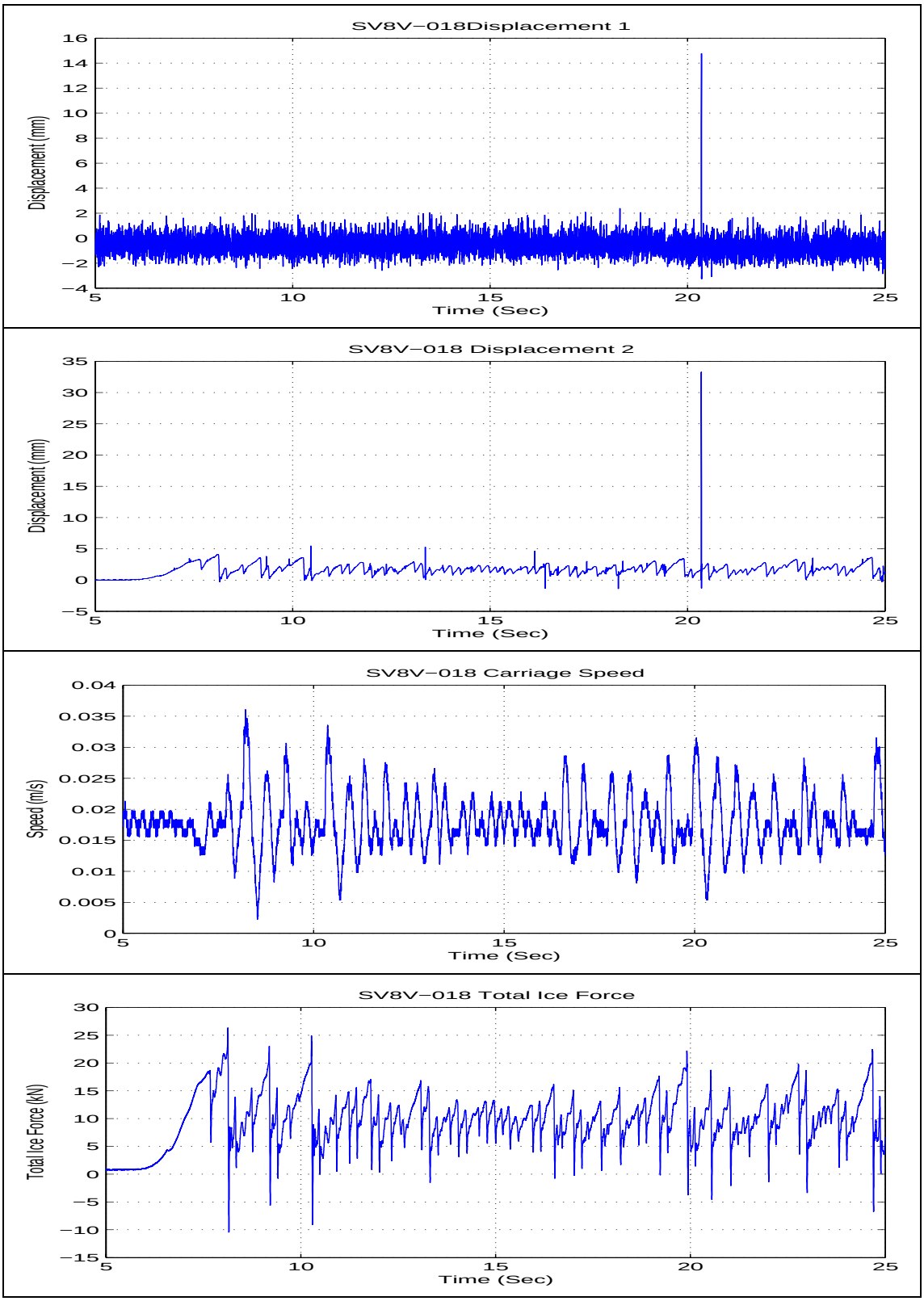

Test SV8V-SW2-038

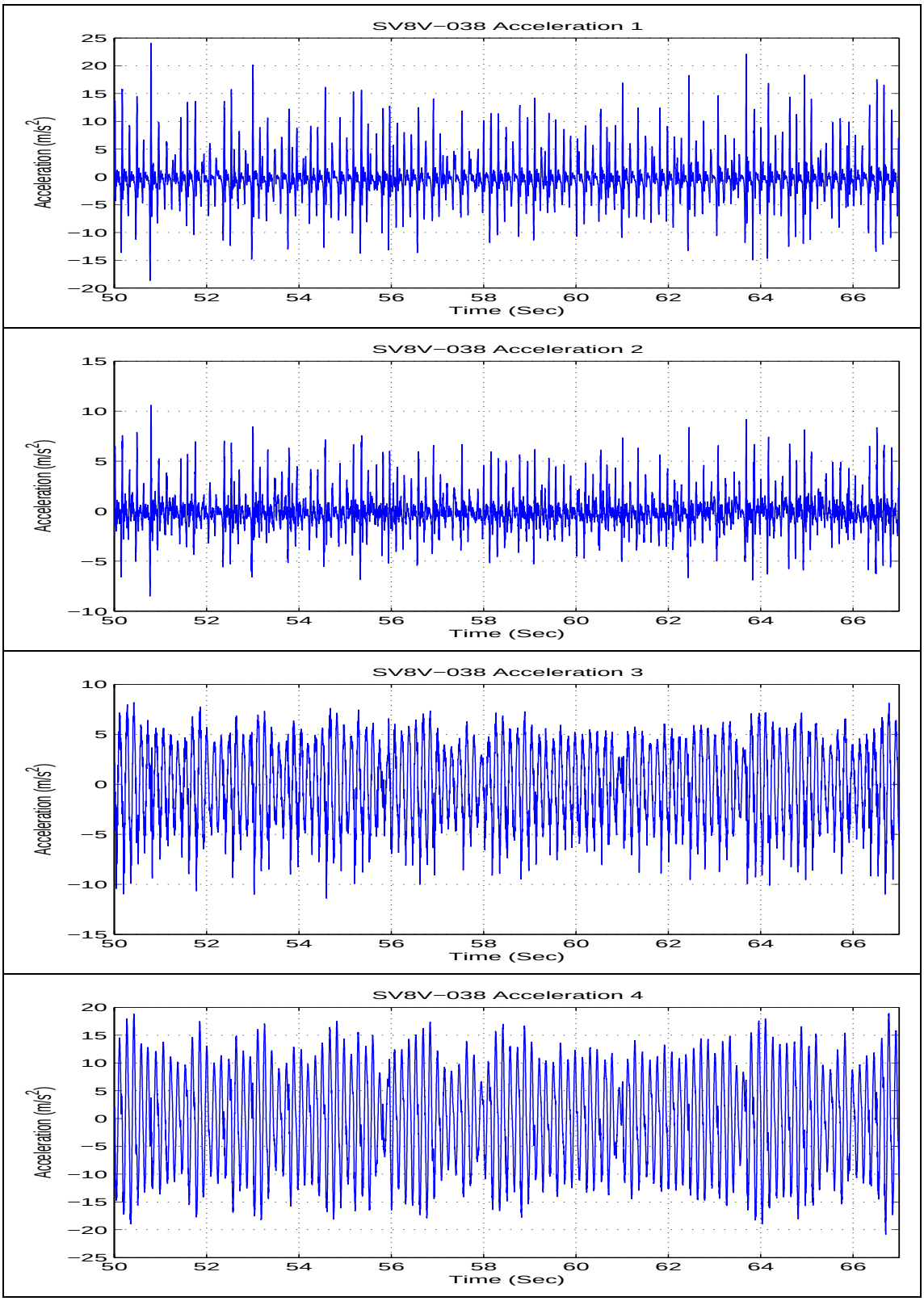

Test SV8V-SW2-038

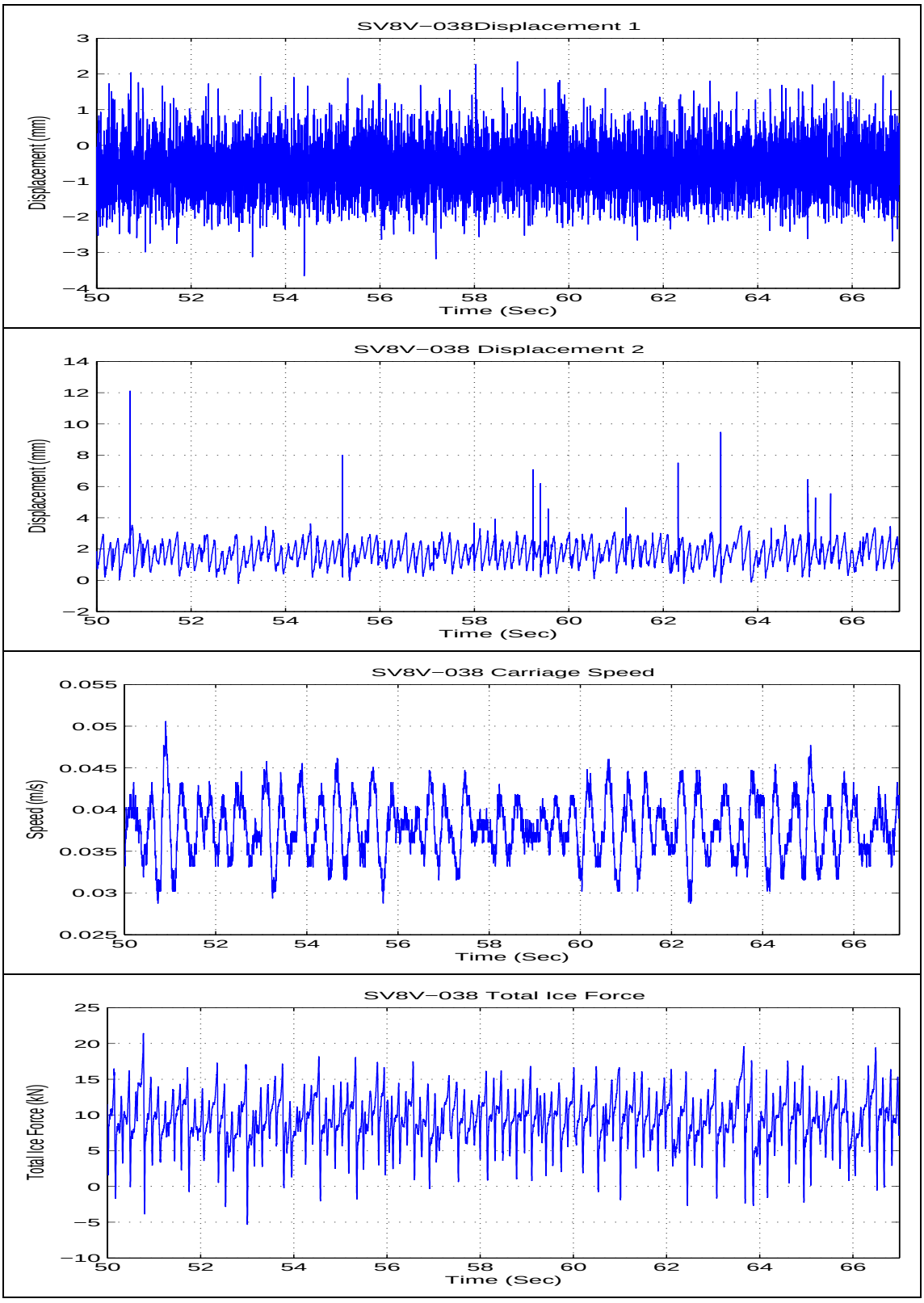

Test SV8V-SW3-098

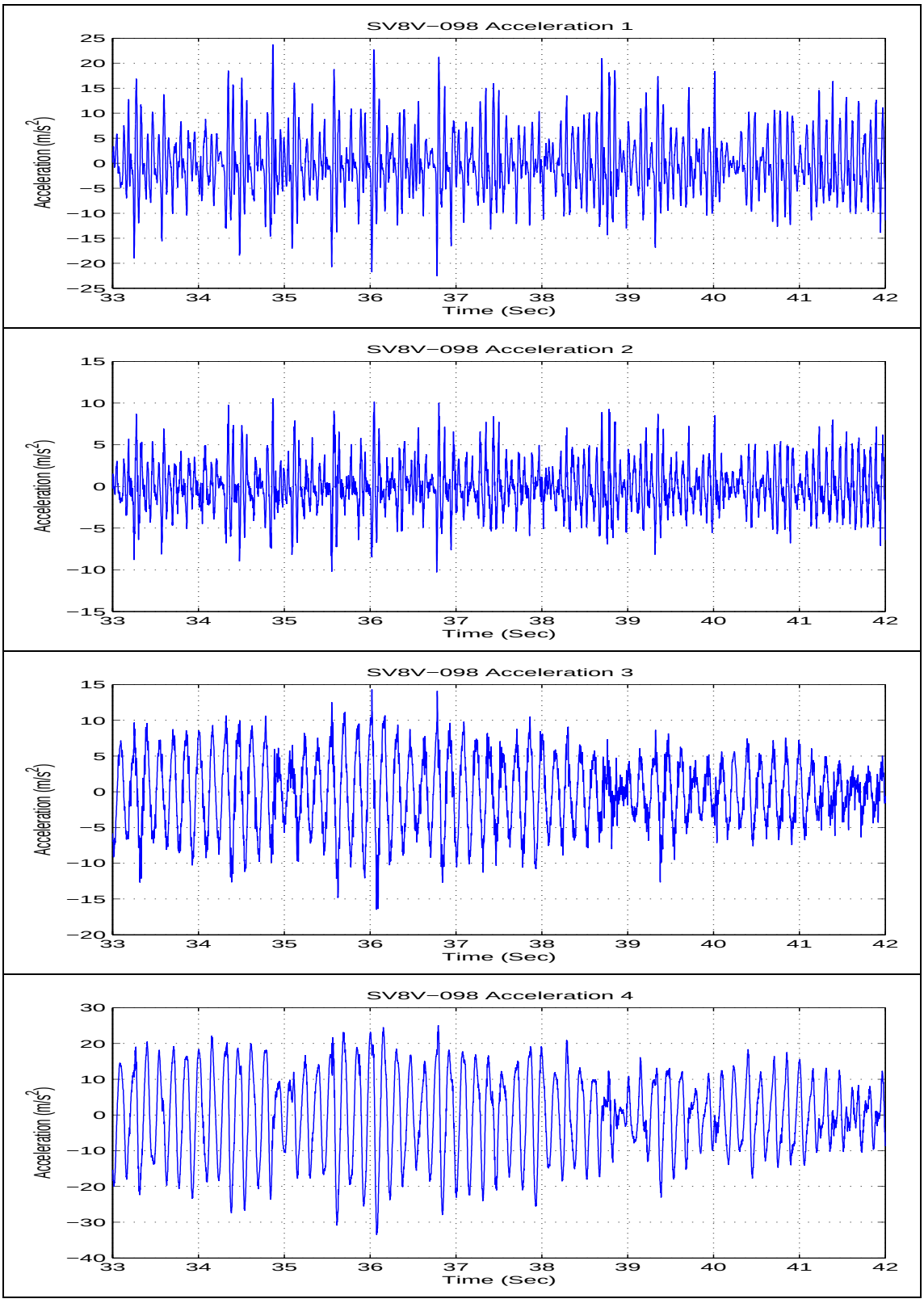

Test SV8V-SW3-098

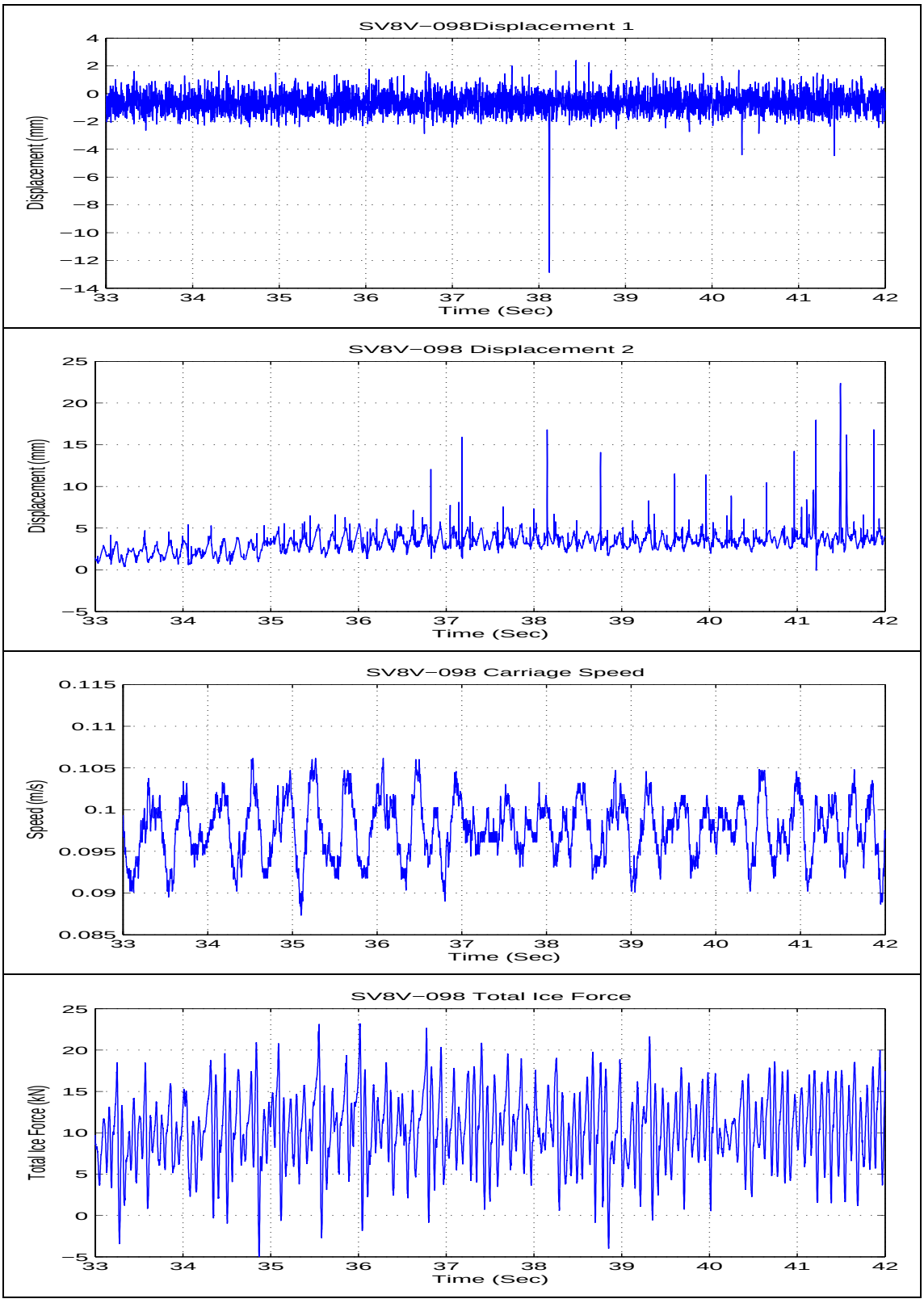

Test SV8V-SW3-118

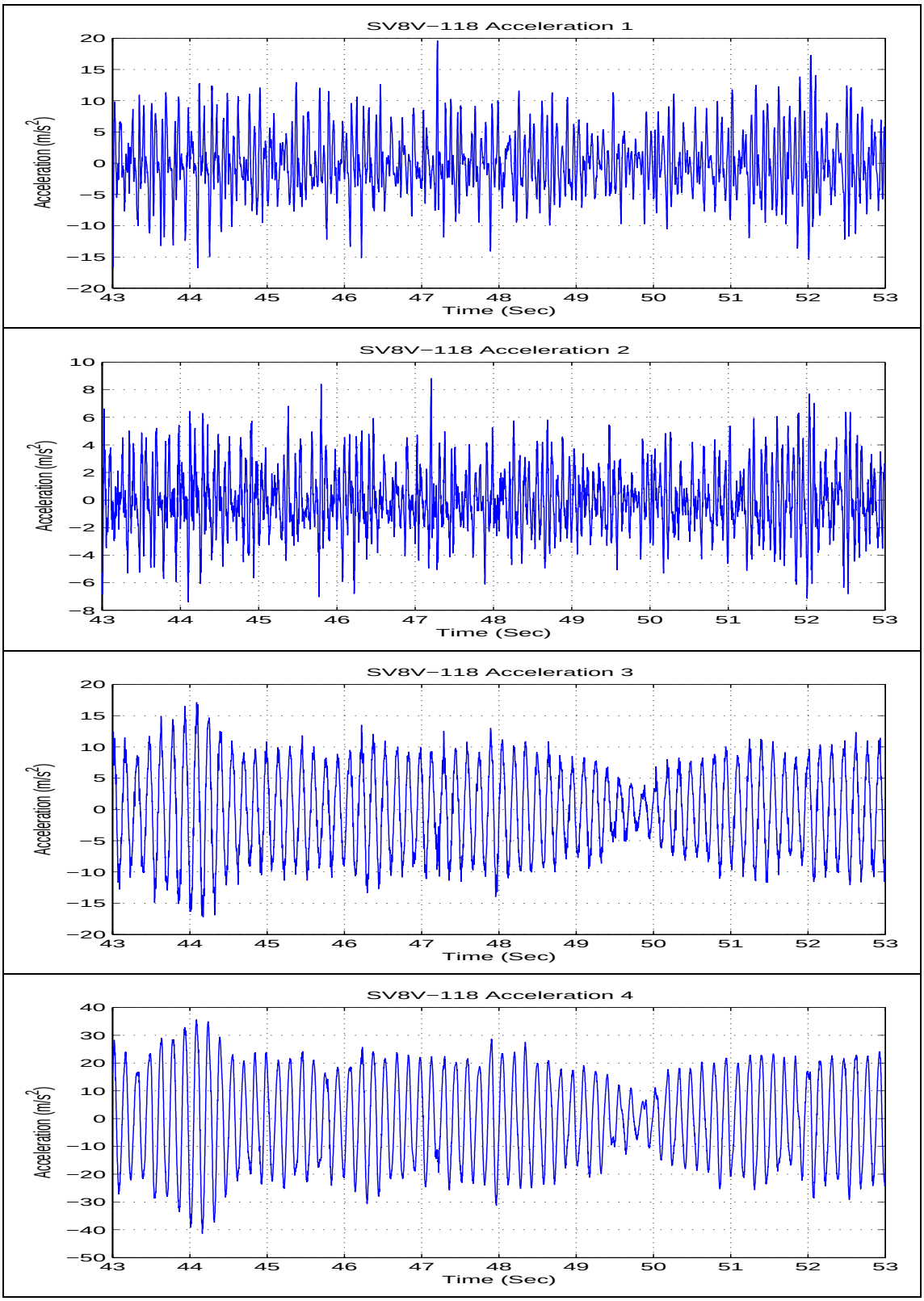

Test SV8V-SW3-118

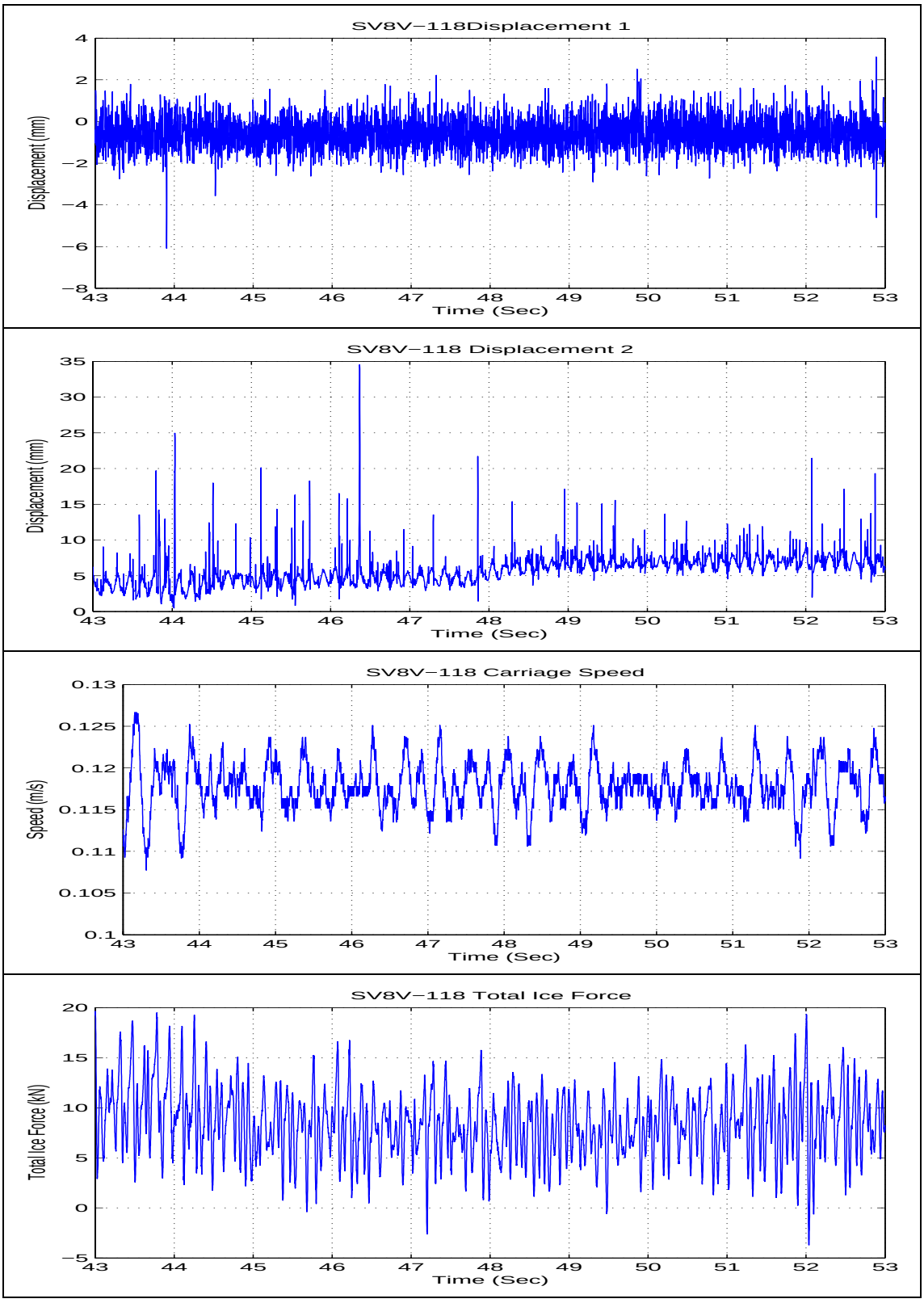

Test SV8V-SW4-198

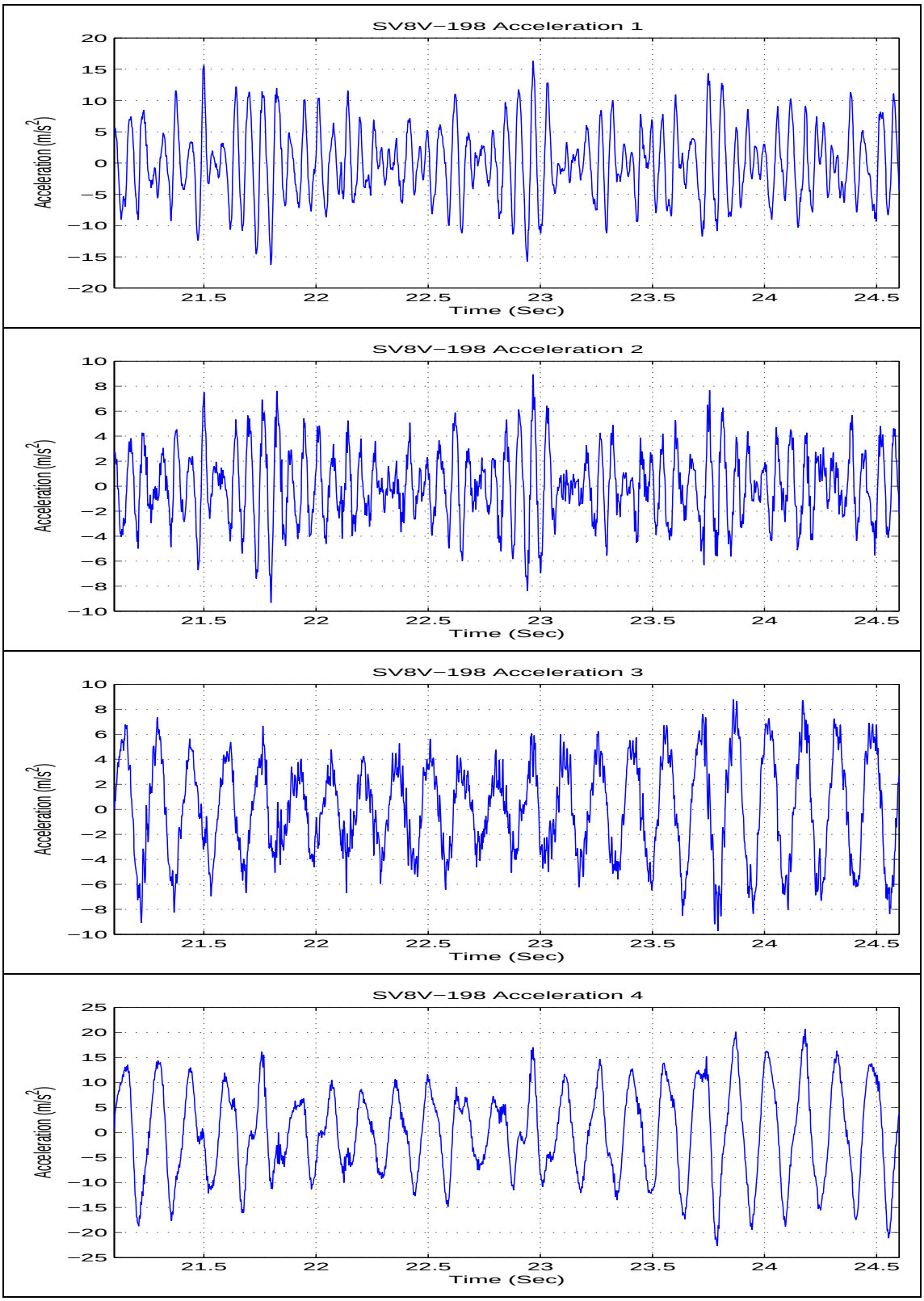

Test SV8V-SW4-198

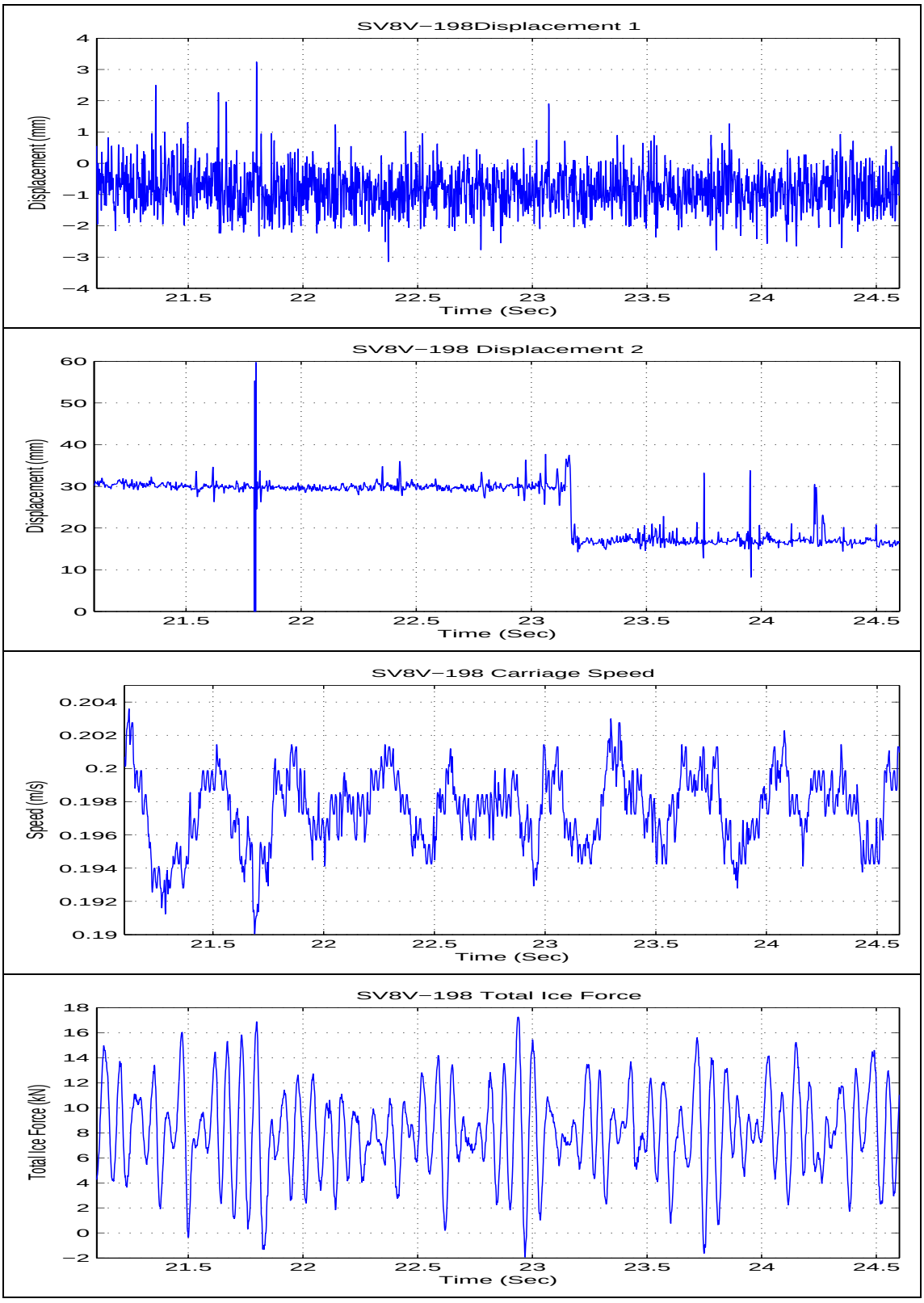

Test SV8V-SW5-308

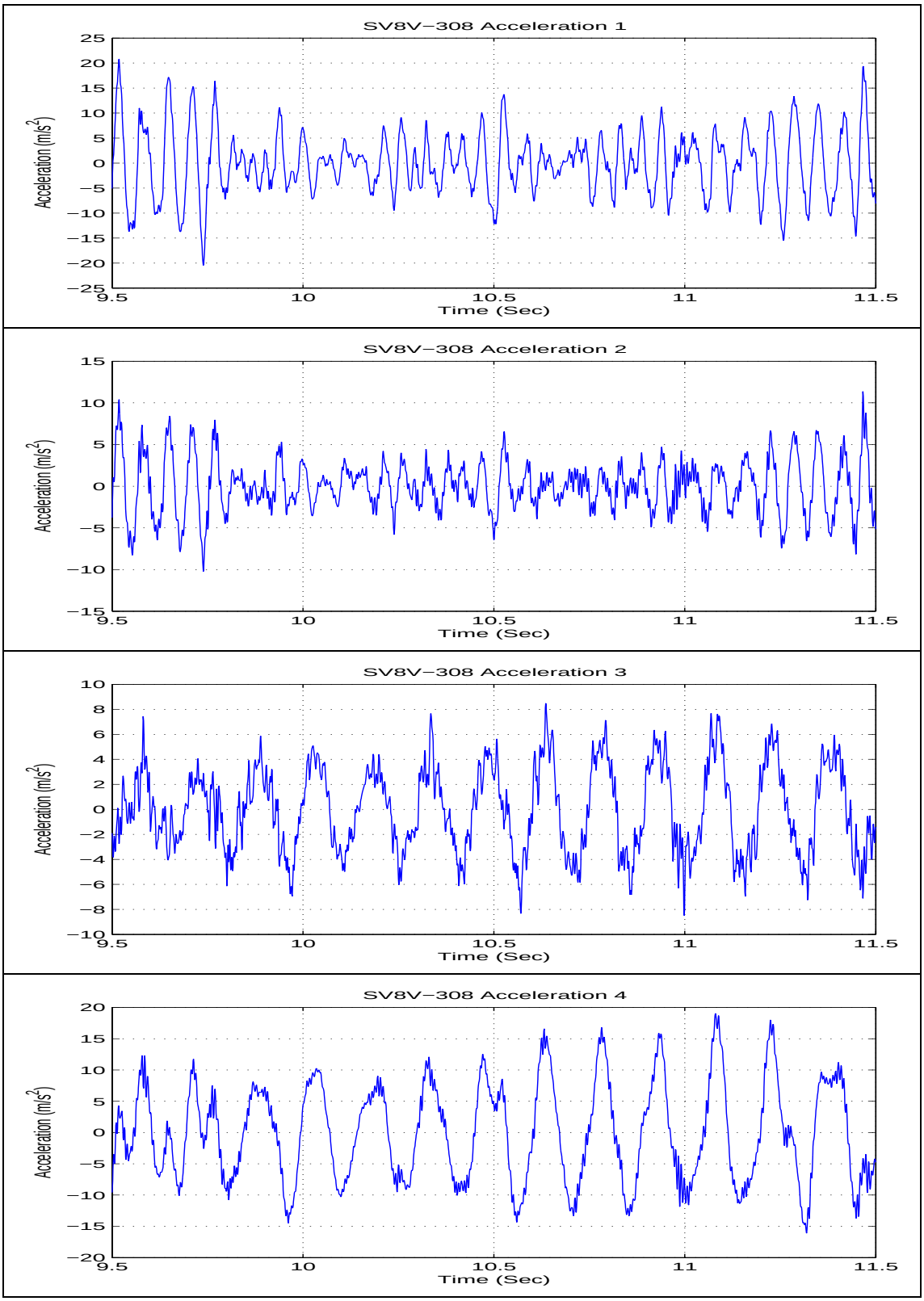

Test SV8V-SW5-308

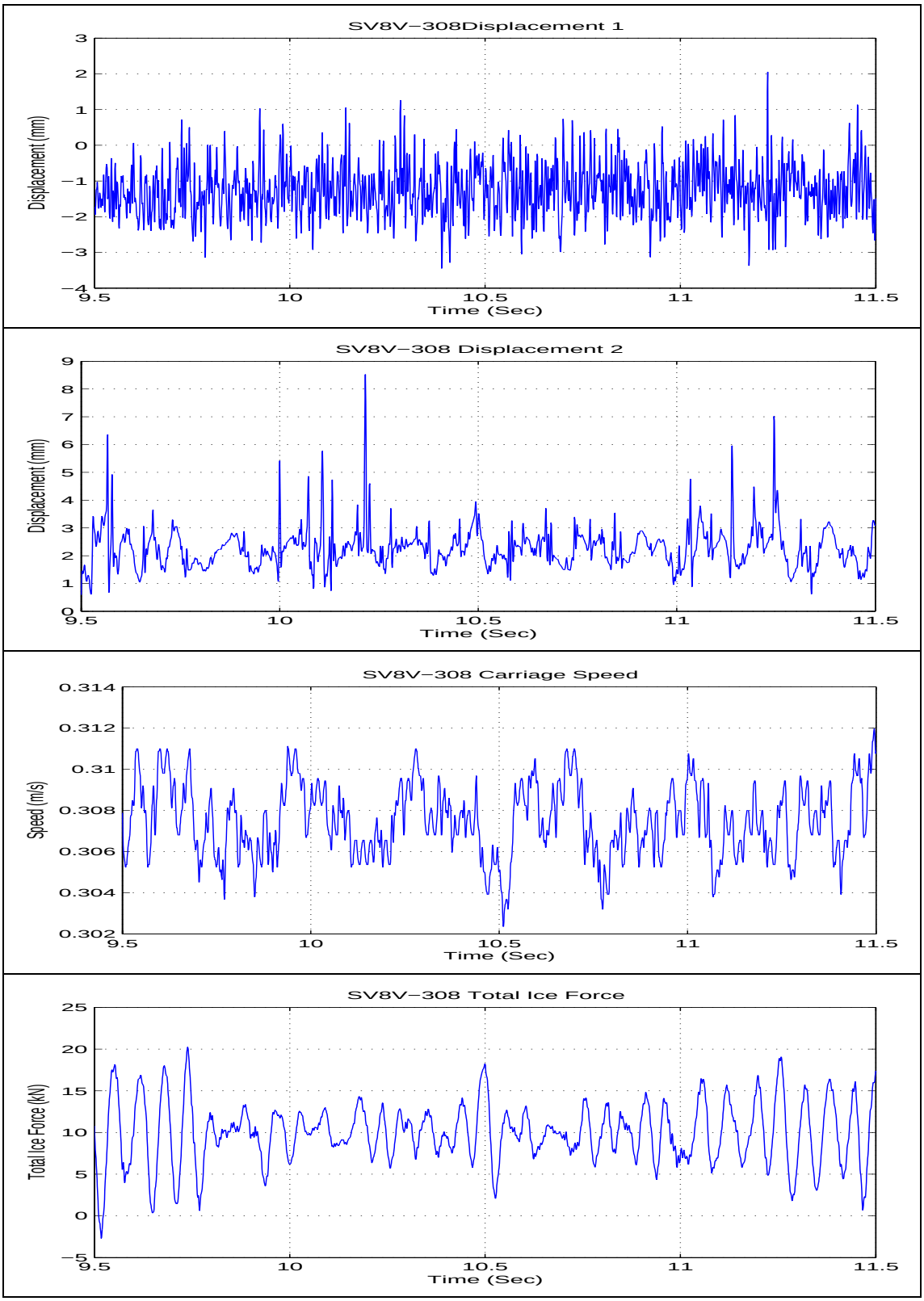

Test SV8C-020

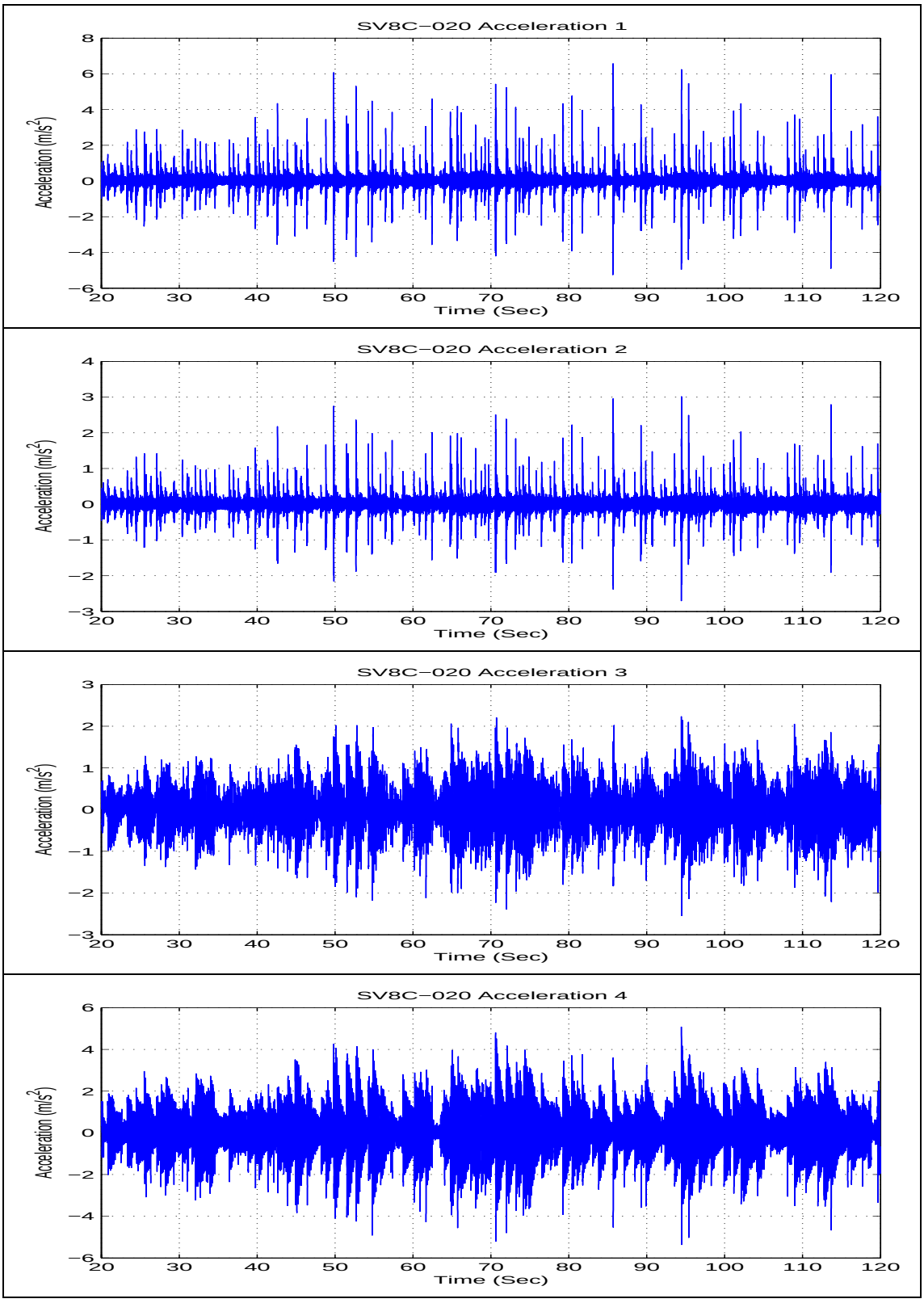

Test SV8C-020

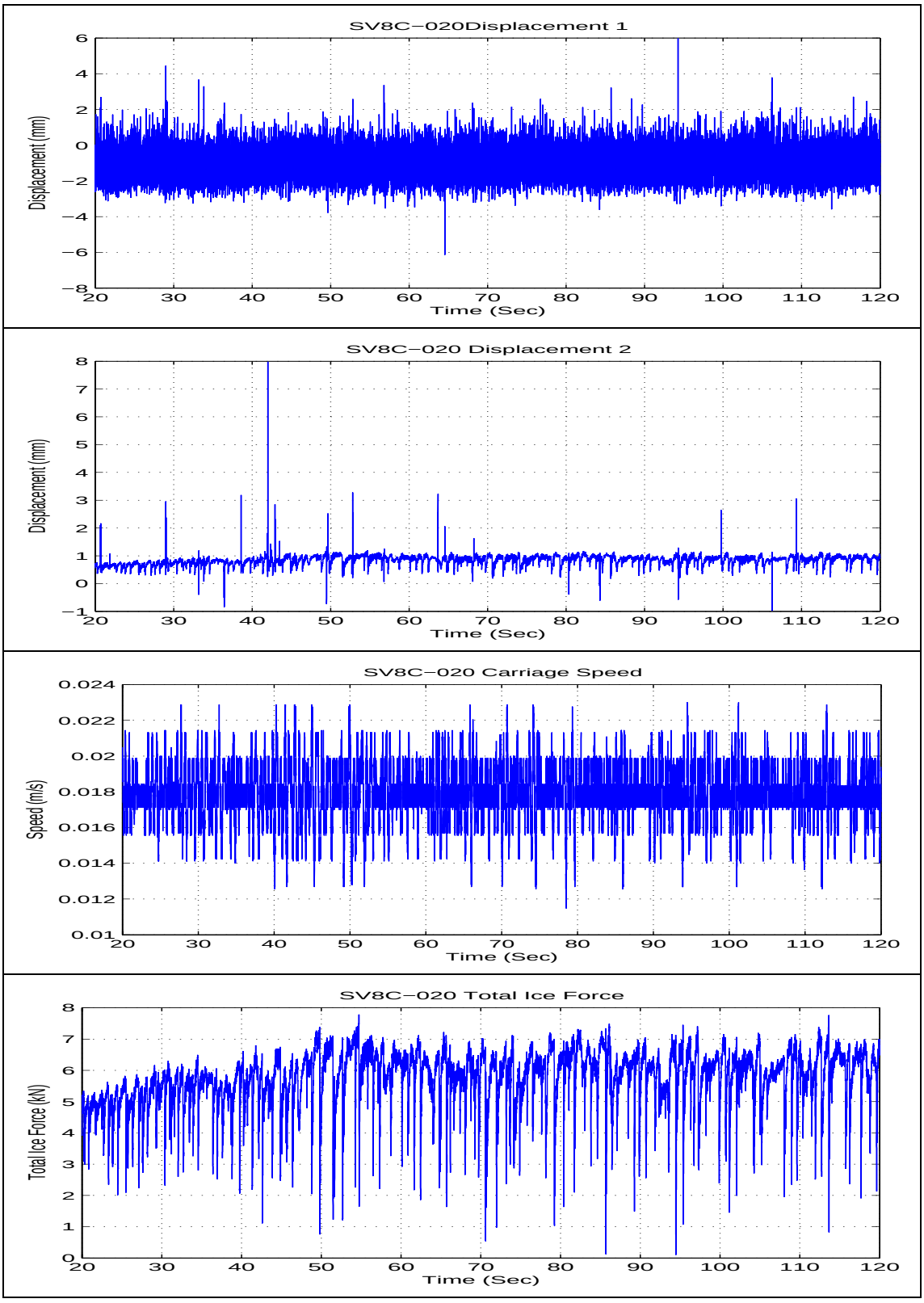

Test SV8C-050

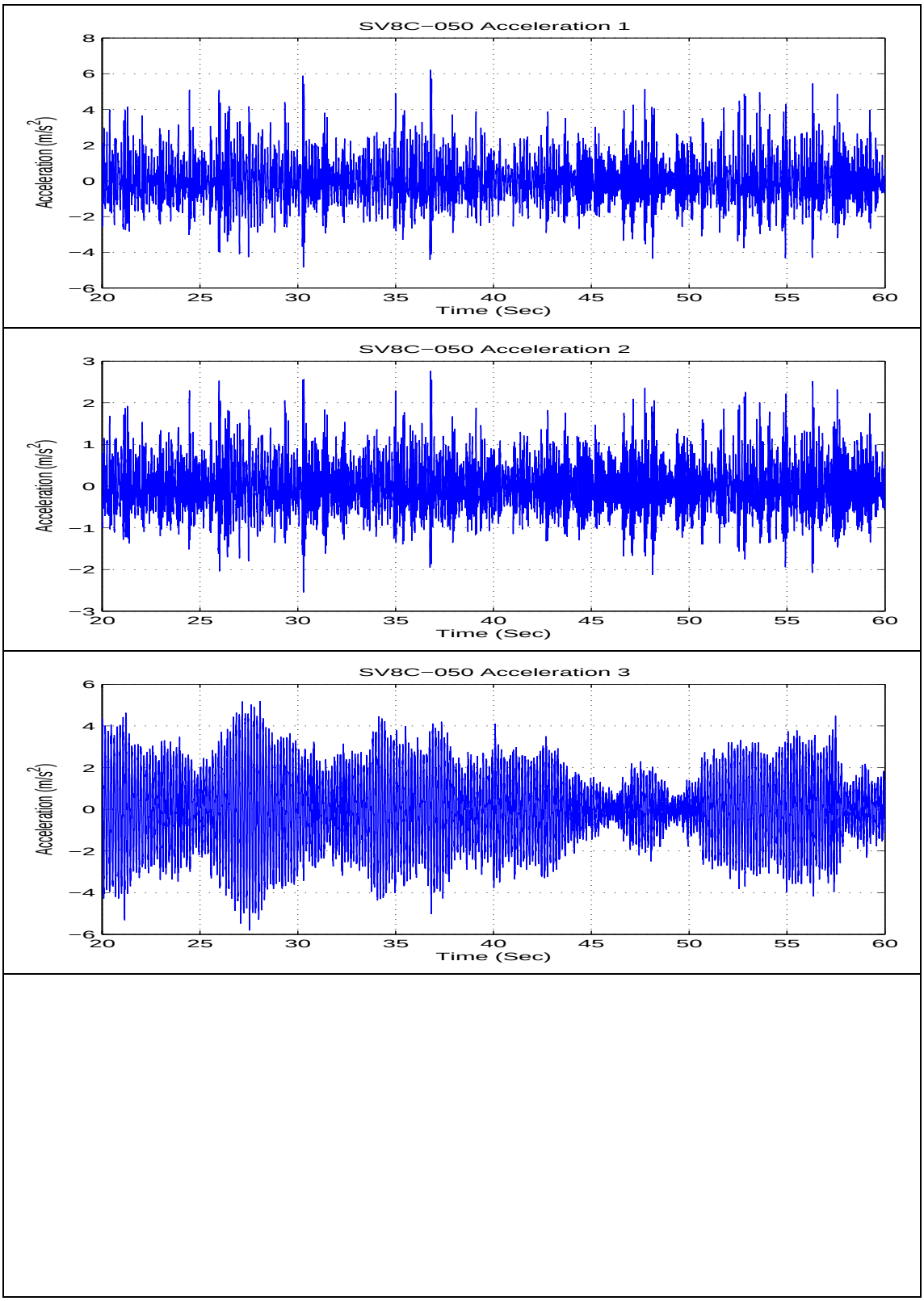

Test SV8C-050

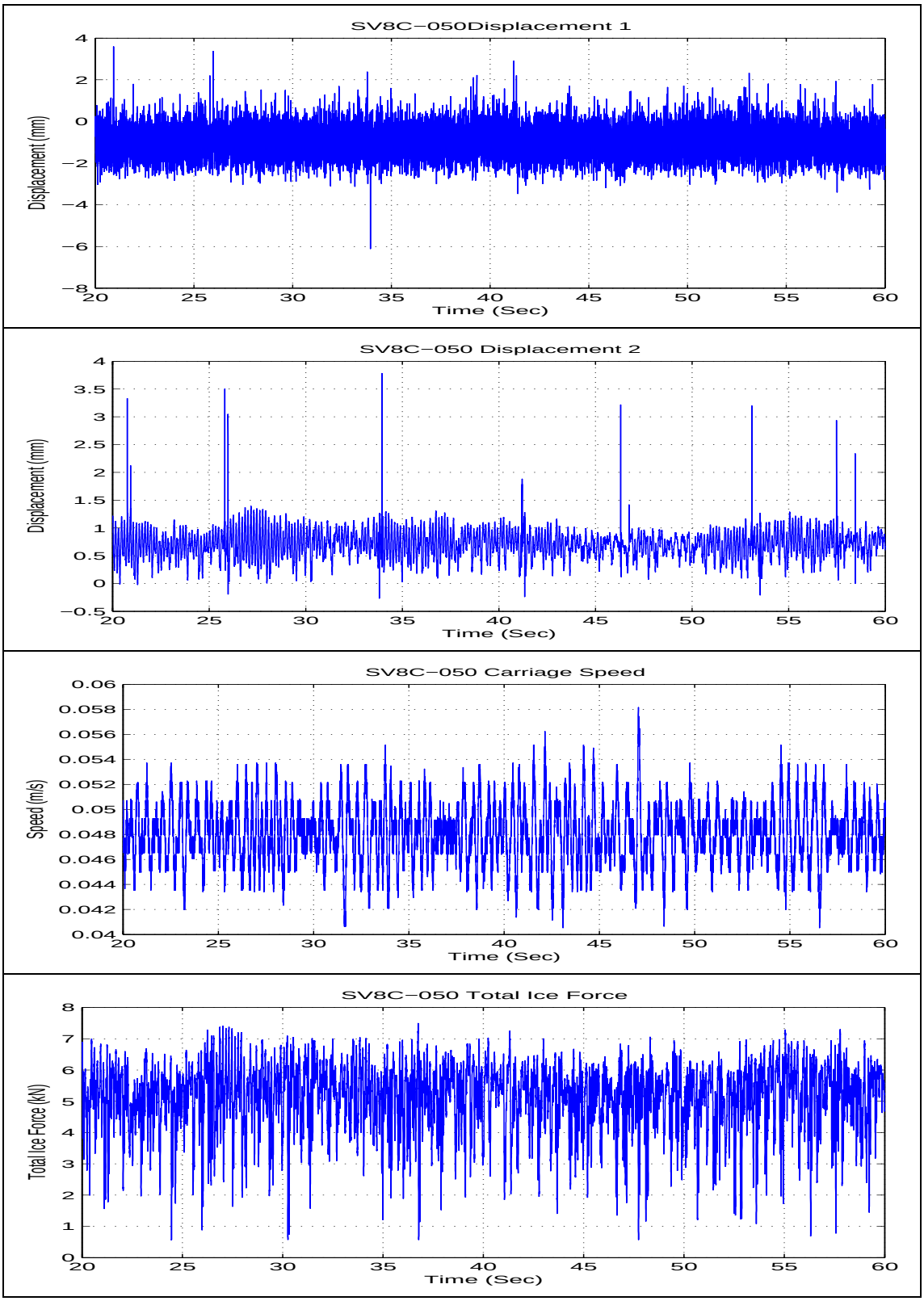

Test SV8C-100

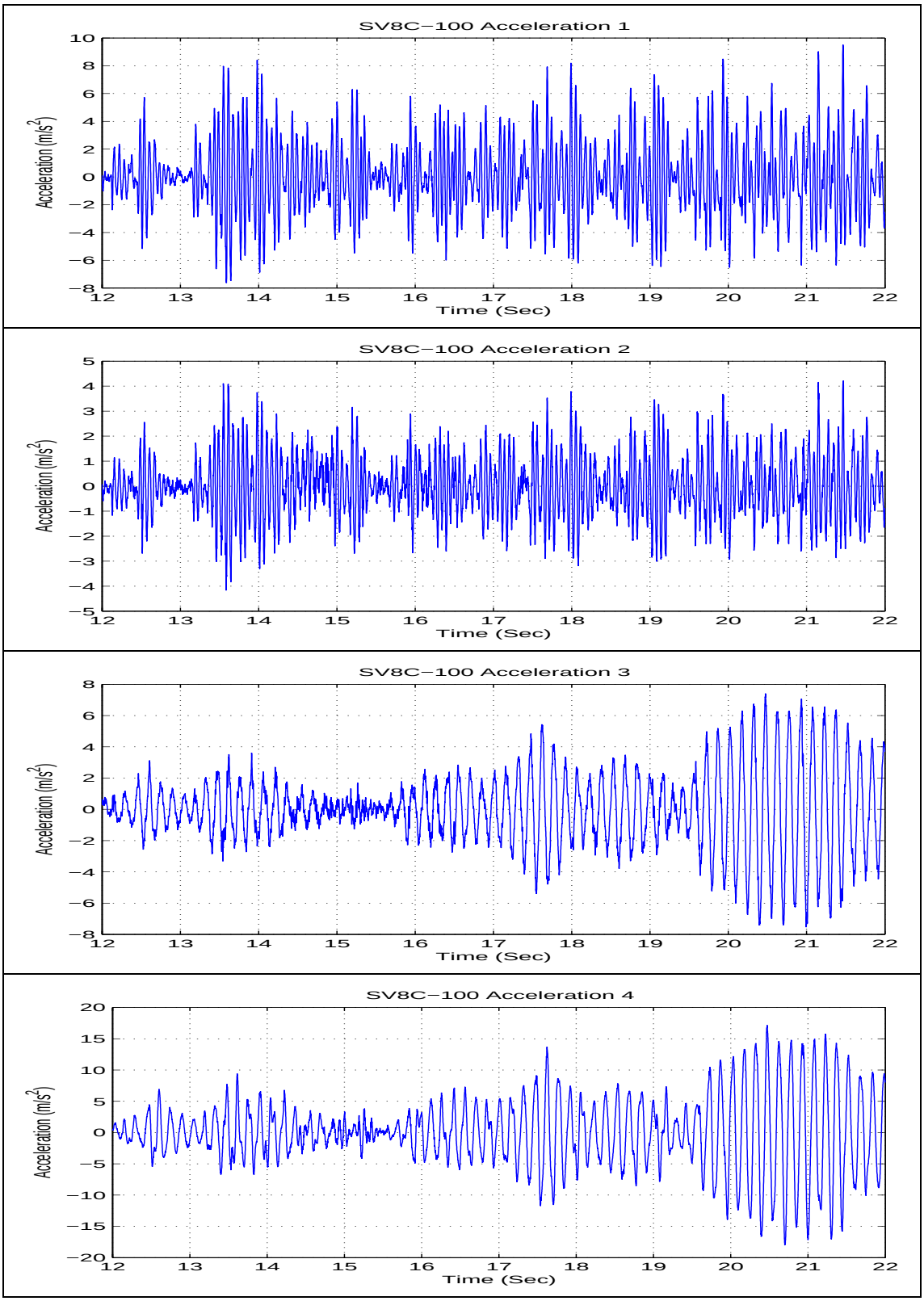

Test SV8C-100

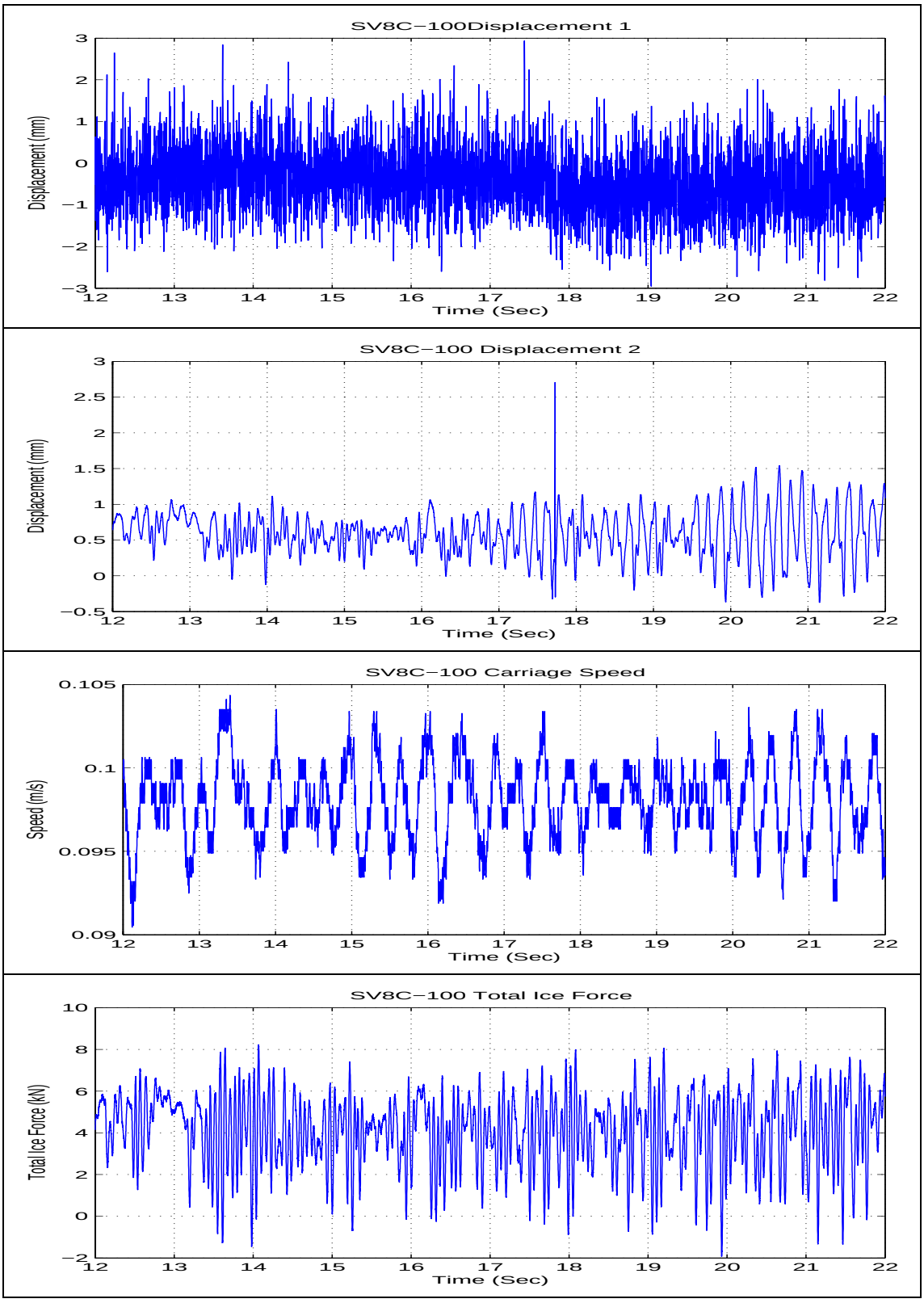

Test SV8C-200

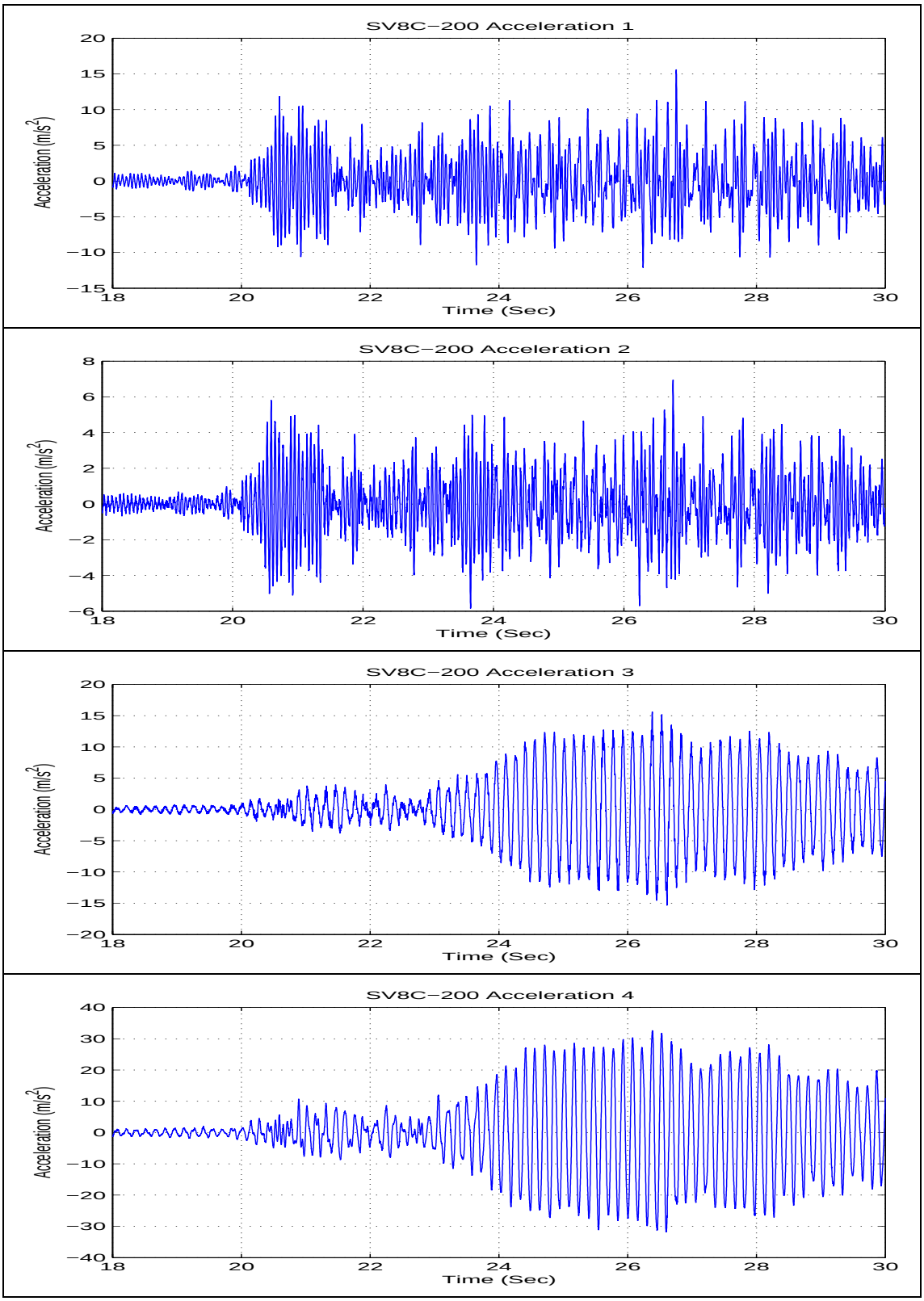

Test SV8C-200

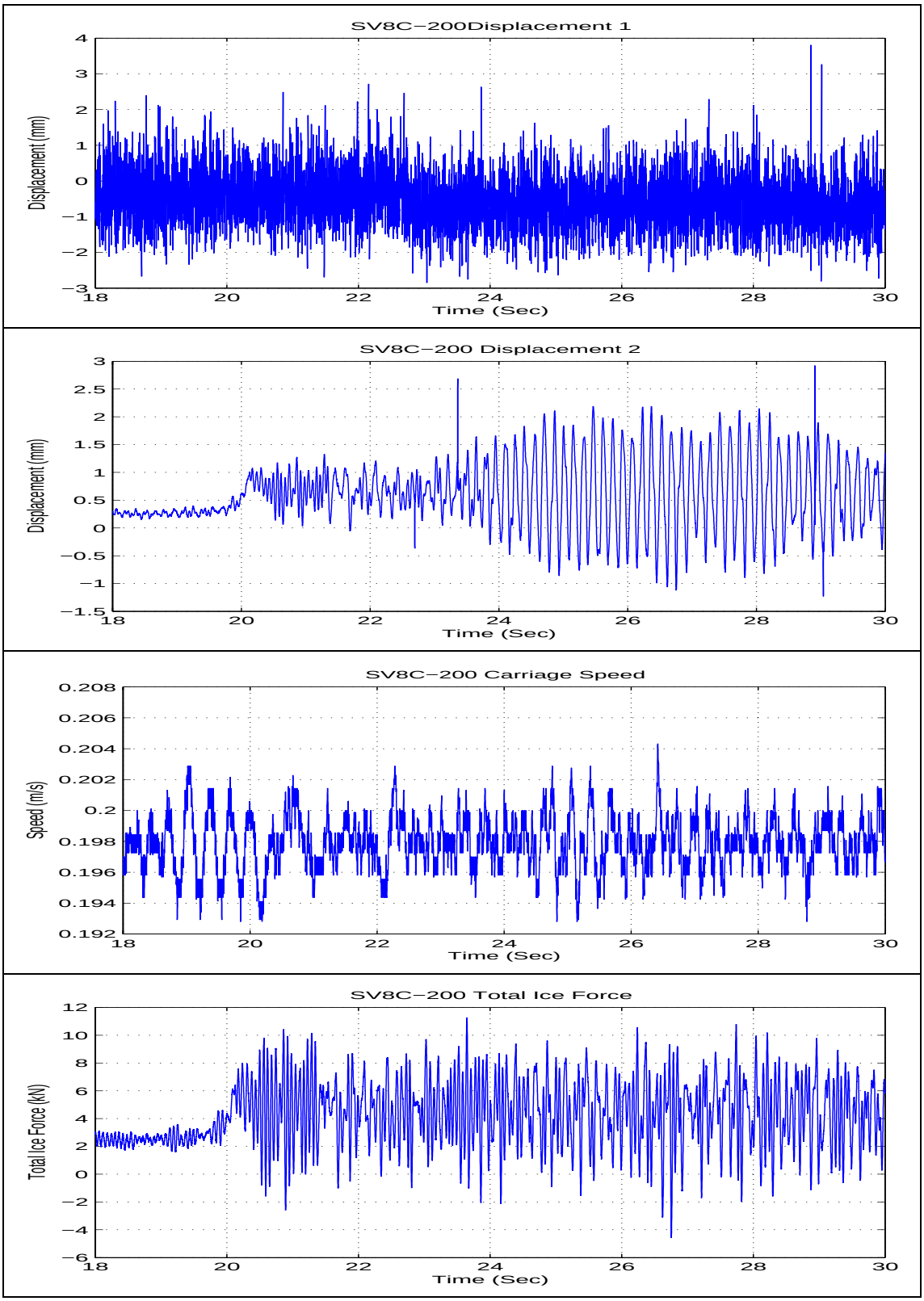

Test SV8C-400

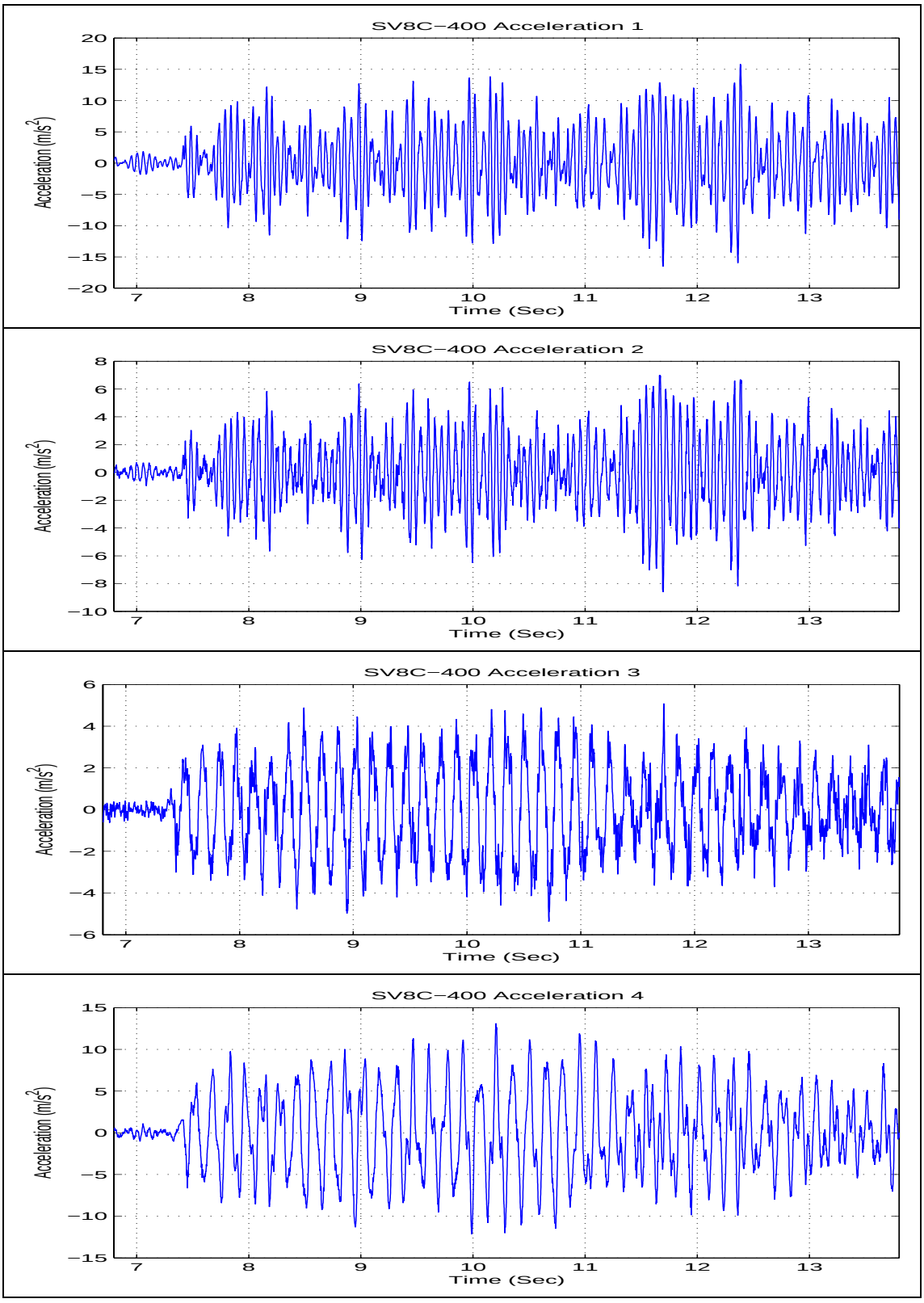

Test SV8C-400

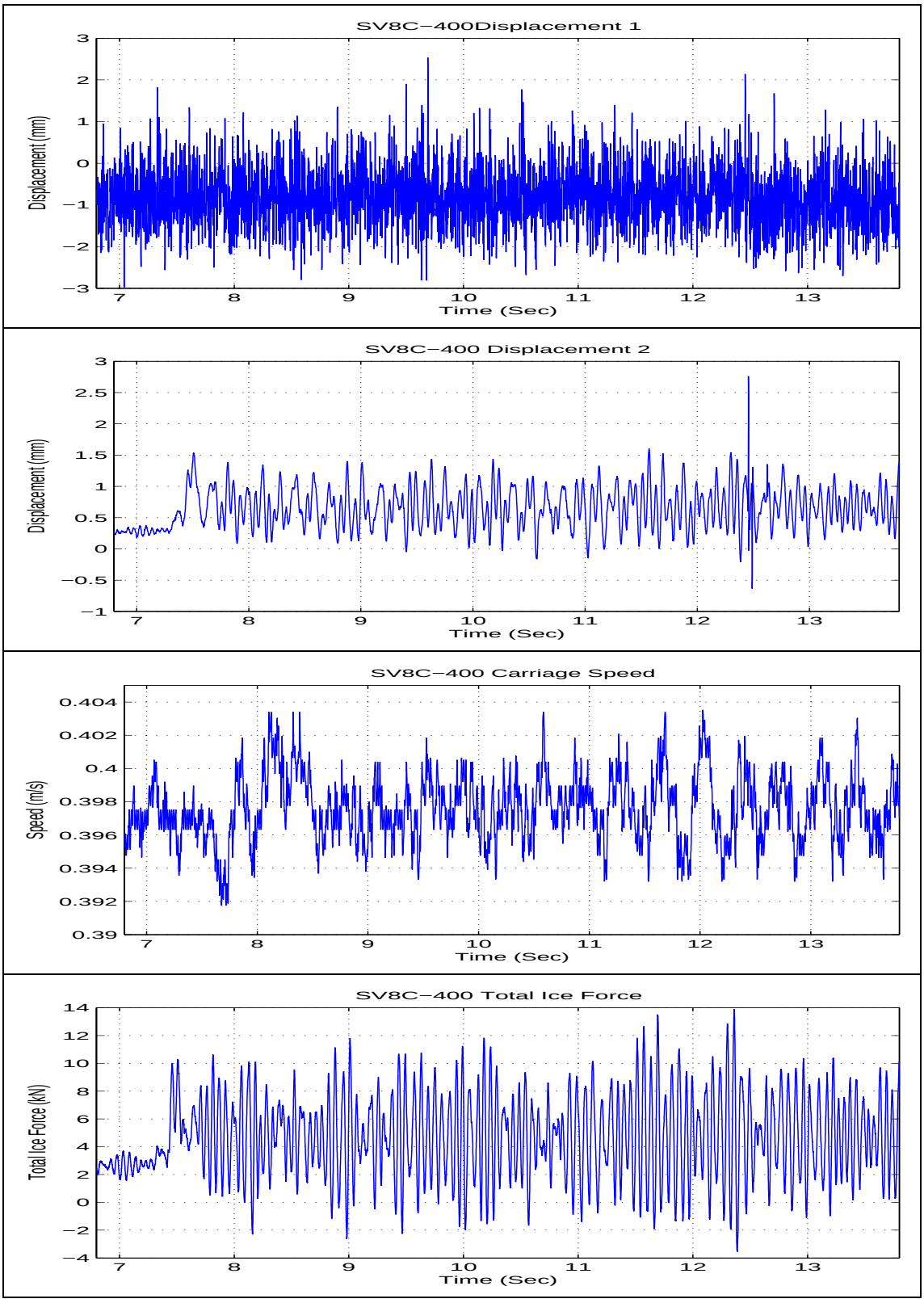

Published by

VTT

Vuorimiehentie 5, P.O.Box 2000, FIN–02044 VTT, Finland
Phone internat. +358 9 4561
Fax +358 9 456 4374

Series title, number and report code of publication

VTT Research Notes 2223
VTT–TIED–2223

Author(s)
Kärnä, Tuomo, Kolari, Kari, Jochmann, Peter, Evers, Karl-Ulrich, Xiangjun, Bi, Määttänen, Mauri & Martonen, Petter

Title

Ice action on compliant structures

Laboratory indentation tests

Abstract

This experimental research addresses the dynamic ice-structure interaction of marine structures. The main objective was to obtain data on the phenomenon known as steady-state vibration of vertical offshore structures. Such data is needed while researchers develop numerical and simplified models of the vibration. A further objective was to find data on ice-induced vibrations of conical structures. A common belief has been that ice can not create significant vibrations on conical offshore structures. Recent full-scale data has shown that this assumption is not correct. Hence, the present project aimed at obtaining laboratory data on this kind of vibrations. The third aim of the project was to demonstrate that additional structural damping can be used to mitigate the dynamic response caused by ice actions.

Tests were done at the ice basin of the ARCTECLAB using the carriage of the ice basin. An experimental structure was installed on the carriage and penetration tests were done on three sheets of columnar grained ice. The dynamic properties of the structure were modified during the test series. Two different indentors were used, a vertical cylinder and a cone. This test report provides detailed descriptions of the test set up and the test programme. The main results are also shown in terms of the measured time signals. The report serves as a background document for more detailed analysis and subsequent exploration of the data.

Keywords
marine structures, offshore structures, steady-state vibrations, ice-induced vibrations, conical structures, dynamic response, measurement, testing, numerical analysis, models

Activity unit
VTT Building and Transport, Puumiehenkuja 2 A, P.O.Box 1806, FIN–02044 VTT, Finland

ISBN	Project number
951–38–6200–3 (soft back ed.) 951–38–6201–1 (URL: http://www.vtt.fi/inf/pdf/)	

Date	Language	Pages	Price
December 2003	English	43 p. + app. 79 p.	C

Name of project	Commissioned by
NEST Networking Studies on Ice and Compliant Structures	EU

Series title and ISSN	Sold by
VTT Tiedotteita – Research Notes 1235–0605 (soft back edition) 1455–0865 (URL: http://www.vtt.fi/inf/pdf/)	VTT Information Service P.O.Box 2000, FIN–02044 VTT, Finland Phone internat. +358 9 456 4404 Fax +358 9 456 4374

This experimental research addresses the dynamic ice-structure interaction of marine structures. The main objective was to obtain data on the phenomenon known as steady-state vibration of vertical offshore structures. Such data is needed while researchers develop numerical and simplified models of the vibration. Tests were done at the ice basin of the ARCTECLAB using the carriage of the ice basin. An experimental structure was installed on the carriage and penetration tests were done on three sheets of columnar grained ice. The dynamic properties of the structure were modified during the test series. Two different indentors were used, a vertical cylinder and a cone. This test report provides detailed descriptions of the test set up and the test programme. The main results are also shown in terms of the measured time signals. The report serves as a background document for more detailed analysis and subsequent exploration of the data.

The experiments were conducted as a joint effort of VTT, Hamburg Ship Model Basin, Helsinki University of Technology and the Dalian University of Technology. The experimental work was financially supported by the Human Potential and Mobility Programme from the European Union through contract HPRI-CT-1999-00035.

Tätä julkaisua myy
VTT TIETOPALVELU
PL 2000
02044 VTT
Puh. (09) 456 4404
Faksi (09) 456 4374

Denna publikation säljs av
VTT INFORMATIONSTJÄNST
PB 2000
02044 VTT
Tel. (09) 456 4404
Fax (09) 456 4374

This publication is available from
VTT INFORMATION SERVICE
P.O.Box 2000
FIN–02044 VTT, Finland
Phone internat. + 358 9 456 4404
Fax + 358 9 456 4374

ISBN 951–38–6200–3 (soft back ed.)
ISSN 1235–0605 (soft back ed.)
ISBN 951–38–6201–1 (URL: http://www.vtt.fi/inf/pdf/)
ISSN 1455–0865 (URL: http://www.vtt.fi/inf/pdf/)